Diss. ETH No. 20706

System Design of a Directly Air Assisted Turbocharged SI Engine Using a Camshaft Driven Valve

A dissertation submitted to
ETH ZURICH

for the degree of
Doctor of Sciences

presented by

Christoph Voser

MSc ETH ME
born October 22, 1982
citizen of Switzerland

accepted on the recommendation of
Prof. Dr. Lino Guzzella, examiner
Prof. Dr.-Ing. Georg Wachtmeister, co-examiner
Dr. Christopher H. Onder, co-examiner

2012

Christoph Voser
christoph.voser@alumni.ethz.ch

Institute for Dynamic Systems and Control
ETH Zurich
Sonneggstrasse 3
8092 Zurich
Switzerland

Für meine Familie

Acknowledgments

This work is part of the hybrid pneumatic engine project at the Institute for Dynamic Systems and Control (IDSC). It has been supported by the Swiss Federal Office of Energy (BfE Switzerland), Robert Bosch GmbH and KPMG.

There are many people who have contributed to this work in various ways, and who deserve my deepst gratitude. First of all, I would like to thank my supervisor, Prof. Dr. Lino Guzzella, for accepting me as a doctoral candidate. Furthermore, I am grateful to Prof. Dr.-Ing. Georg Wachtmeister who accepted to be my co-examiner. Special thanks go to Dr. Christopher Onder for his support and the very helpful discussions, and for accepting to be my co-examiner.

I also want to acknowledge Dr. Christian Dönitz for his valuable contributions to the project.

Furthermore, I want to thank my colleagues and contributing students at the IDSC for their help and support throughout my work. A special thank you goes to Daniel Wagner and Daniel Burch for their devoted support at the engine test bench.

Finally, my thanks go to my parents, my brothers and my girlfriend whose support and encouragement during all the years made this dissertation possible in the first place.

August 2012 *Christoph Voser*

Abstract

The pneumatic hybridization in combination with downsizing and turbocharging is a promising approach to reduce the fuel consumption of spark-ignited (SI) engines while maintaining an excellent driveability. The associated system costs are substantially smaller than those of the well-known electric hybridization.

Hybrid pneumatic engines (HPEs) are equipped with an additional "charge" valve (CV) per cylinder that connects the cylinder to an air pressure tank. The compressed air is used to start the engine. The so-called pneumatic engine start is fast enough to justify the elimination of engine idling and the use of a stop/start functionality. Furthermore, the injection of compressed air into the combustion chamber during the compression phase can recover the driveability. This so-called boost mode is the enabler of strong downsizing and turbocharging.

Thus far, fully variable camless valve-trains have been investigated for the charge valve actuation. These systems are expensive, complex and are not available in series production, which prevented a breakthrough of the HPE technology. This thesis evaluates whether and how camshaft driven systems currently available can be used to control the air exchange. Such systems are simpler and more cost-effective, which makes them more attractive for a realization. The reduced complexity and cost of the valve-train come at a loss of variability which can be overcome by control strategies. Hence, the design of the valve-train system of the charge valve becomes crucial.

First, all pneumatic engine modes available on a directly connected HPE are analyzed with respect to their fuel saving potential, required valve-train variability and air demand. As a result, propelling the vehicle with air is omitted. Thus, the HPE boils down to a turbocharged (TC) SI engine, which uses pressurized air for the engine start and to boost the engine. The tank can still be filled by running the engine as a compressor during deceleration phases. The resulting system is called directly air-assisted TC SI engine. Its fuel saving potential for a downsizing factor of two amounts to 28%, which is only slightly smaller than the 31% achievable with a fully variable valve-train.

The air exchange between the cylinder and the tank depends on the lift profile, the valve diameter and the tank pressure. The lift profile is characterized by its opening instant, closing instant, acceleration and maximum lift. For each mode a design methodology is derived to find an appropriate valve lift profile while respecting the influence of the valve diameter, the tank pressure and other constraints. The methodologies are generic and can be applied to arbitrary engines. All design methodologies are exemplarily applied to the 0.75 l two-cylinder TC SI test bench engine available at the institute.

Since the boost mode is used to improve the driveability of TC SI engines its valve design is linked to a performance criterion. Furthermore, the boost mode with camshaft driven CVs ideally complements the use of a conventional turbocharger. At low engine speeds, the effect of the boost mode is largest. Thus, it compensates the turbo lag, which is most prominent at low engine speeds. Additionally, the torque control is complicated by the limited variability of the mechanical valve-train. An air mass based control strategy actuating the throttle, ignition timing and boost mode timing is analyzed in simulation and then verified experimentally for various operation conditions.

In simulation and experiments it is shown that the engine can also be pneumatically started within 350 ms if a camshaft driven CV is used. Furthermore, the best tank filling performance is achieved at high engine speeds and at low tank pressures.

Finally, the individual design methodologies are merged to an overall system design approach. It guarantees that the system performance is maximized rather than each individual mode. In a concluding design example the valve timings of each mode as well as an appropriate tank size are determined. For a compact class vehicle which is propelled by a 0.75 l TC SI engine it turns out that an air tank of less than 10 l is sufficient.

Zusammenfassung

Die pneumatische Hybridisierung in Kombination mit der Reduktion des Hubraums und der Turboaufladung ist ein vielversprechender Ansatz, um den Kraftstoffverbrauch von Ottomotoren zu senken, ohne dabei Kompromisse in der Fahrbarkeit einzugehen. Die anfallenden Zusatzkosten des Systems sind deutlich kleiner als diejenigen von Elektrohybriden.

Pneumatische Hybridmotoren verfügen über ein zusätzliches Ventil pro Zylinder. Das sogenannte Ladeventil verbindet die Brennkammer mit einem Druckluftank. Die darin gespeicherte Druckluft wird für den Motorstart verwendet. Dieser ist genügend schnell, um auf den Leerlaufbetrieb verzichten zu können und somit eine Stop/Start-Funktionalität abbilden zu können. Die Einblasung von komprimierter Luft in den Brennraum während der Kompressionsphase ermöglicht es, mehr Kraftstoff einzuspritzen. Der sogennante Boost-Modus führt daher zu einer deutlichen Verbesserung des Ansprechverhaltens und der Fahrbarkeit. Er macht die starke Hubraum-Reduktion in Kombination mit der Turboaufladung erst möglich.

Bis anhin wurden vollvariable Ventiltriebe vorgeschlagen für die Regelung des Lufttransfers zwischen dem Tank und den Brennräumen. Diese Ventiltriebe sind teuer, komplex und werden nicht in Serienproduktion gefertigt, was den Durchbruch der pneumatischen Hybridisierung bislang verhinderte. Im Gegensatz dazu sind nockenwellen-getriebene Ventile deutlich einfacher und kostengünstiger. Zudem sind sie bereits verfügbar und werden in Serienfahrzeugen eingesetzt. In dieser Arbeit wird evaluiert, ob und in welcher Form nockenwellen-getriebene Ladeventile mit fixen Steuerzeiten für die Steuerung des Lufttransfers zwischen dem Brennraum und dem Drucktank eingesetzt werden können. Nockenwellen-getriebene Ladeventile verfügen über eine eingeschränkte Variabilität. Durch geeignete Regelstrategien können immer noch alle Modi betrieben werden. Das Hauptaugenmerk liegt aber auf der Auslegung der Ladeventile, insbesondere auf deren Ventilhubkurven.

Im ersten Schritt werden die Betriebsmodi des pneumatischen Hybridmotors auf deren Kraftstoffeinsparpotential, die erforderliche Ventiltriebs-Variabilität und den Luftbedarf untersucht. Daraus folgt, dass auf den

Fahrzeugantrieb mit komprimierter Luft verzichtet wird und somit die komprimierte Luft nur noch zum Starten und Boosten eingesetzt wird. Das Antriebssystem wird folglich neu luftunterstützter turboaufgeladener Ottomotor genannt. Trotz der Vernachlässigung des pneumatischen Motor Modus beträgt das Kraftstoffeinsparpotential bei einer Halbierung des Hubvolumens immer noch 28 %.

Der Luftaustausch zwischen den Brennräumen und dem Tank hängt vom Tankdruck, von der Hubkurve und dem Durchmesser des Ladeventils ab. Die Hubkurve ist gekennzeichnet durch den Öffnungszeitpunkt, den Schliesszeitpunkt, die Beschleunigung und den maximalen Hub. Für jeden Betriebsmodus wird eine Ventil-Auslegemethodik präsentiert, anhand welcher ein geeignetes Hubkurvenprofil ermittelt werden kann. Die Einflüsse von Ventildurchmesser, Tankdruck und anderen Einschränkungen werden berücksichtigt. Die Methoden sind generisch und können für beliebige Motorgrössen mit unterschiedlichen Brennverfahren angewendet werden. Alle Auslege-Methoden werden für den 0.75 l Zweizylinder-Prüfstandsmotor exemplarisch angewendet.

Der Boost Modus wird zur Verbesserung der Fahrbarkeit eingesetzt. Deshalb ist die Auslegung der Ventilhubkurve an eine Fahrbarkeits-Anforderung geknüpft. Der Effekt des Boost Modus mit nockenwellen-getriebenen Ladeventilen ist bei tiefen Drehzahlen am grössten. Der Boost Modus ist folglich hervorragend geeignet, um das Turboloch, welches bei tiefen Drehzahlen besonders ausgeprägt ist, zu überbrücken. Die Drehmomentregelung im Boost Modus wird durch die reduzierte Variabiliät des Ventiltriebs erschwert. Für die Regelung des Drehmoments wird eine luftmassen-basierte Regelstrategie für die Drosselklappe, den Zündwinkel und die Ansteuerung der Ladeventile in Simulation untersucht und mit Messungen auf dem Prüfstand für verschiedene Betriebspunkte verifiziert. Zudem wird in Simulation und Experimenten gezeigt, dass der pneumatische Motorstart auch mit nockenwellen-getriebenen Ladeventilen realisiert werden kann. Mittels der Simulation mit einem Prozessmodell wird zudem gezeigt, dass das Füllen des Tanks bei hohen Drehzahlen und tiefen Tankdrücken am schnellsten erfolgt.

Abschliessend werden die einzelnen Auslege-Methoden zu einer Systemauslege-Methode zusammengeführt, mit der Absicht, die Performance des Gesamtsystems zu maximieren. In einem abschliessenden Beispiel werden die Ventilhubkurven der einzelnen Modi und eine geeignete Tankgrösse für den Prüfstandsmotor ermittelt. Für ein Fahrzeug der Kompaktklasse, welches mit einem 0.75 l aufgeladenen Ottomottor ausgestattet ist, reicht ein Tankvolumen von 10 l.

Contents

1. Introduction

1.1. Motivation

For many reasons the fuel consumption of power-trains has to be reduced, e.g., greenhouse effect, limited resources and their geographic distribution, fuel prices, to name but a few.

A widely accepted method for reducing the fuel consumption in spark-ignited (SI) internal combustion engines (ICEs) is downsizing, i.e., reducing the displacement of an engine [1, 2]. Lower friction and reduced pumping losses result in a lower fuel consumption. The peak power of a larger naturally aspirated (NA) engine can be recovered by using a turbocharger (TC).

Unfortunately, by applying strong downsizing and turbocharging, the turbo lag leads to a loss of driveability and consequently of customer acceptance. The delayed rise of the torque results from the additional inertia brought into the system by the rotor of the turbocharger. It is pronounced if it is combined with downspeeding, i.e., operating the drive train in the highest gear possible. Solutions which cope with this problem are either expensive and complex to control, e.g., multi-stage turbocharging, or they increase the fuel consumption, e.g., waste gate closed strategy or replacing the TC by a mechanical compressor.

Another solution is the electric hybridization of the drive train, where the fast torque response of the electric motor is used to improve the driveability. Aside from the driveability improvement, hybrid electric vehicles offer a substantial fuel economy, which, however, comes at a high added cost and weight for the additional components such as batteries, power electronics and electric motors.

A further solution to the driveability problem of strongly downsized and turbocharged SI engines is in-cylinder boosting, which was proposed in [3, 4, 5]. In that solution, an air mass buffer is added to a conventional ICE. Each cylinder is directly connected to a shared air pressure tank. The air mass flow is controlled by a valve referred to as the charge valve (CV). The resulting engine structure is depicted in Figure 1.1.

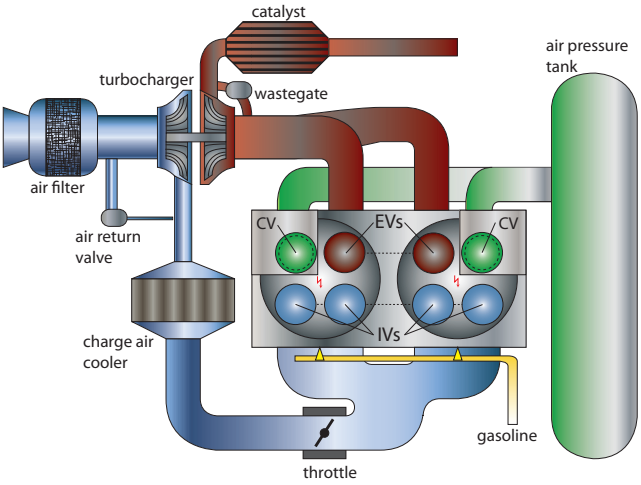

Figure 1.1.: Schematic of the downsized and turbocharged SI engine with a direct connection between the combustion chamber and the air tank: intake valve (IV), exhaust valve (EV).

So far, in-cylinder boosting was predominantly discussed in the context of hybrid pneumatic engines (HPEs) [6, 7, 8]. Besides boosting, the pressurized air available in HPEs is also used to perform a rapid pneumatic engine start [9] and thus serves to avoid idling losses. Moreover, the pressurized air is used to propel the vehicle by means of the so-called pneumatic motor mode. During deceleration phases the engine is run as a compressor to fill the air tank. This mode is often called pump mode. In [6] a fuel savings potential of HPE of up to 35% has been calculated and verified experimentally. The main contribution results from strong downsizing which is enabled by in-cylinder boosting.

HPEs are usually equipped with a fully variable camless valve actuation for the CV because the additional engine modes require a large variability of the valve opening instant, the valve closing instant, and the maximal valve lift. The drawbacks of such a valve actuation system are the high total costs of ownership (investment, maintenance), a high complexity, its limited robustness and the need for an additional power supply for the valve actuation (e.g., electric, hydraulic, pneumatic). Furthermore, such systems are not yet in use in series production cars.

Camshaft driven systems are simpler and more cost-effective, and thus are more attractive for a realization. Furthermore, they are available on the market and are adopted in cars today. The motivation of this thesis is to answer the question of whether and, if yes, with which drawbacks a camshaft driven (CSD) CV can be used for the control of the air transfer between the combustion chamber and an additional air mass buffer.

1.2. Objectives of this thesis

This thesis aims at evaluting the potential of TC SI engines that are equipped with an additional air mass buffer and a CSD CV. Validated simulation models are used to study each mode. Based on the found relations, design methodologies for the CV lift profile of each mode are derived. Furthermore, the loss of variaibility results in a demand of sophisticated control strategies. Several results are validated with experiments on the institute's test bench engine which is described in Appendix A.

1.3. Structure and contributions of this thesis

The work is structured as follows:

- In Chapter 2, all modes of an HPE equipped with fully variable CVs are analyzed with respect to their fuel saving contribution, required valve-train variability and air demand. The analysis is based on simulation and measurement data. From the results, the engine modes which should be realized with a CSD CV are derived. Furthermore, CSD valve-train mechanisms are presented and evaluated.

- In Chapter 3, in-cylinder boosting with a CSD CV is examined with respect to the achievable transient engine performance. The system characteristics and limitations are discussed by using a mean value engine model that is adapted for in-cylinder boosting. A model-based design framework is presented which links the valve system design to a desired engine performance. The content of this chapter was published in [10]. Furthermore, in [11] the concept of using a CSD CV to boost the engine is patented.

- In Chapter 4, the torque control during the turbo lag compensation is discussed. The control is complicated by the limited variability

of the mechanical valve-train. This limited variability gives rise to a trade-off between fuel and pressurized air consumption. An air mass based control strategy actuating the throttle, ignition timing and boost mode timing is analyzed in simulation and then verified experimentally in various operation conditions. The content of this chapter was published in [12].

- Chapter 5 discusses the pneumatic engine start using CSD CVs. A general methodology for an air-optimal CV design is presented which can handle various specifications. The proposed design methodology is based on a validated process model. In a design example the methodology is applied to the two-cylinder test bench engine. The resulting optimized pneumatic start is experimentally verified. The content of this chapter was published in [13].

- In Chapter 6 the tank filling with CSD CVs is discussed. The filling performance characteristics are derived and analyzed. A CV design methodology is then presented and applied in a design example. Furthermore, the performance of a CSD CV with fixed valve timing is compared to the performance of a CSD CV with variable valve timing. The chapter ends with a discussion of other means to fill the tank.

- The previous chapters analyzed each mode individually. Chapter 7 combines all the findings into one system design methodology. This methodology is applied in a design example to find the valve timings for each mode and an appropriate tank size. The behavior of the properly designed system is then analyzed for various parameter configurations, e.g., initial tank pressure or tank volume.

- Finally, the conclusions are drawn in Chapter 8.

Further contributions were published within the framework of the HPE project [6, 9, 14].

2. System Analysis and Valve-Train Considerations

The fuel economy of HPEs results from additional pneumatic engine modes such as the boost mode, the pneumatic motor mode and the pneumatic start mode [5]. The pump mode supplies the pressurized air used in these pneumatic modes. As shown in Figure 2.1, the realization of these modes requires a large variability of the valve opening instant, the valve closing instant, and the maximal valve lift. Thus, HPEs are usually equipped with a fully variable camless valve actuation for the CV. References to the HPE in this thesis are based on the assumption that the CV is fully variable and that the intake and exhaust valves are driven by the camshaft.

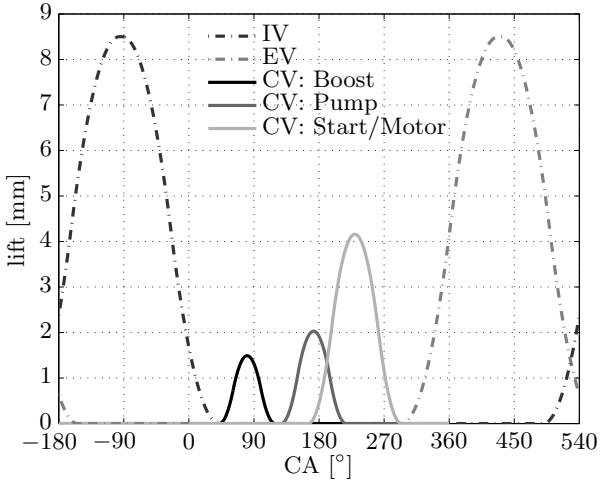

Figure 2.1.: Valve lift profiles of the various engine modes (0 °CA at bottom dead center before compression).

The aim of this thesis is to find a system realization with a camshaft driven valve-train mechanism for the CV. The evaluation process starts

in Section 2.1 with the analysis of the fuel saving contribution of each engine mode in an HPE. Furthermore, the valve-train variability required for the torque control and the air demand are discussed. Based on the results of the HPE analysis, the air assisted TC SI engine is derived in Section 2.2. In Section 2.3.1 the requirements on the valve-train resulting from the engine modes and their transitions are discussed. Section 2.3.2 presents a brief overview of existing CSD valve-train mechanisms. In Section 2.3.3 the available valve-train mechanisms are evaluated. Finally, possible system realizations are presented.

2.1. Analysis of the hybrid pneumatic engine

2.1.1. Fuel economy

The additional engine modes available in an HPE yield a substantial fuel economy. In [15] the contribution of each engine mode has been evaluated in simulation for an HPE with ideal CVs and a perfectly insulated air tank. Figure 2.2 shows the results for a vehicle weighing 1450 kg on the New European Drive Cycle (NEDC) relative to a 2 l NA engine. All engines depicted have the same rated power. The smaller engines are equipped with a turbocharger to recover the rated power. For a downsizing factor of 2, the total saving potential is 31%. The fuel economy resulting from downsizing, which is enabled by the boost mode, amounts to approximately 25%. The contribution of the pneumatic start is 3%. For the pneumatic motor mode a savings potential of approximately 3% is predicted. These predictions were experimentally verified and published in [6]. For the Nissan Micra 1.24 l a fuel economy of 30.6% was measured on the federal test procedure (FTP) drive cycle. The pneumatic motor mode contributed 2.8%.

From the point of view of fuel economy, the boost mode is the most important engine mode since it enables the strong downsizing and turbocharging without a driveability loss. It is followed by the pneumatic motor and pneumatic start mode, both of which contribute the same amount.

2.1.2. Valve-train variability

To achieve a good driveability and comfort, the torque demand of the driver should be met. In the following paragraphs the requirements on

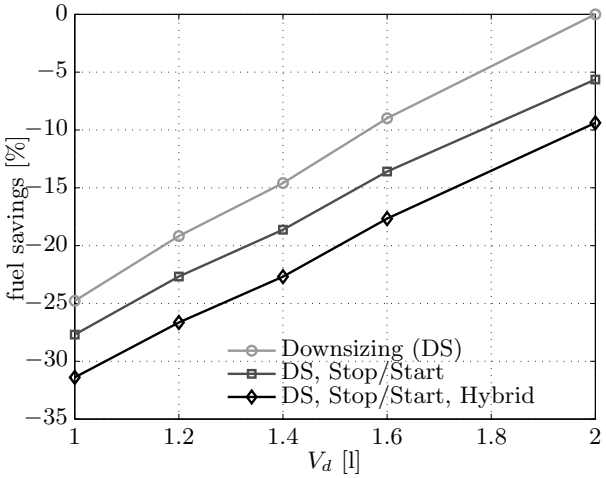

Figure 2.2.: Fuel saving potential for a 1450 kg vehicle in the NEDC relative to a 2 l NA engine [15]. All engines have the same rated power.

the valve-train (VT) variability for the torque control is discussed for each pneumatic engine mode.

Boost mode In the boost mode the torque is controlled by the ignition timing and the amount of air that enters the combustion chamber (assuming stoichiometric conditions). The amount of air is controlled by the throttle position and the CV timing. If too much charge enters the combustion chamber the retardation of the spark timing can be used to adjust the torque to the desired value. The CV timing is not crucial, since another fast actuator (namely the ignition timing) can compensate. Furthermore, the boost mode is mainly applied in transients during a very short period of time.

Pneumatic motor mode In the pneumatic motor mode, it must be possible to set the torque to a desired value. In [16] it is shown that the main actuator for the torque control in the pneumatic motor mode is the CV closing instant. Thus, the torque control requires a rather high VT variability on top of the high variability required to enable all engine modes.

Pneumatic start The pneumatic start does not need to satisfy a given torque demand. Its goal is to reach the idling speed in minimum time. Thus, a precise torque control is not required.

2.1.3. Air demand

If the pump mode is not realized with a fully variable valve-train, its filling performance inevitably is lower. Hence, the available amount of compressed air is smaller. The question arises in which mode the available air should be used, i.e., which fuel savings are achieved with which amount of air. Thus, in the following the air demand of each pneumatic engine mode is analyzed.

Boost mode In the boost mode, a small amount of air is added to the combustion chamber during transients, which are very short. The combustion chamber is mainly filled with air coming from the intake manifold. Thus, the boost mode requires little air only.

Pneumatic motor mode In the pneumatic motor mode the torque is generated by the pressurized air that is injected. The cylinder is mainly filled with air from the tank at a high pressure level. Furthermore, it is operated in the conventional speed range which results in many air injections per second, e.g., for a two-cylinder engine that is operated at an engine speed of 2400 rpm, 40 air injections occur per second. The longer the motor mode is operated the larger is its impact on the fuel economy. However, the amount of air demanded increases rapidly. Thus, the pneumatic motor mode demands a lot of pressurized air.

Pneumatic start As shown in [9], only four air injections are necessary to speed up the two-cylinder engine to its idle speed. Consequently, the air demand of the pneumatic start is rather small.

Table 2.1 summarizes the advantages and disadvantages of the various modes presented. Note that the pump mode which is used to fill the tank is not listed here since tank filling is a prerequisite. If no compressed air is available, the other modes cannot be realized. There are several ways to fill the tank, e.g., by running the engine as an air compressor during deceleration phases. Alternatively, the air tank can be filled by an

Table 2.1.: Analysis of additional pneumatic engine modes.

Mode	fuel savings	VT variab.	air demand
Downsizing and boost mode	+++	small	small
Pneumatic motor mode	+	high	high
Pneumatic start	+	small	small

external compression device which can be driven either mechanically or electrically. Tank filling is discussed in Chapter 6.

2.2. Air assisted TC SI engine

The aim of this thesis is to find a system realization with a CSD valve-train mechanism. The new system realization should be cost-effective and realizable with available valve-train technology. Thus, too complex valve-trains and cylinder head modifications are excluded.

The analysis in the previous section showed that the fuel economy resulting from the pneumatic motor mode is rather low. Its high requirements on the valve-train variability lead to increased costs and complexity. The high air demand requires a larger tank, which complicates the packaging. Furthermore, in the pneumatic motor mode the three-way catalytic converter (TWC) is flooded with cold air (due to the expansion). As a result the TWC is filled with oxygen and the temperature of the catalyst is reduced. Since these drawbacks do not outweigh the low fuel savings, the pneumatic motor mode is omitted.

Without the pneumatic motor mode the system reduces to a TC SI engine where air is used to enhance the driveability and to realize a stop/start functionality. The vehicle is no longer propelled purely with air. Thus, the system name is changed from hybrid pneumatic engine to *air assisted (AA) TC SI engine*. It features the following engine modes:

- conventional combustion mode;
- boost mode;
- pneumatic start;
- tank filling.

According to Figure 2.2, the expected fuel economy for a downsizing factor of 2 is still approximately 28%. The measurement results of [6] show fuel savings of 28% on the FTP without using the pneumatic motor mode.

2.3. Camshaft driven valve-train

In this section an appropriate CSD valve-train mechanism is evaluated for the AA TC SI engine. First, the valve-train requirements of the modes and the mode transitions are formulated. Then, a brief survey of existing CSD valve-train mechanisms is given. Finally, a valve-train mechanism is evaluated.

2.3.1. Requirements on the valve-train

As shown in Figure 2.2 the required valve-train variability is large to enable the valve lift profiles of each engine mode. Each profile has a different

- opening instant (CVO);
- closing instant (CVC);
- valve acceleration (acc.);
- maximal valve lift.

The transitions between the modes pose additional requirements on the valve-train. In the following the mode transitions occurring in an AA TC SI engine are analyzed and classified. A mode transition is considered to be critical if an erroneous actuation of the valve-train leads to high emissions, damage of the engine or an unsatisfied driver demand.

The transition to a fired engine mode is always critical because misfire can occur. Misfire results in an unsatisfied torque demand and high hydrocarbon emissions. In addition, the unburnt fuel might ignite in the exhaust and possibly damage the TWC. The cause of misfire in this context is an air-fuel ratio which substantially deviates from stoichiometric conditions. The transition to the boost mode is particularly critical because air from the tank and fuel are injected. The timing of the fuel and the air injection are crucial. Furthermore, at a tip-in of the driver the boost mode should be activated as fast as possible (e.g., in the next cycle) and as predictably as possible (i.e., reliably). Hence, the actuation

of the air injection has to be precise, reliable, predictable, from one cycle to the next and cylinder individual. The transition to the pump mode is uncritical since no combustion takes place. It is also not crucial that the transition happens immediately.

Table 2.2 summarizes all occurring mode transitions and classifies them into very critical (vc), critical (c) or uncritical (uc). The start mode is

Table 2.2.: Classification of engine mode transitions: vc = very critical, c = critical, uc = uncritical.

From/To	conventional	boost	pump
Conventional	-	vc	uc
Boost	vc	-	uc
Pump	c	vc	-
Start	c	vc	-

only used after the power-train is shut off. Thus, a direct transition to this mode does not occur.

Consequently, when selecting a valve-train mechanism the following aspects have to be considered and carefully evaluated for each occurring mode transition

- cycle-to-cycle resolution (C2C);
- cylinder individual switching (cyl. ind.);
- transition reliability (reliab.);
- maximal engine speed for which the mode transition is possible.

2.3.2. Survey of CSD valve-trains available

Camshaft driven systems are simpler and hence more cost-effective. Furthermore, they are available on the market and are adopted in cars today. This section provides an overview of existing variable, camshaft driven valve-train mechanisms. The survey does not claim to be complete. It should rather point out the existing variety.

Variable valve actuation is a generalized term used to describe any mechanism or method that can change the shape and/or the timing of a valve lift event. In the following two different classifications are given. First, the variability of the valve events is considered. Then, various technical realizations are presented.

Classification by valve event

As shown in [17] the following options exist for variable valve actuation:

1. variable cam phasing;
2. switchable valve lift;
3. cylinder deactivation:
4. continuously variable lift/duration.

Classification by system technology

- Variability of camshaft drive:
  BMW Vanos [18]
- Variability of cam to valve transmission:
  hydraulic: INA UniAir [19, 20]
  mechanical: BMW Valvetronic [21], INA EcoValve [22]
- Variability by additional cam profile link:
  Porsche VarioCam [23], Honda VTEC, Toyota VTT
- Variability by shiftable cam or camshaft:
  Audi valvelift system [24], INA cam shifting [25], INA 3DCam [26]

Furthermore, various designated valve deactivation mechanisms exist [27, 28].

2.3.3. Valve-train evaluation

If the requirements and the available valve-train variabilities are known a suitable valve-train mechanism can be determined. The evaluation is given in Table 2.3.

Cam shifting systems fit the requirements best mainly because the transition is fast, cylinder individual and reliable. Furthermore, the valve lift profile of each mode can be designed individually. The variability in the transmission from cam to valve also fulfills most of the requirements. The mechanical transmission is limited by the adjustment speed. The temperature dependence of the oil properties constrains the reliability of the hydraulic transmission. The variability in the camshaft drive is undesirable since all CVs are phased at the same time which causes timing problems during the mode transitions.

Table 2.3.: Evaluation of valve-train mechanisms. (h) = hydraulic, (m) = mechanical.

Variability	CVO	CVC	lift	acc.	C2C	cyl. ind.	reliab.
Camshaft drive	+	-	-	-	-	-	√
Transmission (m)	+	+	++	-	-	√	√
Transmission (h)	+	+	++	-	+	√	-
Cam shifting	++	++	++	++	++	√	√

2.3.4. Possible system realizations

Cam shifting systems can be combined with cylinder deactivation or auxiliary systems, e.g., external compression device (ext. comp.) or an electric stop/start system (el. SS). A total of eight system realizations of an AA TC SI engine exist with cam shifting, cylinder deactivation, external compressor and electric stop/start system. They are listed in Table 2.4. The last column indicates the total number of cams necessary. Note that the

Table 2.4.: Possible system realizations.

Mode	conv.	boost	pump	start	# cams
#1	cam	cam	cam	cam	4
#2	cyl. deact.	cam	cam	cam	3
#3	cam	cam	ext. comp.	cam	3
#4	cam	cam	cam	el. SS	3
#5	cam	cam	ext. comp.	el. SS	2
#6	cyl. deact.	cam	cam	el. SS	2
#7	cyl. deact.	cam	ext. comp.	cam	2
#8	cyl. deact.	cam	ext. comp.	el. SS	1

boost mode can only be realized by a CSD system. All other modes can also be realized with auxiliary systems.

In the following chapters CV design methodologies and control strategies of each mode are discussed. Each design methodology only considers a fixed valve lift profile in the crank angle (CA) domain, i.e., a fixed cam profile without any additional variability. In Chapter 7 the individual design methodologies are combined and applied on an AA TC SI engine

equipped with a shiftable cam system with four separate cams (realization #1) or three separate cams and a deactivation mechanism (realization #2), respectively.

3. In-Cylinder Boosting: Valve Design

Among the modes described in Section 2.2 the boost mode is the most important one since it enables strong downsizing and, thus, the associated fuel economy. In the boost mode, once the intake valves (IVs) are closed, compressed air is added to the combustion chamber during the compression stroke. Hence, more fuel can be injected, yielding a higher torque. A measured p-V diagram of this mode is depicted in Figure 3.1. This mode substantially enhances the driveability of the power train since a large torque step can be realized from one engine cycle to the next. Furthermore, the exhaust enthalpy flow is increased, which leads to a faster acceleration of the turbocharger.

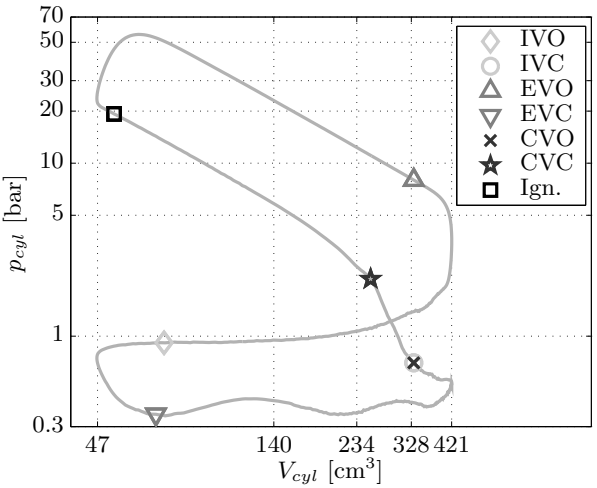

Figure 3.1.: Measured, double-logarithmic p-V diagram of the boost mode with the valve timings of intake valves (IVs), exhaust valves (EVs) and charge valve (CV) (O: opening, C: closing). The engine parameters are listed in Appendix A.

This chapter presents a model-based approach for the design of a CSD CV used for in-cylinder boosting. In such a realization the air mass admitted through the CV cannot be controlled. Hence, all requirements and constraints on the engine performance have to be considered in the design process.

The chapter is structured as follows: Section 3.1 presents the models that are used to study the engine behavior with in-cylinder boosting and shows validation results. In Section 3.2 the performance of an engine equipped with a CSD CV is analyzed using a mean value model of the engine system. Section 3.3 presents the relevant CV design variables, shows their dependencies and discusses arising constraints. Section 3.4 provides a valve design example. Finally, conclusions are drawn.

3.1. Models

The dynamic performance of a TC SI port-fuel injected (PFI) engine with in-cylinder boosting is studied with a mean value model (MVM). In Section 3.1.1 the relevant changes made to a standard MVM are discussed. Section 3.1.2 presents a model for the transferred CV mass and links it to the valve parameters. In Section 3.1.3 the model validation is shown.

3.1.1. TC SI PFI engine model

The modeling approach is standard and well documented in the literature [29]. In this section, only those changes are discussed that are necessary to realize the boost mode.

Intake air mass flow

During boosting the intake conditions are very rich, which decreases the volumetric efficiency because more cylinder volume is occupied with fuel. In contrast, the fuel evaporation leads to an increased cooling of the mixture. Consequently, the density of the mixture is higher. The air mass which enters from the intake manifold into each cylinder m_β is typically modeled as

$$m_\beta = \frac{p_{im}}{R_a \cdot \vartheta_{im,cc}} \cdot \eta_{vol}(\lambda_{ip}) \cdot \frac{V_d}{N_{cyl}}, \tag{3.1}$$

where p_{im} is the intake manifold pressure, R_a is the gas constant of air, $\vartheta_{im,cc}$ is the temperature of the charge entering, V_d denotes the displacement of the engine, N_{cyl} is the number of cylinders, η_{vol} is the volumetric

efficiency (see Appendix B.1), and λ_{ip} is the normalized air/fuel ratio in the intake port.

Torque generation

The Willans approximation [29] is used for the torque generation both in the conventional and in the boosted operation. With the assumption of stoichiometry after CV closing, the fuel mean effective pressure p_{mf} is calculated as

$$p_{mf} = \frac{H_l \cdot N_{cyl}}{V_d \cdot \sigma_0} \cdot (m_\beta + m_{CV}), \tag{3.2}$$

where H_l denotes the lower heating value of gasoline, σ_0 is the stoichiometric air/fuel mass ratio, and m_{CV} stands for the air mass transferred through the CV. Note that m_β and m_{CV} correspond to air masses per cylinder. Furthermore, the terms torque and brake mean effective pressure are used interchangeably in this thesis.

3.1.2. Camshaft driven CV

During boosting, air from the tank enters through the CV. The air transferred through the CV can be modelled as

$$m_{CV} = \frac{p_t}{\sqrt{R_a \cdot \vartheta_t}} \cdot \Psi_{crit} \cdot \frac{1}{\omega_e} \cdot \int_{\phi_{CVO,b}}^{\phi_{CVC,b}} A_{eff}(y_{CV}(\phi))d\phi, \tag{3.3}$$

where p_t is the tank pressure, ϑ_t is the tank temperature, ϕ is the crank angle, ω_e is the engine speed, $\phi_{CVO,b}$ is the CV opening angle, $\phi_{CVC,b}$ is the CV closing angle, $y_{CV}(\phi)$ denotes the CV lift, and A_{eff} denotes the effective flow area. It includes the discharge coefficient which results from stream contraction [30]. For a CSD CV, the lift profile and hence the integral are constant. More details on the derivation of Equation (3.3) are given in Appendix B.2.

CV mass flow

Rewriting Equation (3.3) and introducing new variables yields

$$m_{CV} = \mu_{CV,p} \cdot \frac{p_t}{\omega_e} = \mu_{CV} \cdot \frac{1}{\omega_e}. \tag{3.4}$$

The value of $\mu_{CV,p}$ is constant for a given CV design (assuming that the tank temperature remains constant) and, thus, can be considered as the CV size.

According to Equation (3.4), the mass transferred through a CSD CV is

- proportional to the tank pressure p_t,
- proportional to the CV size $\mu_{CV,p}$, and
- inversely proportional to the engine speed ω_e.

Thus, at low engine speeds a higher air mass is transferred. This fact favors the turbo lag compensation where air is missing, particularly at low engine speeds. Figure 3.2 shows the air admitted as a function of the engine speed for the same CV size ($\mu_{CV,p} = const.$) and two different tank pressures.

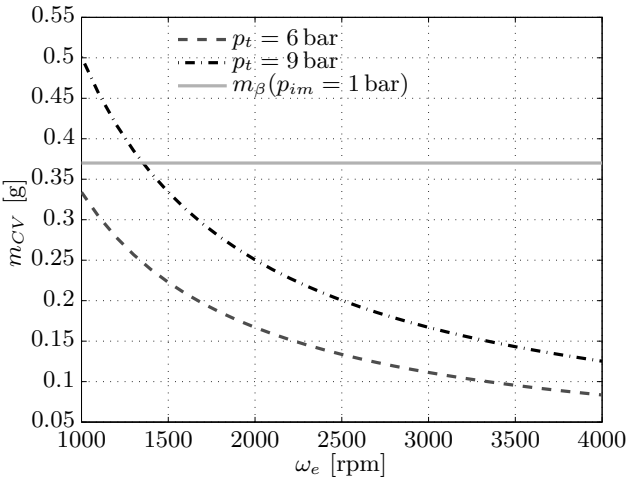

Figure 3.2.: Air mass admitted through the CV as a function of the engine speed for the same CV size ($\mu_{CV,p} = 5.82\,{}^{\text{g}}/_{\text{sbar}}$) but different tank pressures. The solid line approximates the intake air mass at $p_{im} = 1$ bar for the engine data listed in Appendix A.

The variable μ_{CV} denotes the CV mass flow. It significantly influences the engine performance and is a basic property of an engine equipped with in-cylinder boosting. It will be used to evalute the transient engine performance in the design process where the value of the tank pressure is not yet known but has to be determined.

Simplified lift profile

For the derivations below a simplified valve acceleration profile in the crank angle domain is assumed where the magnitudes of the acceleration and deceleration are equal and piecewise constant. Then, the CV lift $y_{CV}(\phi)$ is a function of the acceleration in the crank angle domain $a_{CV} = \frac{d^2 y_{CV}}{d\phi^2}$, the CV opening angle and the CV closing angle. Figure 3.3 shows the simplified valve acceleration profile and the resulting lift profile.

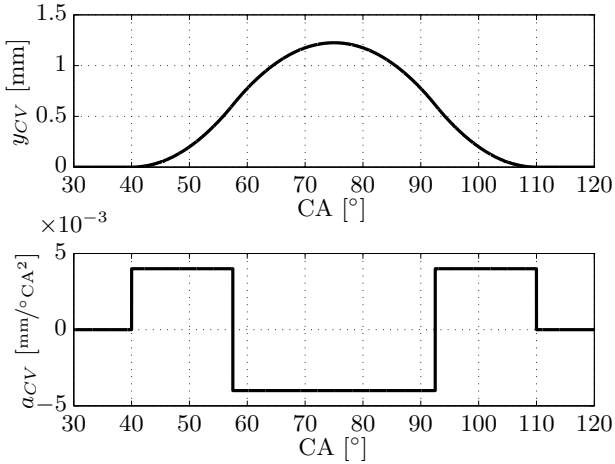

Figure 3.3.: Simplified valve lift and acceleration profiles: $\phi_{CVO} = 40\,^{\circ}\mathrm{CA}$, $\phi_{CVC} = 110\,^{\circ}\mathrm{CA}$, $|a_{CV}| = 0.004\,\mathrm{mm}/^{\circ}\mathrm{CA}^2$.

Effective flow area

The effective flow area A_{eff} can be modelled by

$$A_{eff}(\phi) = \mu\sigma_{CV}\left(\frac{y_{CV}(\phi)}{d_{CV}}\right) \cdot \frac{d_{CV}^2 \cdot \pi}{4}, \tag{3.5}$$

where $\mu\sigma_{CV}$ is the flow coefficient as defined in [30] and d_{CV} denotes the CV diameter. The linear approximation for the flow coefficient can be defined as

$$\mu\sigma_{CV}\left(\frac{y_{CV}(\phi)}{d_{CV}}\right) \approx \mu\sigma_{CV,lin} \cdot \frac{y_{CV}(\phi)}{d_{CV}}. \tag{3.6}$$

It holds well for lift-to-diameter ratios of up to 0.11.

3.1.3. Model validation

The engine used for this analysis is a modified engine where one exhaust valve was replaced by a fully variable valve that is actuated by an electro-hydraulic valve-train system (EHVS). Details on the modification can be found in [5]. The main parameters of the engine modelled are listed in Appendix A.

A specially designed controller for the EHVS allows the injection of a defined amount of air through the CV. This functionality allows an emulation of the behavior of a camshaft driven CV in terms of the mass transfer instead of the lift profile.

Figure 3.4 shows the simulated and measured engine torque trajectories with and without boosting at $\omega_e = 2000\,\mathrm{rpm}$. The solid lines show the case with in-cylinder boosting ($\mu_{CV} = 34.9\,\mathrm{g/s}$). At $t = 0\,\mathrm{s}$, the throttle is fully opened and the boost mode is activated. It remains active in the time frame shown. The engine torque is measured with a torque flange sensor which is located between the dynamometer and an elastic shaft that is connected to the engine. The measured torque signal is post-processed with a non-causal moving average filter over one engine revolution. The oscillations present after the torque step result from the unmodelled elasticity of the shaft. Due to the reciprocating behavior of the engine and since the engine is port-fuel injected, the torque does not immediately rise after the tip-in. The delay from injection update to torque center is approximately one engine cycle. The dashed lines show the situation without boosting where the throttle is fully opened at $t = 0\,\mathrm{s}$.

Figure 3.5 shows the simulated and measured engine torque trajectories with and without boosting at $\omega_e = 2500\,\mathrm{rpm}$.

These results confirm that the MVM approximates the dynamic behavior sufficiently well. It is therefore suited for the subsequent performance analysis.

3.2. Performance driven derivation of the CV mass flow

As shown in Figures 3.4 and 3.5, boosting substantially accelerates the torque build-up. In this section the torque response is studied for different values of μ_{CV} at various engine speeds using the models presented. Based on the results, a method for the derivation of a desired CV mass flow $\mu_{CV,des}$ is introduced which is based on an engine performance criterion.

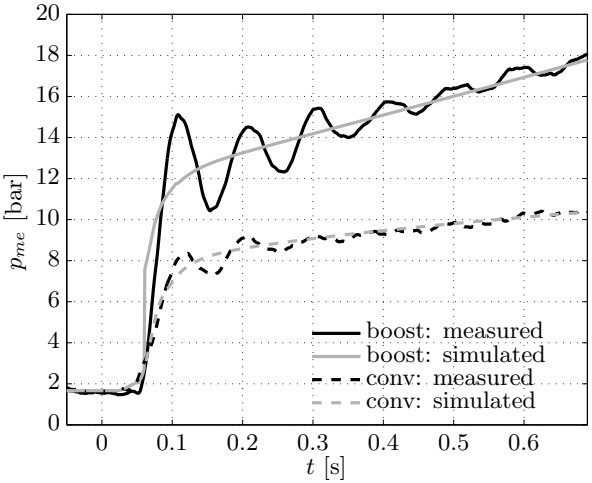

Figure 3.4.: Comparison of measurement and simulation data of the brake mean effective pressure p_{me} for $\mu_{CV} = 34.9\,\mathrm{g/s}$ and $\omega_e = 2000\,\mathrm{rpm}$: $m_{CV} = 0.167\,\mathrm{g}$. Dashed curves: without boost, solid curves: with boost (active for $t \geq 0\,\mathrm{s}$).

3.2.1. Engine performance for various CV mass flows

The fastest torque build-up is achieved if the throttle is fully opened and the boost mode is activated. In this way, the maximum amounts of air and consequently of fuel enter the cylinder. Figure 3.6 shows the torque build-up at constant engine speed for two different values of μ_{CV}. Prior to the activation of the boost mode and before the opening of the throttle is initiated, the engine is operated at $p_{me} = 1.7\,\mathrm{bar}$. The solid lines show the torque development with boosting. The dashed lines show the performance without boosting.

The upper plot shows the engine performance resulting from a CV design with $\mu_{CV} = 34.9\,\mathrm{g/s}$. The maximum stationary torque $p_{me,max}(\omega_e)$ is reached within one second for every engine speed. At low engine speeds the turbo lag is eliminated completely as a result of the inverse proportionality of the CV air mass to the engine speed.

The lower plot shows the performance for $\mu_{CV} = 55\,\mathrm{g/s}$. (Note the differing legend.) For a larger value of μ_{CV}, the torque rise in the boost mode is faster, of course, due to the increased CV air mass. In this case

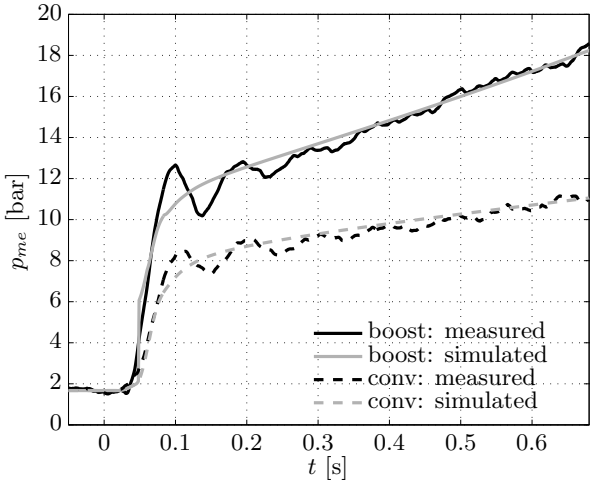

Figure 3.5.: Comparison of measurement and simulation data of the brake mean effective pressure p_{me} for $\mu_{CV} = 34.9\,\mathrm{g/s}$ and $\omega_e = 2500\,\mathrm{rpm}$: $m_{CV} = 0.134\,\mathrm{g}$. Dashed curves: without boost, solid curves: with boost (active for $t \geq 0\,\mathrm{s}$).

the maximum stationary torque for every engine speed is reached within approximately 0.6 s or less.

The performance without the boost mode activation is significantly slower. Especially at low engine speeds, the turbo lag is well noticeable.

Figure 3.6 clearly shows that the boost mode substantially improves the response behavior at low engine speeds. For high engine speeds the responsiveness can be improved also, but to a smaller extent.

The CV air mass affects the performance improvement in two ways: In addition to an instantaneously higher torque, the exhaust enthalpy flow is substantially increased, which leads to a much faster turbocharger acceleration. As a result, the duration of the air injection is reduced such that only little pressurized air is used.

Instantaneous torque

Aside from the time to reach the maximum torque, the instantaneously reachable torque is of interest. It corresponds to the torque that is produced by the sum of the naturally aspirated full load air mass (waste gate open) and the CV air mass at a given engine speed. In Figure 3.6 the in-

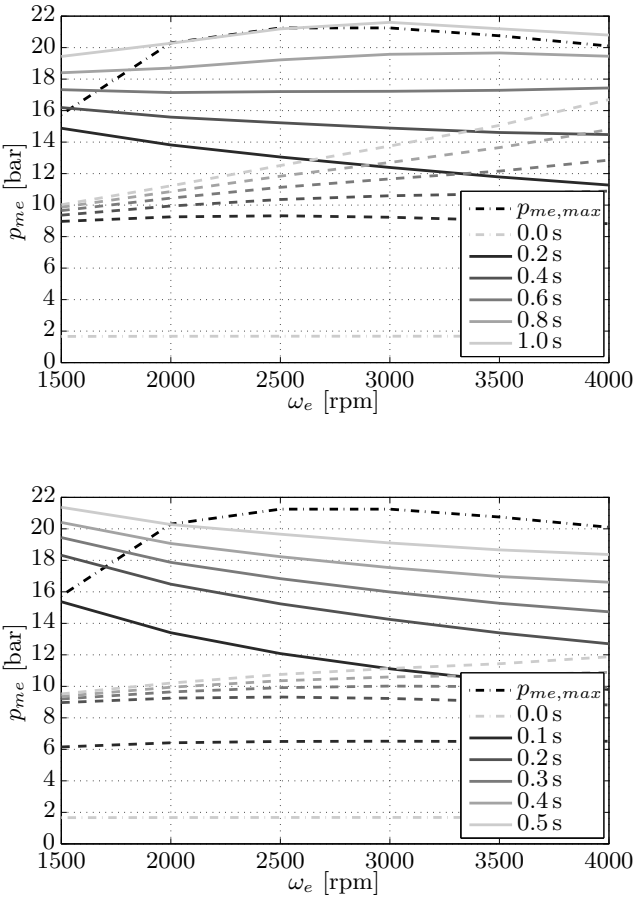

Figure 3.6.: Torque build-up at constant engine speeds: Dashed lines show the performance of the TC SI engine without boost, solid lines depict the performance with boost. Gray dash-dot line indicates engine torque before throttle step and boost mode activation. Upper plot: $\mu_{CV} = 34.9\,\mathrm{g/s}$: $m_{CV} = 0.167\,\mathrm{g}$ at 2000 rpm. Lower plot: $\mu_{CV} = 55\,\mathrm{g/s}$: $m_{CV} = 0.263\,\mathrm{g}$ at 2000 rpm. Note: The time interval between the various lines is smaller in the lower plot: $\Delta t = 0.1\,\mathrm{s}$.

stantaneous torque line corresponds to the line of $t \approx 0.2\,\mathrm{s}$ (due to throttle and intake manifold dynamics). It is noticeable how the instantaneously reachable torque decreases with increasing engine speed as a result of the smaller air mass admitted.

Overboost

At low engine speeds it is possible to overboost the engine, i.e., to temporarily obtain more than the maximum stationary torque. In that operating region the combustion is susceptible to knock. Increased turbulence due to air injection reduces this susceptibility [31]. In the simulation results presented in Figure 3.6 the knock limit is not considered. Hence, the torque values obtained are rather high.

3.2.2. Desired CV mass flow

As described above, the value of μ_{CV} significantly influences the dynamic behavior of the engine. The value of μ_{CV} can be found by formulating a benchmark torque response, i.e., the time $\Delta t_{step,des}$ to achieve a desired torque step from $p_{me,1}$ to $p_{me,2}$, at a given engine speed $\omega_{e,des}$ as illustrated in Figure 3.7. With the engine model and the chosen performance requirement, the value for $\mu_{CV,des}$ can be determined by using a simple solver since the problem is convex. Note: To determine $\mu_{CV,des}$ an MVM of a conventional TC SI engine is sufficient. Only the charge cooling constant needs to be identified.

Of course, the value of $\mu_{CV,des}$ cannot be chosen arbitrarily. It is subject to physical constraints, e.g., valve lift profile or CV diameter. These are discussed in the following section.

3.3. CV design

Whereas the previous section showed how the value of $\mu_{CV,des}$ can be determined on the basis of a performance requirement using a mean value model (MVM), this section describes how a desired value of μ_{CV} can be realized by an appropriate selection of the CV design variables. The CV mass models presented in Section 3.1.2 are used for this purpose. First, the relevant CV design variables are presented. Then, constraints are discussed. Finally, the dependencies of the CV design variables are shown.

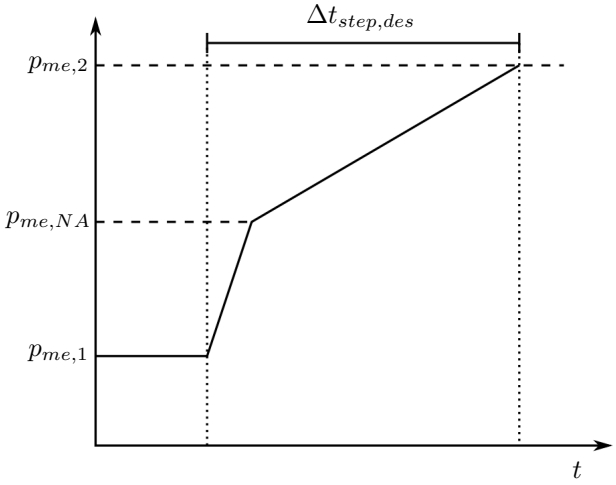

Figure 3.7.: Desired torque step at a constant engine speed $\omega_{e,des}$. The variable $p_{me,NA}$ denotes the torque at $p_{im} = 1\,\text{bar}$.

3.3.1. Relevant CV design variables

The relevant CV design variables are

$\phi_{CVO,b}$	CV opening angle;
$\phi_{CVC,b}$	CV closing angle;
$a_{CV,b}$	CV acceleration profile;
d_{CV}	CV diameter;
$\tilde{p}_{t,b}$	Minimum tank pressure.

The minimum tank pressure $\tilde{p}_{t,b}$ is considered in the following derivations. It is assumed that

$$p_t \geq \tilde{p}_{t,b} \tag{3.7}$$

which guarantees that $\Delta t_{step,des}$ is always reached. For a larger tank pressure an even smaller step time, $\Delta t_{step} < \Delta t_{step,des}$ can be achieved since the air mass transferred through the CV is larger due to its proportional dependence on the tank pressure.

The goal of the CV design process is to find values for the design variables which fulfill

$$\mu_{CV,des} = \frac{\tilde{p}_{t,b}}{\sqrt{R_a \cdot \vartheta_t}} \cdot \Psi_{crit} \cdot \int_{\phi_{CVO,b}}^{\phi_{CVC,b}} A_{eff}(y_{CV}(\phi, a_{CV,b}), d_{CV}) d\phi. \quad (3.8)$$

The derivation of the CV design variables is under-determined since there is one equation for five variables. Additional constraints reduce the feasible design space. In the following, the most important constraints are discussed.

3.3.2. Constraints

The constraints presented here generally hold for in-cylinder boosted SI engines and are independent of the model complexity.

Spatial constraint

Adding a CV to the cylinder head might reduce the area available for IVs and EVs. If the fitting of the CV requires the downsizing of the IVs and/or the EVs, the volumetric efficiency of the conventional combustion mode might be deteriorated, possibly reducing the peak power capability. However, depending on the cylinder head design the downsizing might not be necessary, resulting in an unaltered volumetric efficiency.

Valve timing constraint

The earliest opening of the CV is possible around IV closing (IVC). An overlap of several degrees is acceptable, but blowing charge out through the IVs has to be avoided because pressurized air is wasted. Hence, shifting IVC in favor of the CV opening has an impact on the gas exchange performance in the conventional combustion mode.

Safety constraint

Any flow of air/fuel mixture from the cylinder to the tank has to be avoided. Hence, throughout the opening period of the CV, the cylinder pressure p_{cyl} has to be smaller than or equal to the tank pressure.

$$p_{cyl}(\phi) \leq \tilde{p}_{t,b} \qquad \phi \in [\phi_{CVO,b}, \phi_{CVC,b}] \quad (3.9)$$

The maximum cylinder pressure in the interval $[\phi_{CVO,b}, \phi_{CVC,b}]$ is reached at CV closing and when the in-cylinder mass is maximal, i.e., equal to $m_{cyl,max}$. To avoid the flow of mixture to the tank in the entire operation range, the design has to fulfill the following constraint

$$\tilde{p}_{t,b} \geq f_s \cdot p_{cyl}(\phi_{CVC,b}) = f_s \cdot \frac{R_{cyl} \cdot \vartheta_{cyl}(\phi_{CVC,b})}{V_{cyl}(\phi_{CVC,b})} \cdot \underbrace{\frac{1}{x_a} \cdot \left(m_{\beta,max}(\omega_e^*) + \frac{\mu_{CV,des}}{\omega_e^*} \right)}_{m_{cyl,max}}, \tag{3.10}$$

where $\vartheta_{cyl}(\phi)$ is the temperature of the mixture in the cylinder, $V_{cyl}(\phi)$ is the cylinder volume at the crank angle ϕ and R_{cyl} is the gas constant of the mixture in the cylinder (air, fuel, residual gas). The dependency of R_{cyl} on the normalized air/fuel ratio at the time of ignition λ_c is small and therefore can be neglected. The variable $f_s \geq 1$ is an additional safety factor which accounts for variable uncertainties, e.g., temperature uncertainties at $\phi_{CVC,b}$. The variable $m_{\beta,max}$ is the maximum air mass from the intake manifold, ω_e^* is the engine speed for which the cylinder mass is maximal and x_a is the air mass fraction. Their derivations are presented in Appendix B.3.

Note that Equation (3.10) relates the minimum tank pressure to the CV closing and provides its upper boundary. The higher the tank pressure is, the later the CV can be closed. This safety constraint holds for PFI as well as for direct-injection engines if the fuel injection duration and mixture formation require the fuel injection to start before the CV is closed.

To relax the requirements on the spatial constraints and to reduce the compression work, it is recommended to choose the CV closing angle at its maximum value. Hence, for a larger minimum tank pressure the CV can close later, and vice versa.

For $p_t > \tilde{p}_{t,b}$, more air is admitted through the CV and, thus, the cylinder pressure at CV closing $p_{cyl}(\phi_{CVC,b})$ increases. Since this increase is smaller than the increase of the tank pressure, no mixture flows to the tank. Hence, if Equation (3.10) is fulfilled for $p_t = \tilde{p}_{t,b}$, it is fulfilled for all $p_t \geq \tilde{p}_{t,b}$. The proof of this statement is given in Appendix B.4.

Mechanical constraints on the lift profile

Camshaft driven valves have a fixed acceleration and jerk profile in the crank angle domain [32]. Stress limitations apply in the time domain. Thus, the maximum engine speed determines the limits for the acceleration in the CA domain. Since the turbo lag is more of an issue at low engine speeds and the admitted air mass decreases with increasing engine speed, the use of the boost mode is neither effective nor necessary at high engine speeds. By allowing the activation of the boost mode only up to $\omega_{e,b} < \omega_{e,max}$, the CV acceleration in the CA domain can be increased. Its maximum value is

$$a_{CV,b} = \frac{d^2 y_{CV}(\phi)}{d\phi^2} = \frac{\ddot{y}_{CV,max}}{\omega_{e,b}^2}, \tag{3.11}$$

where $\ddot{y}_{CV,max}$ is the maximum valve acceleration in the time domain. Furthermore, the large pressure difference across the CV, the CV diameter, the CV opening duration and the maximum boost speed $\omega_{e,b}$ influence the valve spring design, which is discussed in Appendix B.5.

Multi-functionality

Additional constraints on the CV design parameters may arise if additional engine modes are to be realized. For instance if the tank is filled by operating the engine as an air compressor, the CV diameter might need to be larger than a minimum value to achieve an acceptable filling performance. In case boosting is applied as part of an AA TC SI engine or an HPE, other engine modes may cause additional constraints on the CV design parameters, e.g., minimum tank pressure to realize a rapid pneumatic engine start [9, 13]. In Section 7.1 a system design methodology is presented which considers all engine modes of an AA TC SI engine.
Note that the CV diameter is common to all modes.

3.3.3. CV design variable dependencies

In the design process it is desirable to know how the different variables influence each other. Every feasible combination of CV variables has to fulfill Equations (3.8) and (3.10). In this section, the dependencies of the variables are evaluated analytically and numerically.

Analytic solution

With the simplified lift profile and the linear approximation of the flow coefficient given in Equation (3.6), the integral in Equation (3.8) can be evaluated analytically. The resulting expression for the desired CV mass flow becomes

$$\begin{aligned}\mu_{CV,des} =& \mu\sigma_{CV,lin} \cdot a_{CV,b} \cdot \frac{(\phi_{CVC,b} - \phi_{CVO,b})^3}{32} \\ & \cdot \frac{\pi \cdot d_{CV}}{4} \cdot \frac{\tilde{p}_{t,b}}{\sqrt{R_a \cdot \vartheta_t}} \cdot \Psi_{crit}.\end{aligned} \tag{3.12}$$

This relation holds for the design subspace in which the maximum lift is smaller than 11% of the CV diameter (area of validity of the linear approximation of $\mu\sigma_{CV}$).

For a constant value of $\mu_{CV,des}$ the following holds:

- An increased valve acceleration allows the CV diameter to be decreased.
- An earlier CV opening allows a considerable decrease of the CV diameter since $\phi_{CVC,b} - \phi_{CVO,b}$ is cubic in Equation (3.12). The sensitivity can be expressed as

  $$S_{dCV,CVO} = \frac{\partial d_{CV}/d_{CV}}{\partial \phi_{CVO,b}/\phi_{CVO,b}} = \frac{3 \cdot \phi_{CVO,b}}{\phi_{CVC,b} - \phi_{CVO,b}}. \tag{3.13}$$

  Especially for a late CV opening the sensitivity is very high: For $\phi_{CVC,b} = 110\,°\text{CA}$ and $\phi_{CVO,b} = 60\,°\text{CA}$, advancing the CV opening by 1 °CA leads to a decrease of the CV diameter by 6% and of the area by 11.6%.
- An increase of the minimum tank pressure allows a decrease of the CV diameter. Note that if the tank pressure is increased $\phi_{CVC,b}$ could also be increased (which results from the flow-to-tank constraint given in Equation (3.10)). Hence, the reduction of the CV diameter could be even larger.

Numeric solution

Since the linear approximation of the flow coefficient holds in a limited range only, the solutions over a wide design range are obtained by numerical evaluation of the integral term. For these investigations the CV

Table 3.1.: Parameter values used for the numerical evaluation.

Variable	value	unit
$\mu_{CV,des}$	34.9	g/s
$a_{CV,b}$	0.004	mm/°CA²
ω_e^*	2500	rpm
$m_{\beta,max}(\omega_e^*)$	0.83	g
$\vartheta_{cyl}(\phi_{CVC,b})$	360	K
ϑ_t	330 [1]	K
R_a	287	J/kg K
R_{cyl}	273.5	J/kg K
x_a	0.84	
f_s	1.1	

acceleration is set to be constant. Table 3.1 lists the parameter values chosen for this evaluation.

Figure 3.8 shows that the latest CV closing angle increases with increasing tank pressure. This relationship results from Equation (3.10). Figure 3.9 depicts the resulting diameter for various CV openings and tank pressures. The CV closing is always set to its maximum value according to Equation (3.10).

The following conclusions can be drawn:

- A low tank pressure requires a large CV diameter;
- A late CV opening also results in a large CV diameter. The limited time for the mass exchange has to be compensated by a larger flow area;
- CV diameters smaller than 10 mm can be realized.

[1] The temperature in the air tank is equal to the ambient temperature since an uninsulated tank is considered to reduce the susceptibility to engine knocking. The temperature of the injected air ϑ_t is increased due to heat transfer from the engine block ($\vartheta_e \approx 353\,\mathrm{K}$) and the warm CV pipe. At the test bench, $\vartheta_t = 330\,\mathrm{K}$ is typically measured. In general, the value of ϑ_t mainly depends on the routing of the CV pipe, i.e., if the air enters on the intake side the temperature is lower than if it enters on the exhaust side.

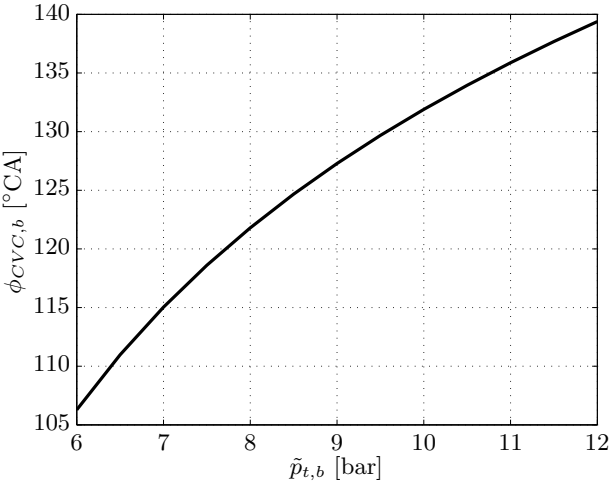

Figure 3.8.: CV closing $\phi_{CVC,b}$ as a function of the design tank pressure $\tilde{p}_{t,b}$.

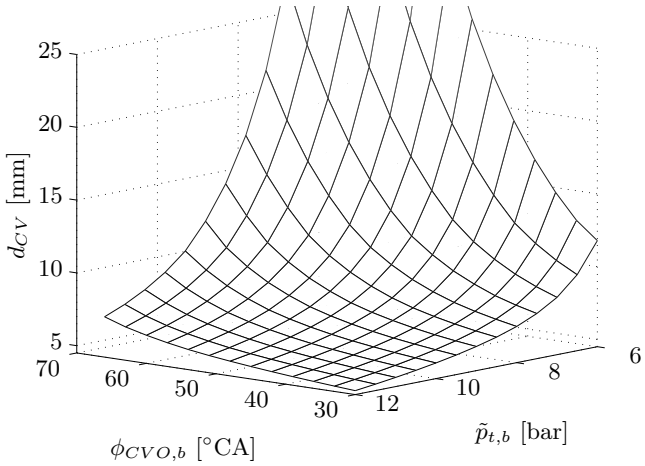

Figure 3.9.: CV diameter d_{CV} as a function of design tank pressure $\tilde{p}_{t,b}$ and CV opening angle $\phi_{CVO,b}$.

3.4. Design example

The goal is to find values for the CV design variables which fulfill the following specifications:

- At $\omega_e = 2000\,\text{rpm}$, full load has to be reached within 1 s. Therefore, the performance specifications are: $\Delta t_{step} = 1\,\text{s}$, $\omega_{e,des} = 2000\,\text{rpm}$, $p_{me,1} = 1.7\,\text{bar}$, $p_{me,2} = 20.3\,\text{bar}$.
- The CV diameter has to be minimal.
- The IV closing is at $\phi_{IVC} = 42\,^\circ\text{CA}$.
- The maximum CV acceleration in the crank angle domain is $a_{CV,b} = 0.004\,\text{mm}/^\circ\text{CA}^2$.
- The minimum tank pressure is $\tilde{p}_{t,b} = 8\,\text{bar}$.
- The engine parameters are those listed in Appendix A.
- The values in the bottom section of Table 3.1 are used.

Design process

1. Find the desired CV mass flow $\mu_{CV,des}$ by means of the mean value model: $\mu_{CV,des} = 34.9\,\text{g/s}$.
2. Determine the engine speed ω_e^* for which the cylinder air mass is maximal using Equation (B.3): $\omega_e^* = 2500\,\text{rpm}$ and calculate the corresponding maximum cylinder mass $m_{cyl,max} = 1.15\,\text{g}$
3. Find the limit of $\tilde{p}_{t,b} \cdot V(\phi_{CVC,b})$ with Equation (3.10): $\tilde{p}_{t,b} \cdot V(\phi_{CVC,b}) = 124.1\,\text{J}$.
4. Find $\phi_{CVC,b}$ for $\tilde{p}_{t,b} = 8\,\text{bar}$ using the data of the engine geometry and the value of $\tilde{p}_{t,b} \cdot V(\phi_{CVC,b}) \rightarrow \phi_{CVC,b} = 122.0\,^\circ\text{CA}$.
5. The sensitivity analysis yields the result that for a minimum CV diameter the CV has to open as early as possible $\rightarrow \phi_{CVO,b} = \phi_{IVC} = 42\,^\circ\text{CA}$.
6. The CV diameter can be found by solving Equation (3.8) with the values known for the other variables $\rightarrow d_{CV} = 8.5\,\text{mm}$.

Hence, the following set of values for the design variables fulfills the desired performance criterion, all specifications and all constraints:

$$\begin{array}{lll} \phi_{CVO,b} & = 42.0 & ^\circ\text{CA} \\ \phi_{CVC,b} & = 122.0 & ^\circ\text{CA} \\ a_{CV,b} & = 0.004 & \text{mm}/^\circ\text{CA}^2 \\ d_{CV} & = 8.5 & \text{mm} \\ \tilde{p}_{t,b} & = 8.0 & \text{bar.} \end{array}$$

Alternative CV realizations with equal $\mu_{CV,des}$

Table 3.2 lists the values of the design example with three alternative realizations which have the same CV mass flow $\mu_{CV,des}$. Alternative 1 has a smaller minimum tank pressure. However, the required CV diameter is significantly larger. By opening the CV substantially earlier the CV diameter can be reduced again while still having a small minimum tank pressure as shown in Alternative 2. Engines equipped with variable intake valve timing can be used to achieve such early IVCs. The values for the CV diameter and the IVC in Alternative 3 correspond to those of the test bench engine (see Appendix A), i.e., a very late IVC and a large CV diameter.

Table 3.2.: CV realizations for $\mu_{CV,des} = 34.9\,\text{g/s}$.

Variable	unit	example	alt. 1	alt. 2	alt. 3
$\phi_{CVO,b}$	°CA	42.0	42.0	15.0	66.0
$\phi_{CVC,b}$	°CA	122.0	106.3	106.3	123.8
$a_{CV,b}$	$\text{mm}/^\circ\text{CA}^2$	0.004	0.004	0.004	0.004
d_{CV}	mm	8.5	19.2	8.5	19.0
$\tilde{p}_{t,b}$	bar	8.0	6.0	6.0	8.3

3.5. Conclusion

By using a mean value model adapted for in-cylinder boosting, the injection of air through a CSD CV significantly improves the response characteristics at low engine speeds. The mass transferred through the CV is proportional to the tank pressure and the CV size, and inversely proportional to the engine speed.

In the model-based design framework presented, all relevant limitations such as mixture flow to the tank, spatial limitations and mechanical limitations on the lift profile are discussed. The design is linked to the most important characteristic of the concept, namely the performance during transients. With this framework it is possible to design the CV for any AA TC SI engine. The sensitivities of the CV design variables $\{\phi_{CVO,b}$, $\phi_{CVC,b}$, $a_{CV,b}$, d_{CV}, $\tilde{p}_{t,b}\}$ are presented and a design example is given which is applicable to arbitrary engines.

In this chapter the focus was on the CV design. In the following chapter control issues are discussed and control strategies are presented. Their performance is studied in simulation and verified by experiments.

4. In-Cylinder Boosting: Control

In the previous chapter it was shown that in-cylinder boosting substantially improves the speed of the torque build-up, which is a measure for the driveability. In addition to the speed of the torque build-up, the driveability is also influenced by the conditions for which the boost mode is activated, e.g., a torque value requested or a gradient of a torque request. Various driving styles can be mapped by the formulation of these conditions, which is up to the OEM and is not discussed any further in this chapter.

This chapter focuses on the torque control once the decision to activate boosting is taken. The major challenge of the control is that the CV air mass can only take on the values zero or m_{CV}. Hence, the activation or deactivation of the boost mode always leads to a step in the cylinder air mass. Appropriate control actions of the throttle and the ignition timing are necessary to achieve a smooth torque response, especially in the transition back from boosted to conventional combustion. The control strategies presented aim at maximizing the driveability and the driver comfort while keeping space requirements of the pressure tank at a minimum since packaging is a major concern. Accordingly, the main objective of this chapter is the derivation of a control strategy for the throttle, the ignition timing and the boost mode timing during the turbo lag compensation that is applicable in practice.

The chapter is structured as follows: In Section 4.1, the relevant models are discussed. Section 4.2 presents the control problem formulation. In Section 4.3, the control problem is solved by numerical optimization. In Section 4.4, the optimization results are used to derive a structure for a causal controller. The controller settings are varied to analyze the tradeoff between the consumption of fuel and pressurized air. A minimal-air control strategy is derived and analyzed for several torque steps at various engine speeds. Section 4.5 shows the experimental verification of the predicted performance of the causal control strategy on an engine test bench for various operating conditions. In Section 4.6 the sensitivity of the air consumption to the tank pressure is analyzed. The conclusions are described in Section 4.7.

4.1. Model and system parameterization

In the following, various control strategies are derived which will be analyzed in simulation using the mean value model (MVM) presented in the previous chapter.

Here, only the engine torque model is presented in more detail since it is used for the controller design. According to the Willans approximation [29], the brake mean effective pressure p_{me} for stoichiometric conditions is calculated by

$$\begin{aligned} p_{me} &= e_{\omega} \cdot e_{ign}(u_{ign}) \cdot \frac{H_l \cdot N_{cyl}}{V_d \cdot \sigma_0} \cdot (m_{\beta} + m_{CV}) - p_{me0}, \\ &= k_e \cdot e_{ign}(u_{ign}) \cdot (m_{\beta} + m_{CV}) - p_{me0}, \end{aligned} \tag{4.1}$$

where e_{ω} is an engine speed dependent efficiency term, e_{ign} is an ignition dependent efficiency term and p_{me0} accounts for pumping and friction losses. The variable u_{ign} is the ignition time offset towards late from its maximum brake torque (MBT) value.

Ignition efficiency

The ignition efficiency e_{ign} is set by the spark timing. According to [29], the following relation between the ignition efficiency and the spark timing u_{ign} is valid

$$e_{ign}(u_{ign}) = 1 - k_{ign} \cdot u_{ign}^2 \leq 1, \qquad u_{ign} \leq 0, \tag{4.2}$$

where, in a first approximation, k_{ign} is independent of the operation point [33]. A measurement based identification of k_{ign} is necessary. For $u_{ign} = 0$, it is assumed that the ignition timing is optimal, i.e., that it yields the maximum brake torque.

Desired air mass

The variable $m_{a,des}$ is defined as the amount of air per cylinder which is required to generate the desired torque $p_{me,des}$ for stoichiometric conditions and optimal ignition timing ($e_{ign} = 1$)

$$m_{a,des} = \frac{p_{me,des} + p_{me0}}{k_e}. \tag{4.3}$$

System parameterization

In this chapter the CV mass flow is chosen to be $\mu_{CV} = 34.9\,\mathrm{g/s}$. In the previous chapter, it was shown that this value is a reasonable choice for the engine described in Appendix A.

4.2. System description and control problem formulation

The objective of the turbo lag compensation controller is to track a reference value of the torque by a coordinated control action of the engine actuators. The torque request originates from a vehicle subsystem or the driver [34]. It can be controlled by the amount of fresh charge admitted to the cylinder and by the spark timing. For the control, three actuators are considered, namely

- the throttle plate position u_{th}: It can lead to an increase or decrease of the torque within several engine cycles due to the intake manifold and TC dynamics;
- the ignition timing u_{ign}: It can only decrease the torque but within one engine cycle;
- the boost mode activation u_{CV}: It always leads to a torque increase within just one engine cycle.

Table 4.1 summarizes the properties of each actuator.

Table 4.1.: Torque actuators and their properties.

Actuator	bandwidth $u_i \to p_{me}$	time constant in no. of cycles	torque	relevant dynamics
u_{th}	medium	several	$\updownarrow$	intake TC
u_{ign}	high	1	$\downarrow$	-
u_{CV}	high	1	$\uparrow$	-

The turbine actuator, e.g., waste gate or variable nozzle turbine, is not considered here since it is usually much slower than the actuators listed above. Since boosting is very transient only fast actuators can be used

for the control. The engine considered is equipped with a slow waste gate actuator. Therefore it is assumed that the waste gate is closed during the transients to enable a fast torque build-up.

The effects of the boost mode activation and the retarding of the spark timing are complementary. Their coordinated actuation allows for a high bandwidth of the torque control. It can be used to compensate for the slower dynamics of the intake manifold and the TC speed. The high bandwidth comes at a price. Retarding the spark timing decreases the engine efficiency. In addition, boosting the engine requires pressurized air, which is limited.

4.2.1. Control problem

According to [35], when tipping in, the driver expects good driveability and comfort. In this subsection, the control problem of the turbo lag compensation is presented by formulating these driver expectations as mathematical constraints. For this purpose, the illustration given in Figure 4.1 is used.

Driveability

Good driveability is characterized by as much torque as possible as fast as possible. Hence, the torque request has to be met in minimum time t_{step}. This goal is achieved if the boost mode is activated and the throttle is fully opened, i.e., the exhaust enthalpy and consequently the TC acceleration are maximized.

Figure 4.1 schematically shows the effect of activating the boost mode and opening the throttle at t_{tip-in} as well as how the air mass in the cylinder m_a suddenly increases and with it the torque. As a result of the increasing TC speed the intake manifold pressure and, thus, the intake air mass increase.

Comfort

In addition to a fast torque build-up, the driver wants a smooth and predictable torque development when tipping in, i.e., the torque trajectory has to remain constant once the desired torque is reached at t_{step},

$$p_{me}(t) = p_{me,des}(t) \quad t \geq t_{step}. \tag{4.4}$$

Consequently, the boost mode cannot be switched off immediately after the desired torque is reached because it would lead to a drop of the air

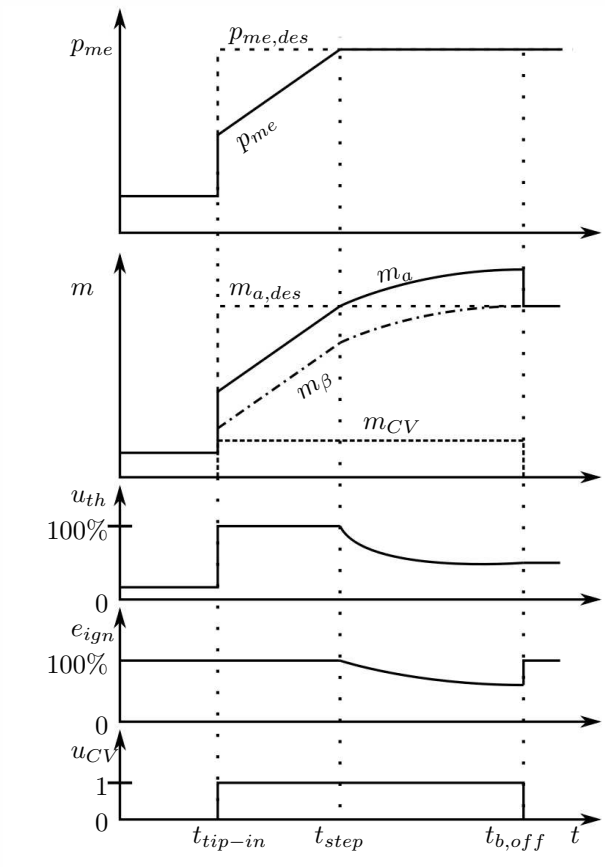

Figure 4.1.: Schematic representation of the torque control inputs during a transient with turbo lag compensation.

mass in the cylinder below the desired value $m_{a,des}$ and, hence, to a drop of the torque. Consequently, the boost mode remains active for $t \geq t_{step}$ which results in excessive charge in the cylinder: $m_a > m_{a,des}$. To keep the torque at the desired level, the spark timing has to be retarded. Consequently, the ignition efficiency decreases.

Accordingly, to avoid a drop of the torque, the deactivation of the boost mode must occur when the intake air mass is equal to the desired air mass

at $t_{b,off}$:

$$m_\beta(t_{b,off}) = m_{a,des}(t_{b,off}). \tag{4.5}$$

At the same instant, the spark timing has to be reset to MBT, i.e., $e_{ign} = 1$, since no more excess charge is in the combustion chamber.

Note that for $t_{step} \leq t \leq t_{b,off}$, the torque control is not unique because there is a single condition, $p_{me} = p_{me,des}$, for two degrees of freedom, namely the spark timing, which affects the ignition efficiency term $e_{ign}(u_{ign}) \leq 1$ and the intake air mass m_β, which is mainly a function of the throttle position.

4.2.2. Ignition control

The high bandwidth of the ignition allows the adjustment of the ignition timing once the intake air mass and the CV mass in the cylinder are known. If there is excessive charge in the cylinder, the ignition efficiency has to be decreased. The desired value of the ignition efficiency is

$$e_{ign,des}(t) = \min\left\{\frac{m_{a,des}(t)}{m_\beta(t) + m_{CV}}, 1\right\}. \tag{4.6}$$

This relation is derived from Equations (4.1) and (4.3). The desired ignition efficiency can be realized by retarding the spark timing according to

$$u_{ign} = -\sqrt{\frac{1 - e_{ign,des}}{k_{ign}}}. \tag{4.7}$$

By assuming that the ignition timing is always adjusted according to the formulation given in Equation (4.6), the condition given in Equation (4.4) can be reformulated to:

$$m_\beta(t) \geq m_{a,des}(t) - m_{CV} \quad t \geq t_{step}. \tag{4.8}$$

4.2.3. Controller structure

The resulting controller structure contains three controllers as shown in Figure 4.2. The boost controller is the main controller. It controls the boost mode activation and deactivation, and it determines the desired ignition efficiency $e_{ign,des}$ and the desired intake air mass $m_{\beta,des}$ based on the desired torque and the estimated intake air mass. The desired values are then realized by two independent controllers: a slow throttle controller and a fast ignition controller.

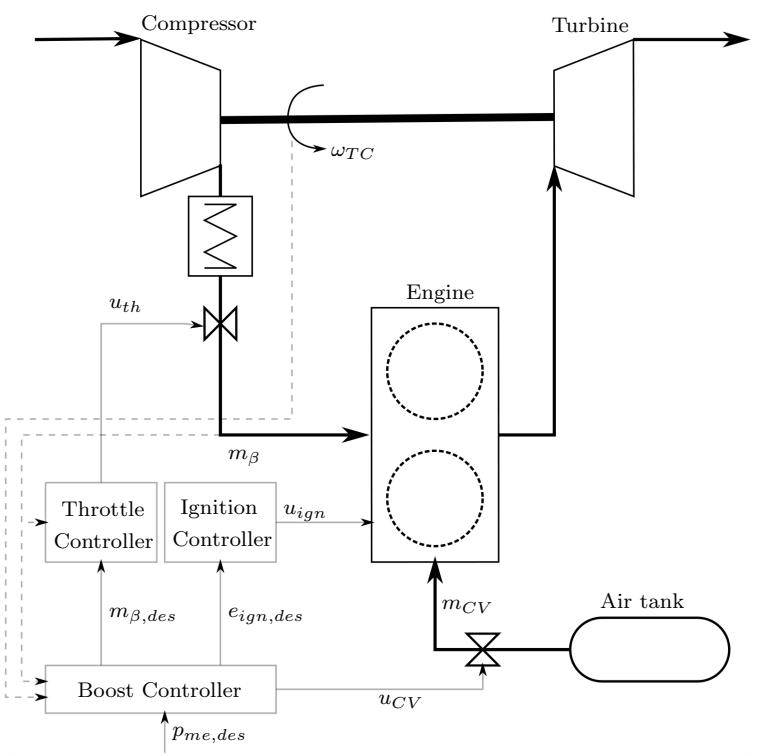

Figure 4.2.: Control architecture overview.

The only constraint on the slower throttle actuation is given in Equation (4.8). Apart from that, it can be arbitrarily chosen:
One possibility is to keep the throttle open. Due to the resulting charge excess the spark timing must be retarded. Consequently, the efficiency decreases but the exhaust enthalpy is increased.
Another possibility is to reduce the intake manifold pressure in order to reduce the amount of excess charge and, thus, to avoid retarding the spark timing. However, the exhaust enthalpy and the TC acceleration are lower.

In the following section the throttle actuation is studied in an optimal control framework. The objective of the optimal throttle actuation is to minimize the consumption of pressurized air and extra fuel due to a retarded spark timing.

4.2.4. Limitations

The operating range of the boost mode is limited by several constraints. The most important ones are discussed below.

Minimum ignition efficiency

The ignition efficiency cannot be reduced to arbitrary values. A too late ignition leads to an unstable combustion or can cause misfire. Furthermore, a late ignition results in high exhaust temperatures, which might damage the turbine. Thus, a lower limit exists for the ignition efficiency

$$e_{ign} \geq e_{ign,min}. \tag{4.9}$$

The value of the minimum ignition efficiency typically amounts to $e_{ign,min} = 0.66$. Using Equations (4.1) and (4.6) the above condition can be transformed to

$$\frac{p_{me,min} + p_{me0}}{k_e} = \frac{e_{ign,min}}{1 - e_{ign,min}} \cdot m_{CV} = \frac{e_{ign,min}}{1 - e_{ign,min}} \cdot \frac{\mu_{CV,p}}{\omega_e} \cdot p_t. \tag{4.10}$$

Consequently, a lower torque limit $p_{me,min}$ exists for which a smooth transition is possible. The lower torque limit depends on the CV size $\mu_{CV,p}$ and on the operating point. For a larger CV or a higher tank pressure the lower torque limit is higher. The opposite holds for a higher engine speed. Figure 4.3 shows the values of the lower torque limit in various operating points for a valve size of $\mu_{CV,p} = 5.82\,\mathrm{g/sbar}$ ($m_{CV} = 0.167\,\mathrm{g}$ at $p_t = 6\,\mathrm{bar}$ and $\omega_e = 2000\,\mathrm{rpm}$). The thick line approximates the NA full load curve.

Minimum intake air mass for boosting

In a SI PFI engine, the intake air mass transports the fuel into the cylinder. The amount of fuel transported is limited though. Assuming a stoichiometric combustion, this limitation can be formulated as a minimum normalized air/fuel ratio in the intake port

$$\lambda_{ip} = \frac{m_\beta(t)}{m_{CV} + m_\beta(t)} \geq \lambda_{ip,min}. \tag{4.11}$$

Consequently, boosting cannot be activated before the intake mass has reached the following value

$$m_\beta(t) \geq \frac{\lambda_{ip,min}}{1 - \lambda_{ip,min}} \cdot m_{CV} = \frac{\lambda_{ip,min}}{1 - \lambda_{ip,min}} \cdot \frac{\mu_{CV,p}}{\omega_e} \cdot p_t. \tag{4.12}$$

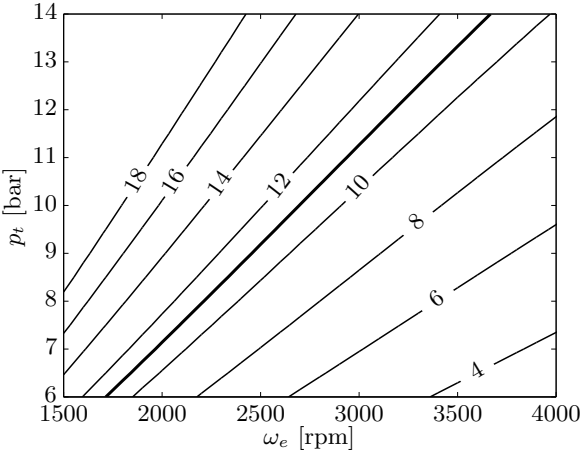

Figure 4.3.: Lower torque limit $p_{me,min}$ as a function of the engine speed and the tank pressure for the constant valve size $\mu_{CV,p} = 5.82\,{}^{\mathrm{g}}/_{\mathrm{sbar}}$ and $e_{ign,min} = 0.66$: $m_{CV} = 0.167\,\mathrm{g}$ at $p_t = 6\,\mathrm{bar}$ and $\omega_e = 2000\,\mathrm{rpm}$.

The boost mode activation instant depends on the CV size $\mu_{CV,p}$ and on the operating point. For a larger CV and a higher tank pressure the required intake air mass increases. The opposite holds for a higher engine speed. The minimum normalized air/fuel ratio in the intake port typically is $\lambda_{ip,min} = 0.25$.

4.3. Optimal control strategy

As stated above, the optimal throttle actuation for the phase $t \in [t_{step}, t_{b,off}]$ has to minimize the weighted sum of pressurized air used Δm_{CV} and extra fuel mass used $m_{f,b}$, which results from retarding the spark timing.

The optimal control problem formulation is

$$\min_{u_{th}:\,[t_{step},\,t_{b,off}]\;\in\;[0,\;100\%]} \quad \frac{1}{\sigma_0} \cdot \Delta m_{CV} + w \cdot m_{f,b} \tag{4.13}$$

subject to

$$m_\beta(t) \;\geq\; m_{a,des}(t) - m_{CV} \tag{4.14}$$

$$m_\beta(t_{b,off}) \;=\; m_{a,des}(t_{b,off}), \tag{4.15}$$

where w is a weighting factor. The deactivation instant of the boost mode $t_{b,off}$ is free. The amount of pressurized air is normalized with σ_0 in order to bring the cost terms to the same order of magnitude.
The time duration of the optimal solution lasts

$$\Delta t_{b,opt} = t_{b,off} - t_{step}. \tag{4.16}$$

The amount of pressurized air used is

$$\Delta m_{CV} = \frac{N_{cyl}}{4 \cdot \pi} \cdot \mu_{CV} \cdot \Delta t_{b,opt}. \tag{4.17}$$

The amount of extra fuel used is [1]

$$m_{f,b} = \frac{\omega_e \cdot N_{cyl}}{4 \cdot \pi \cdot \sigma_0} \cdot \int_{t_{step}}^{t_{b,off}} \max\{m_\beta(t) + m_{CV} - m_{a,des}(t), 0\} dt. \tag{4.18}$$

4.3.1. Numerical optimization

The optimal throttle profile is found by a direct numerical optimization with single shooting. The throttle profile is discretized in time. The values of the throttle profile are constant on each time interval and they are the parameters subject to optimization. The value of the cost function is determined by simulating the MVM for a given throttle profile. The constrained nonlinear problem is solved using a gradient-based method.

Note that the torque build-up phase, where the throttle is wide open and the boost mode is active, is not part of the optimization. As soon as the torque request is fulfilled for the first time, i.e., $p_{me} = p_{me,des}$, the optimized throttle profile starts to be applied. The simulation is stopped once the final condition of Equation (4.15) is fulfilled.

4.3.2. Results and discussion

Figures 4.4 and 4.5 show the optimization results for two different weighting factors for a torque step from 1.7 bar to 16.7 bar at an engine speed of $\omega_e = 2000$ rpm. Table 4.2 lists the resulting costs, the values of the total turbo lag compensation time Δt_b and of the total pressurized air mass used $m_{a,b}$. Furthermore, the duration with retarded spark timing Δt_{spd} is given. The variable $V_{t,b}$ denotes the tank volume which $m_{a,b}$ occupies

[1] Only the effect of the retarded spark timing is considered. Simulations have shown that other effects, e.g., increased pumping losses due to throttling, are second order effects and, thus, have a negligible influence on the amount of extra fuel.

at a tank pressure of 8 bar and a tank temperature of 330 °K. These values are taken from Chapter 3 and are typical for the engine used in the model.

Table 4.2.: Optimal costs for $w = 2$ and $w = 6$.

w [−]	$m^o_{f,b}$ [mg]	Δm^o_{CV} [g]	$\Delta t^o_{b,opt}$ [s]	$m_{a,b}$ [g]	$V_{t,b}$ [l]	Δt_b [s]	Δt_{spd} [s]
2	64.68	2.84	0.51	5.46	0.65	1.04	0.31
6	44.92	3.62	0.65	6.24	0.74	1.18	0.20

Figure 4.4 shows the results for a weighting factor of $w = 2$. Besides the optimal throttle and ignition efficiency trajectories, the actual throttle position α_{th}, the steady-state TC speed for the desired torque $\omega_{TC,des} = \omega_{TC}(p_{me,des})$, the intake manifold pressure p_{im} and the pressure after the compressor p_{aC} are depicted.
At $t = 0\,\text{s}$, the boost mode is activated and the throttle is fully opened. As a result, the torque increases. Once the desired torque is reached, the optimal throttle profile is applied. It is noticeable that the optimal solution consists of two intervals:

Interval I: Throttling Between $0.53\,\text{s} \leq t \leq 0.73\,\text{s}$, the intake air mass is reduced to $m_{a,des}(t) - m_{CV}$ by throttling. Consequently, there is no need to retard the spark timing.

Interval II: Wide open throttle After $t = 0.73\,\text{s}$, the throttle is wide open (WOT). The intake air mass increases and the spark timing must be retarded. This leads to a substantial increase in exhaust enthalpy and, hence, to an increased TC acceleration. At $t = 1.04\,\text{s}$, the final condition in Equation (4.15) is met, and the simulation is stopped.

Figure 4.5 shows the results for a weighting factor of $w = 6$, i.e., the case where the extra fuel consumption is penalized more severely. Since the weighting factor does not affect the time which is necessary to reach the desired torque, all trajectories are equal up to that instant. Thereafter, a different throttle profile is applied. The optimal solution also consists of these two intervals, throttling and WOT. However, the throttle is opened later and the final condition is reached later. Consequently, the amount of pressurized air increases while the duration with a retarded spark timing and, thus, the amount of extra fuel decrease.

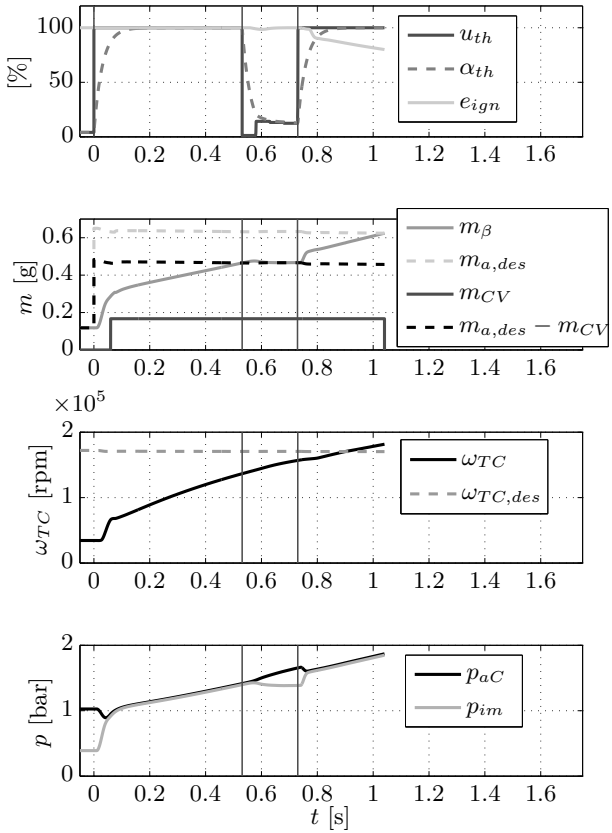

Figure 4.4.: Simulated turbo lag compensation for $w = 2$: Torque step from 1.7 bar to 16.7 bar at 2000 rpm: α_{th} is the actual throttle position.

These results confirm that the amount of extra fuel consumed decreases at the expense of a higher air consumption. Further simulations have shown that the optimal torque control generally consists of these two characteristic intervals, independently of the demanded torque increase, the engine speed, the CV design and the engine size.

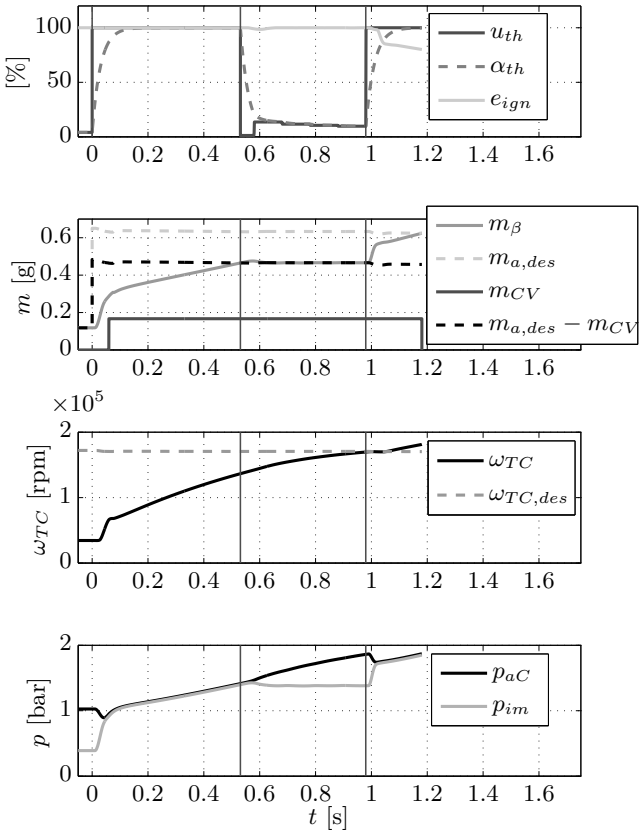

Figure 4.5.: Simulated turbo lag compensation for $w = 6$: Torque step from 1.7 bar to 16.7 bar at 2000 rpm.

4.4. Causal control strategy

Due to its complexity, model dependence and lack of robustness, the optimal feedforward throttle control law is not applicable in practice. In this section, a causal throttle control strategy is derived based on the optimization results which can be applied for various torque steps and engine speeds. Its performance is analyzed in simulation with respect to the consumption of air and extra fuel.

In most vehicles, torque measurement data are not available. Hence, an air mass based throttle control strategy is proposed. A precise torque model is required to achieve a good torque tracking performance. Note that the control law applied for the ignition timing given in Equation (4.6) is also air mass based.

The causal throttle control is realized by a gain-scheduled PI feedback controller with a feedforward part and anti-reset windup. Its goal is to eliminate the difference between the desired value of $m_{\beta,des}$ and the current intake air mass m_β. The same throttle controller is also used for the torque control if no turbo lag compensation is realized. Consequently, the integration of the new controller in the overall control structure is simple. The controller architecture is depicted in Figure 4.2.

To account for the two intervals found by the optimization, the value for the desired intake air mass is changed between two different setpoint values:

1. The main objective in the first phase is to accelerate the TC while avoiding an efficiency decrease. It combines the results of the torque build-up part and the interval I of the optimization problem. The desired intake air mass is chosen as

$$m_{\beta,des}(t) = m_{a,des}(t) - m_{CV}. \tag{4.19}$$

2. In the second phase, the objective is to realize a fast TC acceleration in order to minimize the duration with retarded spark timing. This phase corresponds to the WOT interval in the optimization. The desired intake air mass is chosen to be

$$m_{\beta,des}(t) = m_{a,des}(t). \tag{4.20}$$

Phase transition: The previous section showed that the switch to the WOT interval depends on the weighting factor. This characteristic is transformed to a TC speed dependent condition because the TC speed is the slowest of the system dynamics. Accordingly, the first phase with the smaller setpoint value is active as long as the TC speed $\omega_{TC}(t)$ is lower than the desired TC speed $\omega_{TC,des}(t)$ times a threshold value c_{thr}

$$\omega_{TC}(t) < c_{thr} \cdot \omega_{TC,des}(t). \tag{4.21}$$

The TC speed can be either measured with a TC speed sensor or estimated with an observer [36].

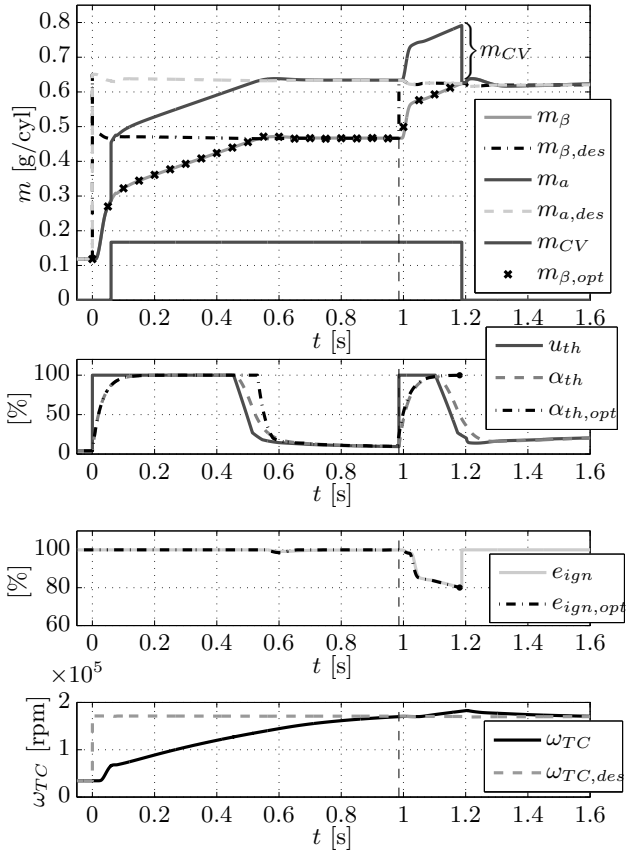

Figure 4.6.: Simulated turbo lag compensation with the causal control strategy for $c_{thr} = 0.99$: Torque step from 1.7 bar to 16.7 bar at 2000 rpm.

4.4.1. Results and discussion

The performance of the causal throttle controller in a torque step from 1.7 bar to 16.7 bar at 2000 rpm is studied in simulation for two different threshold values. Figures 4.6 and 4.7 show the resulting trajectories.

Figure 4.6 shows the performance for a threshold value of $c_{thr} = 0.99$. This corresponds to the optimization case with $w = 6$. As opposed to the optimal throttle actuation $\alpha_{th,opt}$, the throttle closes slightly before the total cylinder air mass m_a reaches the desired value $m_{a,des}$ in order

to keep the intake air mass on the desired value. During the throttling phase the throttle controller precisely tracks the desired intake air mass $m_{\beta,des}$. Just before the two TC speed trajectories intersect, the condition in Equation (4.21) is no longer fulfilled. The setpoint value of the desired intake air mass instantaneously changes, which causes the full opening of the throttle. Furthermore, the ignition timing is retarded. Once the final condition $m_\beta = m_{a,des}$ is fulfilled, simultaneously the boost mode is switched off and the spark timing is reset to MBT. A small overshoot in the air mass is due to the fact that when the boost mode is switched off, the pressure in the exhaust manifold decreases and, hence, the volumetric efficiency increases. Relaxing the final constraint is one possibility to decrease the overshoot.

The performance data of the optimal and causal control strategies are listed in Table 4.3. The resulting deviations from the optimal solution are small. The earlier closing of the throttle in the causal strategy marginally affects the use of pressurized air and extra fuel because the relation between the effective throttle position and the air mass flow through the throttle is highly nonlinear. For $\alpha_{th} > 40\%$ the control authority is small, i.e., opening the throttle more does not yield a larger intake air mass. Note that the optimal trajectories end at $t = 1.18\,\mathrm{s}$ (indicated with a black dot) because the final condition in Equation (4.15) is reached and the simulation is thus stopped. They would continue as in the causal case, i.e., deactivate the boost mode, simultaneously reset the spark timing and close the throttle.

Table 4.3.: Performance data of optimal and causal control strategies for $c_{thr} = 0.99$ and causal strategy for $c_{htr} = 0.7$.

c_{thr}	strategy	$m_{a,b}$ [g]	$m_{f,b}$ [mg]	Δt_b [s]	# rev.
0.99	optimal	6.24	44.9	1.18	≈ 39
	causal	6.28	46.0	1.19	≈ 39
	error	+0.6%	+2.3%	+0.6%	
0.7	causal	5.20	77.0	1.0	≈ 33

Figure 4.7 shows the turbo lag compensation for a threshold value of $c_{thr} = 0.7$, which corresponds to any weighting factor $w \in [0, 1.5]$. As a result of the low threshold, the setpoint value for the throttle controller

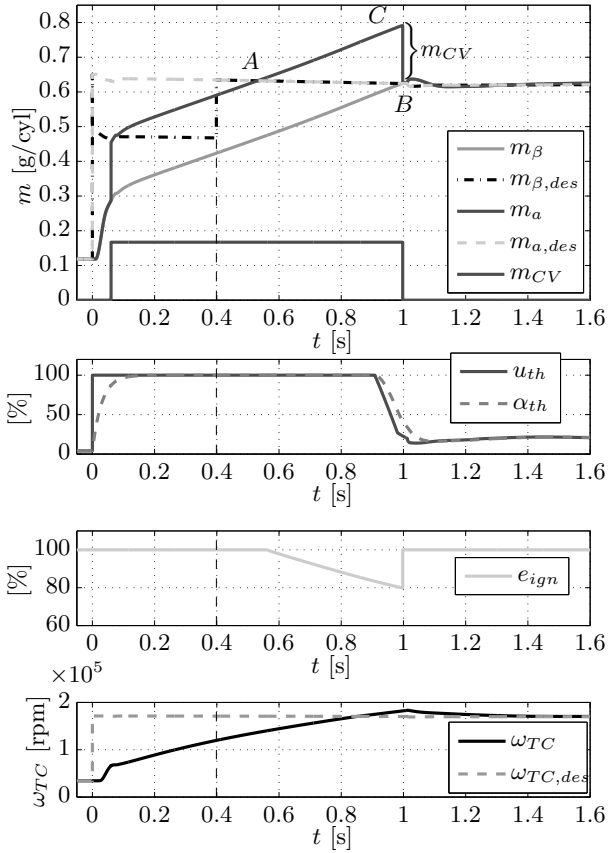

Figure 4.7.: Simulated turbo lag compensation with the causal control strategy for $c_{thr} = 0.7$: Torque step from 1.7 bar to 16.7 bar at 2000 rpm.

is increased before throttling starts. Consequently, the throttle remains wide open. The turbo lag compensation is faster, and less air is used at the expense of a higher amount of extra fuel, see Table 4.3.

Pressurized air versus extra fuel trade-off

Figure 4.8 shows the extra fuel versus the pressurized air consumption for various values of $c_{thr} \in [0, 1.03]$. As expected, the use of pressurized air is minimal if no throttling occurs, i.e., $c_{thr} \leq 0.7$. Consequently, this strategy is referred to as the minimal-air control strategy. It can be

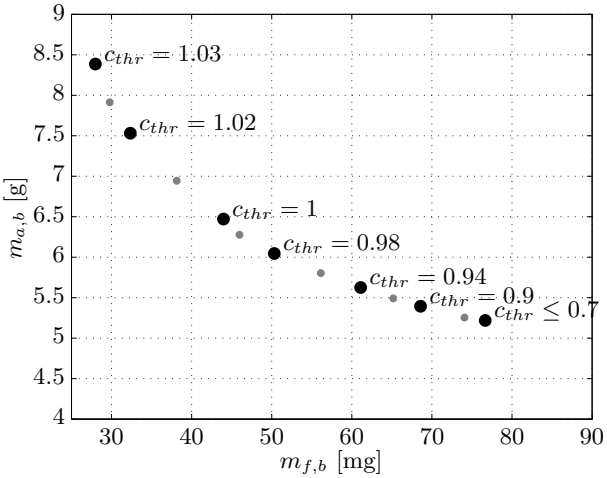

Figure 4.8.: Simulated values of $m_{f,b}$ vs. $m_{a,b}$ for various threshold values $c_{thr} \in [0, 1.03]$ and a torque step from 1.7 bar to 16.7 bar at 2000 rpm.

realized by a single setpoint value for the entire turbo lag compensation: $m_{\beta,des}(t) = m_{a,des}(t)$. The TC speed information is thus not necessary, which makes this strategy very simple and cost-effective to apply.

Figure 4.8 shows that the minimal-air control strategy consumes 24% less pressurized air than the one which uses 50% less extra fuel. Thus, for the same number of boosts, the tank volume can be decreased by 24%. Accordingly, the requirements for the packaging are substantially relaxed.

Figure 4.8 also shows that the extra fuel consumption can be decreased by more than 50% if a large threshold value is chosen. For a vehicle that consumes 4 liters of gasoline on 100 km on the NEDC, the fuel consumption increases by 0.4% if there are 18 turbo lag compensations, i.e., after every gear shift-up and in every acceleration phase, and if the minimal-air control strategy is used (77 mg fuel per boost). A more fuel efficient control strategy lowers the fuel consumption increase on the NEDC to 0.2%. These calculations show that the fuel consumption increase due to boosting is very small and that, thus, the saving potential of a more fuel efficient strategy which requires more tank volume is negligible.

This analysis leads to the conclusion that the substantially relaxed space requirements of the minimal-air control strategy clearly exceed the marginal fuel consumption increase associated with it.

4.4.2. Analysis of minimal-air control strategy

In the previous section, one particular torque step was analyzed. In this section, the air and extra fuel consumption data for torque steps from 1.7 bar to various loads and at various speeds are analyzed in simulation. The results are shown in Figure 4.9.

The first subplot shows that for a constant engine speed, a linear relationship exists between the boost time and the desired torque. Furthermore, the boost time decreases with increasing engine speed due to the higher exhaust enthalpy flow which leads to a faster TC acceleration.

The resulting air consumption is depicted in the second subplot. It decreases with increasing engine speed because the boost time is shorter as a result of the higher exhaust enthalpy. To reach a higher torque more air is used because of the longer boost time.

The third subplot shows the amount of extra fuel for various torque steps and engine speeds. At constant engine speed, the amounts of extra fuel are very similar for all torque steps considered. The amount of extra fuel is proportional to the area in the triangle ABC shown in Figure 4.7. Note that the offset between $m_a(t)$ and $m_\beta(t)$ is constant ($= m_{CV}$). Due to this fact and because $m_a(t)$ increases almost linearly during boosting in the depicted air mass range, the area of the triangle which is obtained for a smaller value of $m_{a,des}$ is approximately the same. For increasing engine speeds the amount of extra fuel decreases, which is due to the smaller CV air mass per cycle and the faster TC acceleration, which in turn is due to the increased exhaust enthalpy flow.

Note that it is assumed that the tank pressure remains constant during the turbo lag compensation, i.e., that the tank is infinitely large. The analysis in Appendix B.6 shows that the error in the air mass for a small tank is less than 4%.

4.5. Experimental verification

In this section, the feasibility of the minimal-air control strategy is verified in experiments. First, some implementation issues are discussed. Then, the measurement results of two turbo lag compensations are presented and discussed.

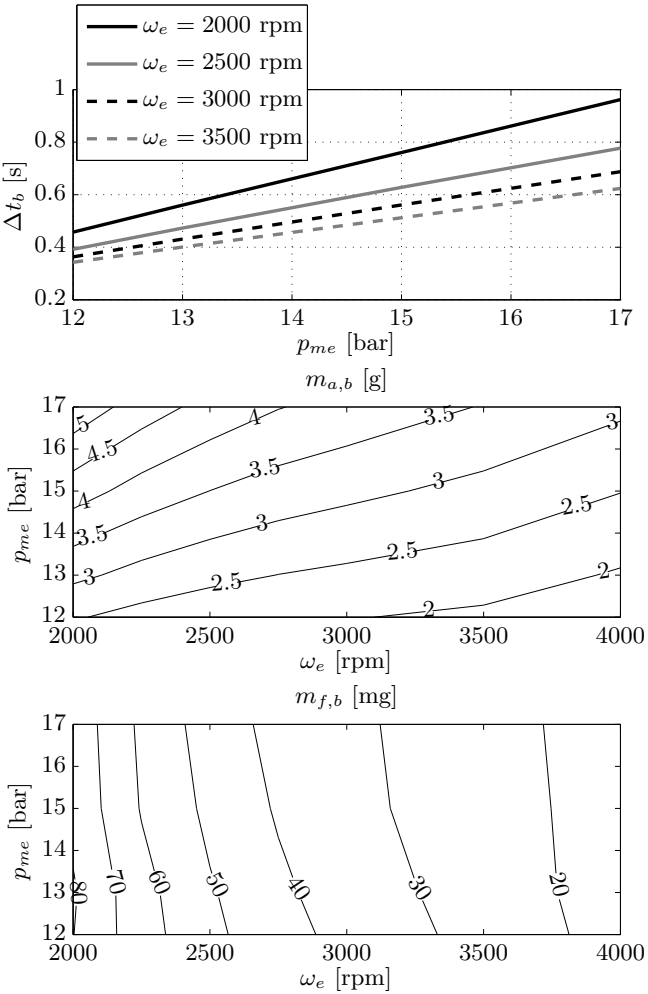

Figure 4.9.: Simulated values of Δt_b, $m_{a,b}$ and $m_{f,b}$ for torque steps from 1.7 bar to the indicated values. Each step is performed at constant engine speed.

4.5.1. Test bench implementation

The experiments were conducted on the test bench described in [10]. Further details are given there. In this subsection, the most important components of the implementation are briefly presented.

Intake air mass estimation

The intake air mass estimator is the most important component of the implementation since all control signals $\{u_{th}, u_{ign}, u_{CV}\}$ depend on it. The intake air mass estimator is based on [37] with the extensions presented in Appendix B.1. Since the test bench engine is port-fuel injected, the entire fuel mass enters through the intake valves. However, only part of the air enters from the intake port. The missing air mass needed for a stoichiometric combustion ($\lambda = 1$) is injected through the CV. As a result, the normalized air/fuel ratio in the intake port λ_{ip} can take on very low values ($\lambda_{ip} < 0.4$). The rich intake conditions lead to increased charge cooling and hence a larger density. On the other hand, they decrease the volumetric efficiency due to the volume occupied by fuel.

Injection control

The fast dynamics of the turbo lag compensation require a high bandwidth control of the injection. Transport delays, sensor dynamics and robustness requirements limit the bandwidth of the λ-feedback loop. As a result, the injection is feedforward controlled while the boost mode is active, i.e., no λ-feedback is used. The injection time is calculated from the estimated cylinder air mass, i.e., $m_\beta + m_{CV}$, taking into account the wall-wetting dynamics.

Spark timing control

With Equation (4.2) the desired ignition efficiency is calculated. The spark timing is then determined by the relation given in Equation (4.7).

4.5.2. Results and discussion

Figures 4.10, 4.11 and 4.12 show three measured turbo lag compensations. The torque and the intake air mass trajectories are compared with the corresponding simulation results. Table 4.4 lists the number of boosted

combustion cycles, the measured air consumption and the simulated air consumption.

Table 4.4.: Number of boosted combustion cycles and the amount of compressed air used in simulation and in experiments.

Data set	# boosts		$m_{a,b}$		
ω_e	sim	meas	sim	meas	error
2000 rpm	32.0	31	5.22 g	5.05 g	−3.2%
2500 rpm	33.2	32	4.35 g	4.20 g	−3.4%
1700 rpm	23.9	23	4.64 g	4.46 g	−3.9%

Figure 4.10 shows the measurement results of a turbo lag compensation at $\omega_e = 2000$ rpm. The desired torque of 16.7 bar is reached within approximately 0.57 s. This value matches the result described in [10]. The measured and the simulated torque trajectories match well, and so do the trajectories of the simulated and the estimated intake air masses $m_{\beta,sim}$ and m_β. The spark timing is retarded by up to 17 deg, which corresponds to an ignition efficiency of 82%. The deviations in the normalized air/fuel ratio are within ±4%, which the three-way catalytic converter can easily cope with.

The performance data is given in Table 4.4. Due to the reciprocating engine used in the experiment, the number of boosted combustion cycles and $m_{a,b}$ can only take on discrete values. In each boosted combustion cycle, 0.167 g of air is injected. This value is the discretization of $m_{a,b}$. The error resulting from one additional boosted combustion for this experiment is 3.3%. Accordingly, the deviation between simulation and experiment given in Table 4.4 is in the order of one boosted combustion cycle. In the MVM simulation the reciprocating nature is neglected and, hence, the value of $m_{a,b}$ and the number of boosted combustion cycles are continuous.

Figure 4.11 shows the measurement results at an engine speed of $\omega_e = 2500$ rpm. The desired torque of 16.7 bar can be reached within approximately 0.57 s. The major difference to the case shown previously is that the CV mass is smaller due to the higher engine speed, see Equation (3.4). Furthermore, the turbo lag compensation is faster. It only lasts $\Delta t_b = 0.82$ s. The duration with delayed spark timing is notably shorter, which is due to the larger enthalpy flow (as a result of the higher engine speed) and the concomitant faster TC acceleration. Hence, the

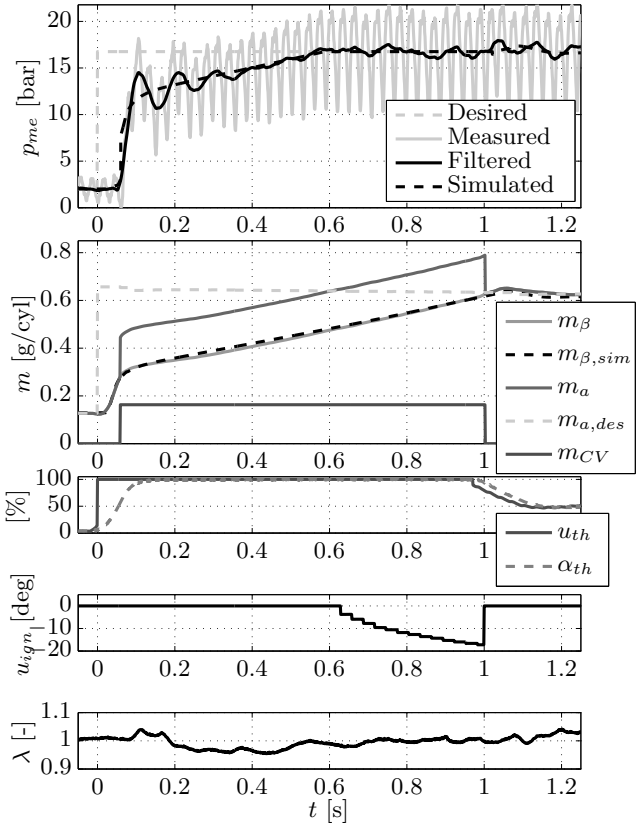

Figure 4.10.: Measured turbo lag compensation at $\omega_e = 2000\,\text{rpm}$ for a torque step from 1.7 bar to 16.7 bar using the minimal-air control strategy.

amount of pressurized air used is smaller, $m_{a,b} = 4.2\,\text{g}$, as predicted in the results shown in Figure 4.9. As in the previous experiment, simulation and measurement data match well. The deviation in the total CV air mass is again in the order of one boosted combustion.

Figure 4.12 shows the measurement results of a turbo lag compensation at $\omega_e = 1700\,\text{rpm}$. In this case the desired torque of 15.2 bar can be reached within approximately 0.4 s as a result of the higher CV air mass. Due to the smaller engine speed the enthalpy flow is smaller and the duration with retarded spark timing is relatively long. Note that once

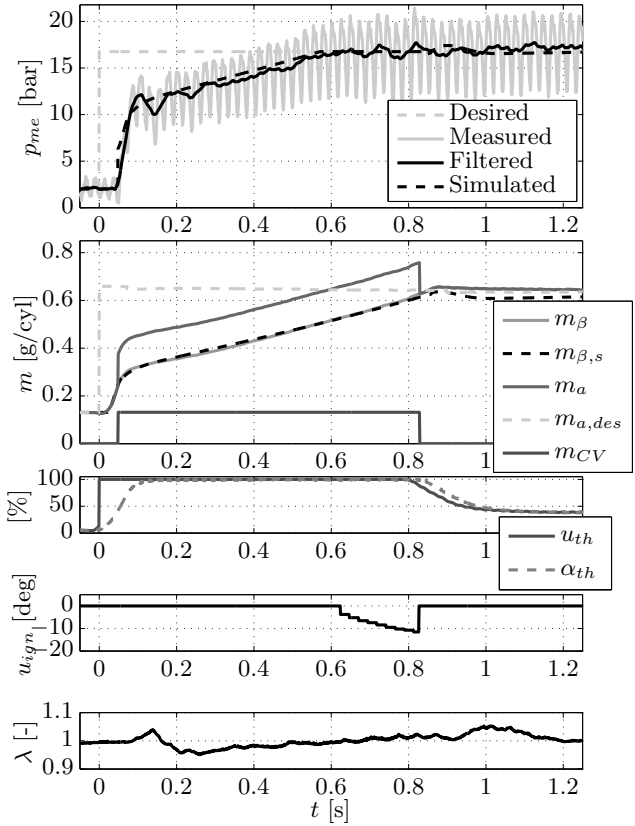

Figure 4.11.: Measured turbo lag compensation at $\omega_e = 2500\,\text{rpm}$ for a torque step from 1.7 bar to 16.7 bar using the minimal-air control strategy.

the boost mode is deactivated, the desired torque cannot be held since it is larger than the maximum steady-state torque. Hence, the engine was overboosted. Even with a fully open throttle, the desired torque is not reached because the control authority of the throttle for values $\alpha_{th} > 40\%$ is very low as mentioned in Section 4.4.1. As above, the deviation between simulation and experiment in the total CV air mass is in the order of one boosted combustion cycle.

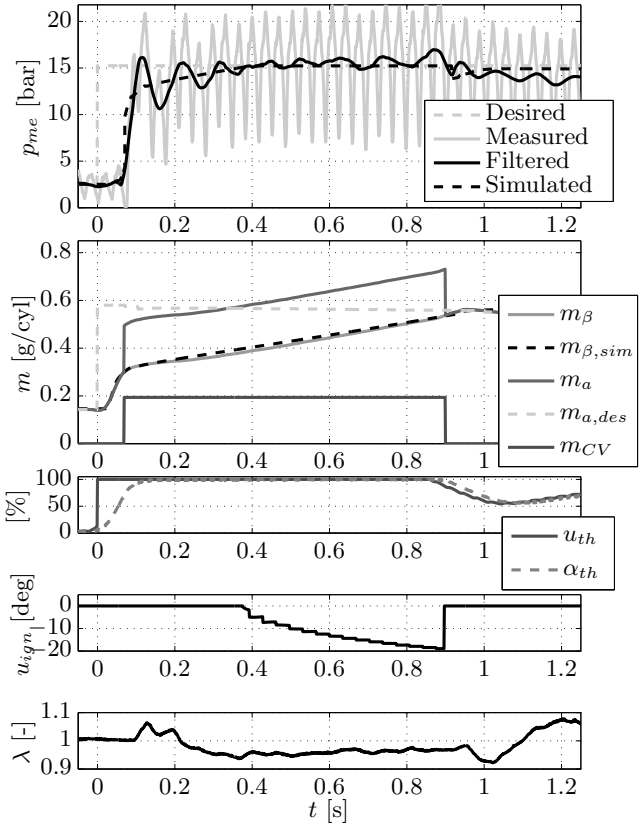

Figure 4.12.: Measured turbo lag compensation at $\omega_e = 1700\,\text{rpm}$ for a torque step from 1.7 bar to 15.2 bar using the minimal-air control strategy.

4.6. Boost mass sensitivity

So far, the boost air mass $m_{a,b}$ was determined for torque steps from $p_{me}(0) = 1.7\,\text{bar}$ and at the minimum tank pressure. In this section the sensitivity to higher tank pressures and higher initial torques is studied in simulation. As in Section 4.4.2 the analysis is performed for $\mu_{CV} = 34.9\,\text{g/s}$ and by applying the minimal-air control strategy. The variable $\tilde{m}_{a,b}$ denotes the boost mass which results for a torque step from $p_{me}(0) = 1.7\,\text{bar}$ and at the minimal tank pressure.

4.6.1. Sensitivity to the tank pressure

During the operation of the engine the tank pressure will certainly vary. According to Equation (3.4) the air mass transferred per cycle increases with the tank pressure. A higher CV mass per cycle leads to a faster TC acceleration and thus to a shorter boost time Δt_b. In this section the sensitivity of the total boost mass to the tank pressure is analyzed. For this analysis a design which yields a minimum tank pressure of $\tilde{p}_{t,b} = 6\,\text{bar}$ is assumed. Hence, the CV size becomes $\mu_{CV,p} = 5.82\,\text{g/sbar}$.

Figure 4.13 shows the simulation results. The upper plot shows the air mass used as a function of the tank pressure. The lower plot shows the ratio of the air mass used $m_{a,b}$ and the nominal air mass $\tilde{m}_{a,b}$ as a function of the ratio of the tank pressure and the minimum tank pressure $\tilde{p}_{t,b}$. Several conclusions can be drawn:

1. The boost air mass increases with an increasing tank pressure. However, the sensitivity is smaller than 1, i.e., the relative increase in the boost mass is smaller than the relative increase in the tank pressure;

2. At low engine speeds, where the boost mode is used predominantely, the sensitivity to the tank pressure is low, e.g., for the double tank pressure only 20% more air is used. The relative increase in the boost mass is larger at high engine speeds;

3. The dependence on the final torque value is low.

Note that these results can also be used to compare the air demand of various CV designs, since the CV mass flow μ_{CV} depends on the tank pressure (see Equation (3.4)). For the two CV designs of Figure 3.6

$$\mu_{CV,1} = \mu_{CV,p} \cdot \tilde{p}_{t,b} = 34.9\,\text{g/s}, \tag{4.22}$$

$$\mu_{CV,2} = \mu_{CV,p} \cdot p_t = 55\,\text{g/s}, \tag{4.23}$$

the pressure ratio amounts to

$$\frac{p_t}{\tilde{p}_{t,b}} = \frac{\mu_{CV,2}}{\mu_{CV,1}} = 1.58. \tag{4.24}$$

According to Figure 4.13, for this pressure ratio and an engine speed of 2000 rpm, the more aggressive design $\mu_{CV,2}$ requires 15% more air to reach $p_{me} = 17\,\text{bar}$. However, the torque step takes half the time. Hence, the air consumption does not scale linearly with the transient performance.

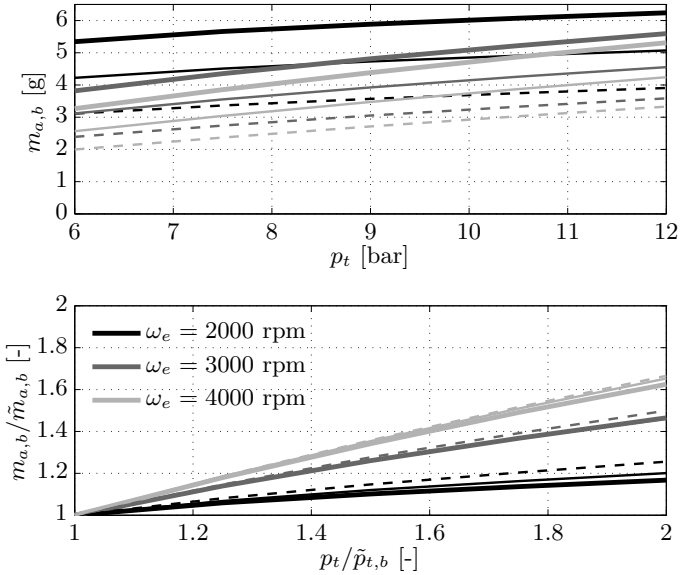

Figure 4.13.: Top: Boost air mass for various tank pressures, engine speeds and torques. Bottom: Ratio of boost air mass and nominal boost air mass for various tank pressures, engine speeds and torques. Both: $p_{me}(0) = 1.7\,\text{bar}$ and $\tilde{p}_{t,b} = 6\,\text{bar}$. Dashed: $p_{me} = 13\,\text{bar}$. Thin solid: $p_{me} = 15\,\text{bar}$. Thick solid: $p_{me} = 17\,\text{bar}$.

Approximation

For the implementation in a quasi-static simulation it is desirable to have an algebraic relation which can be used to calculate the air mass used for boosting. From the simulation results shown in Figure 4.13 the following relations are derived

$$m_{a,b}(p_t, \omega_e, p_{me}) = f_{pt}(p_t, \omega_e) \cdot \tilde{m}_{a,b}(\omega_e, p_{me})$$
$$f_{pt}(p_t, \omega_e) = 1 + f_\omega(\omega_e) \cdot \left(\frac{p_t}{\tilde{p}_{t,b}} - 1 \right),$$

where f_ω is a function which only depends on the engine speed. Note that the correction factor for the tank pressure f_{pt} is independent of the final torque value.

4.6.2. Sensitivity to the initial torque

In-cylinder boosting is also used if the engine torque is larger than $p_{me}(0) = 1.7\,\text{bar}$. This section describes how the the boost mass changes as a function of the initial torque. The analysis is performed at the minimum tank pressure. Figure 4.14 shows the simulation results.

The following conclusions can be drawn:

1. The boost mass decreases with increasing initial torque since the initial TC speed is higher. Hence, the acceleration time of the TC is shorter;
2. The absolute decrease of the boost mass shown in the lower plot is independent of the final torque value. This can be explained by the fact that the duration in the NA region is very short. The TC acceleration is relevant;
3. The absolute decrease of the boost mass is larger at higher engine speeds.

Approximation

As with the tank pressure it is possible to describe the influence of the initial torque in an algebraic relation

$$\begin{aligned} m_{a,b}(p_{me}(0), \omega_e, p_{me}) &= \tilde{m}_{a,b}(\omega_e, p_{me}) - m_{pme0}(\omega_e, p_{me}(0)) \\ m_{pme0}(\omega_e, p_{me}(0)) &= \min\{-k_1 \cdot p_{me}(0) + k_2(\omega_e), 0\}, \end{aligned}$$

where $k_1 > 0$ is a constant and $k_2(\omega_e)$ is a function which only depends on the engine speed.

4.7. Conclusion

In this chapter a novel torque control system for the turbo lag compensation of an engine with in-cylinder boosting using a camshaft driven CV was investigated in simulation and verified by experiments. Clearly, the combination of boost mode and ignition timing allows a high bandwidth control for the torque, although the limited variability of the deactivatable camshaft driven CV does not allow the continuous adjustment of the CV mass. However, a slight increase in fuel consumption is inevitable. The torque control during the turbo lag compensation process is best illustrated in Figure 4.1 and is characterized by the following control actions:

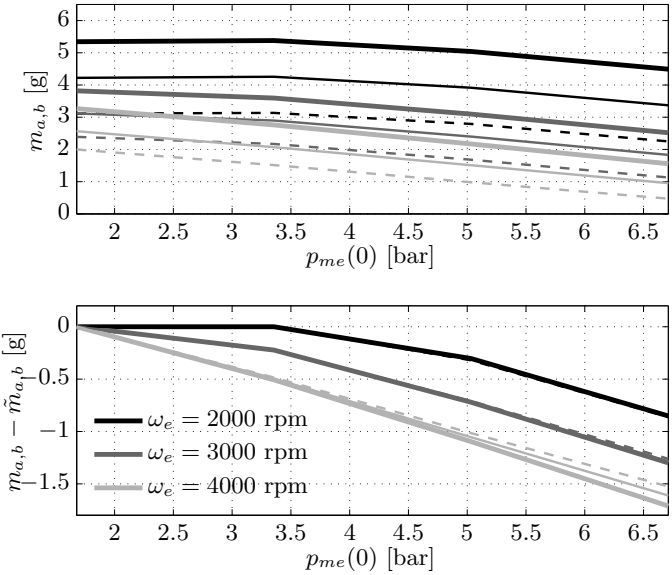

Figure 4.14.: Top: Boost air mass for various initital torques, engine speeds and final torques. Bottom: Difference of the boost air mass and the nominal boost air mass for various initial torques, engine speeds and final torques. Dashed: $p_{me} = 13\,\text{bar}$. Thin solid: $p_{me} = 15\,\text{bar}$. Thick solid: $p_{me} = 17\,\text{bar}$.

1. Fully open the throttle and simultaneously activate the boost mode;
2. When the desired torque is reached, retard the spark timing to keep the torque at the desired level;
3. When the desired intake air mass is equal to the desired cylinder air mass, simultaneously deactivate the boost mode and reset the ignition timing to optimal.

Based on the results determined in an optimal control framework, this causal throttle controller was derived. The simplest and most cost-effective realization is the minimal-air control strategy where only one setpoint value is used for the throttle controller: $m_{\beta,des} = m_{a,des}$. This strategy uses up to 24% less pressurized air, which substantially simplifies the packaging. The associated fuel consumption penalty in real driving con-

ditions is marginal. In experiments, the capability of this control strategy was verified at several engine speeds and for various torque steps.

Note that these results were determined for a closed the waste gate. If an open waste gate strategy is applied, the waste gate might be open at $p_{me} = 1.7\,\text{bar}$. To avoid a substantial increase of the air mass, the waste gate has to close immediately and very fast.

5. Pneumatic Engine Start

An inherent property of ICEs is their limited operability below a minimum rotational speed. Starting an engine means accelerating it up to a specific speed above which it is normally operated. Due to its inertia and the low starter power, a conventional start of an ICE takes up to 1 second. An engine shutdown during idling phases implying such long start times is not accepted by the driver. Therefore, conventional ICEs normally are not shut down during idling phases.

However, idling losses comprise a significant amount of the total fuel consumption. On the NEDC they amount to 6% for a 2 liter NA gasoline engine as shown in Section 2.1. In order to exploit this fuel saving potential by eliminating the idling phases while still satisfying driver demands, the duration of an engine start needs to be reduced.

A common approach to reducing the engine start time is the installation of a powerful electric starter (ES) and an appropriate battery. This strategy can be pursued with hybrid electric vehicles since they are equipped with more powerful electric motors and batteries than conventional engines. However, they induce additional weight and cost. According to [38], start times of 300 ms are achievable with this setup.

Several authors [39, 40] investigated a method for fast starts of gasoline engines with direct fuel injection. The idea behind this approach is to inject fuel into the stopped engine. If the engine has stopped at an appropriate position, the fuel can be ignited at standstill to restart the engine without using the ES. However, a controlled engine shutdown is indispensable to enforce the engine to stop at an appropriate position. Robustness under all operating conditions and emissions due to incomplete combustion at low engine speeds are critical issues with this approach. In [38] the investigations were extended to ES-assisted engine starts to reduce the start time and the emissions.

A cost and weight effective alternative is to use compressed air that can be injected directly into the cylinders. The compressed air is stored in a tank and is injected during the expansion stroke where it produces a positive torque that accelerates the engine. The engine is driven purely pneumatically without burning fuel. In [9] the pneumatic start of an

engine equipped with a fully variable EHVS for the actuation of the CVs was investigated. In this setup, the CV lift profile can be adapted on a cycle to cycle basis. However, an EHVS increases the complexity and cost of the system.

In this chapter pneumatic engine starts using CSD CVs are investigated. Camshaft driven CVs are characterized by a valve lift profile which cannot be varied during the operation of the engine. On the other hand, the level of complexity can be significantly reduced. The goal is to optimize the CV design for minimum air consumption with the constraint of a maximally allowable engine start time.

The chapter is structured as follows: In Section 5.1, the model and the setup of the engine as well as the boundary conditions for the optimization of the CV design are introduced. Additionally, an engine stop strategy is proposed. In Section 5.2, the design problem is formulated as a constrained minimization problem. A design methodology to solve this optimization problem is presented. Section 5.3 shows the application of this methodology in a design example whose results are verified experimentally on a test bench engine. In Section 5.4 various system analyses are conducted with the properly designed system. The chapter ends with a conclusion.

5.1. Model and setup

For the determination of the optimal CV parameters a process model of the engine is used to simulate the start. A detailed description of the model can be found in Appendix C. This section presents a model of the electric starter, the parameters of the valve lift profile and the role of the initial engine position. Note that in this chapter $\phi = 0\,°\text{CA}$ corresponds to the TDC after the compression stroke.

5.1.1. Electric starter

In contrast to [9] the focus here is on CSD CVs. In such a realization the valve lift profile is fixed. Furthermore, the valve can only be actuated by a rotating engine. For the initial actuation of the CVs and for other reasons as described by [39] an ES is indispensable. Furthermore, the ES helps reduce the start time since it is an additional torque supplier during the pneumatic engine start.

In order to precisely predict the behavior of the engine during the start phase, a good model of the ES is crucial. Since the operation of the ES takes place under highly dynamic conditions, the model of the ES needs to be identified during transient operation. The behavior of the ES is modeled as a static torque-speed relationship $T_{ES}(\omega_e)$ for engine speeds below 200 rpm. For higher engine speeds it is assumed that the engine and the ES are disconnected. A least squares approach is used to find a polynomial fit for the torque-speed relationship. Figure 5.1 shows the experimental validation of the relationship found. Only the first half of the first engine revolution is shown because in this phase the dynamics of the ES are dominant.

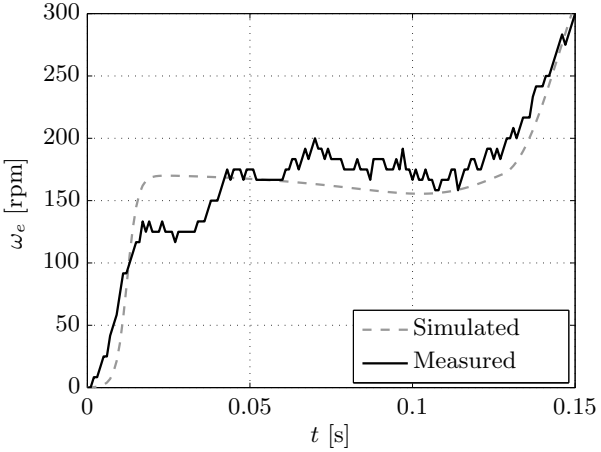

Figure 5.1.: Trajectories of the measured and simulated engine speed during an engine start (first half oef the engine revolution, where ES is active). The measurements are taken on the engine described in Appendix A.

5.1.2. Valve lift profile

The same simplified valve lift model is used as the one described in Section 3.1.2, i.e., the magnitudes of the acceleration and the deceleration are equal and piecewise constant. Note that the maximum valve lift is limited to $y_{CV,max}$ by the actuator chosen. Furthermore, to avoid the collision of the valve with the piston the valve lift profile must fulfill the following

condition

$$y_{CV}(\phi) \leq \min \left\{ \frac{V_{cyl}(\phi)}{A_{cyl}}, y_{CV,max} \right\}, \tag{5.1}$$

where A_{cyl} is the cross-sectional area of the cylinder.

To minimize throttling losses across the CV, the valve should be opened and closed as fast as possible. Consequently, the valve acceleration has to be maximal. In contrast to the IVs and the EVs, the CV is only actuated at low engine speeds. Since mechanical stresses apply in the time domain, the maximum CV acceleration in the CA domain can be chosen higher than the one of the IVs and EVs. A reasonable value for the CV acceleration can be found with

$$a_{CV,s} = a_{IV} \cdot \left(\frac{\omega_{e,max}}{\omega_{e,s,max}} \right)^2, \tag{5.2}$$

where a_{IV} denotes the acceleration of the IVs in the CA domain, $\omega_{e,max}$ is the maximum engine speed and $\omega_{e,s,max}$ is the maximally allowable engine speed during the pneumatic start operation.

Given the maximum valve lift $y_{CV,max}$ and the valve acceleration $a_{CV,s}$, the remaining parameters of the CV lift profile are the CV timings $\phi_{CVO,s}$ and $\phi_{CVC,s}$. A methodology to find appropriate values is presented in Section 5.2.

5.1.3. Initial engine position

The duration of the pneumatic engine start strongly depends on the time which elapses until pressurized air is injected for the first time. The earlier pressurized air is injected, the faster the engine start is. The duration until the CV opens at $\phi_{CVO,s}$ is mainly influenced by the size of the ES and the initial engine position ϕ_0. Hence, the engine should be shut down such that the piston which is in the compression stroke comes to rest close to the CV opening angle.

The rest position can be influenced by the actuation of the throttle during the engine shutdown. To find an appropriate value for the initial engine position in the model, several experimental engine shutdowns were performed with constant throttle opening u_{th} and the rest position was recorded. Figure 5.2 shows the results for the two-cylinder engine described in Appendix A. The best performance is achieved with a throttle opening of $u_{th} = 2\%$ because the variance is smallest and the mean position is closest to the top dead center (TDC). Higher values yield a

rest position which is further away from the TDC. Smaller throttle opening values yield a poor repeatability of the rest position, which is not desirable. Thus, for the design methodology an initial engine position of $\phi_0 = 95\,°\text{CA}$ before TDC (bTDC) is chosen.

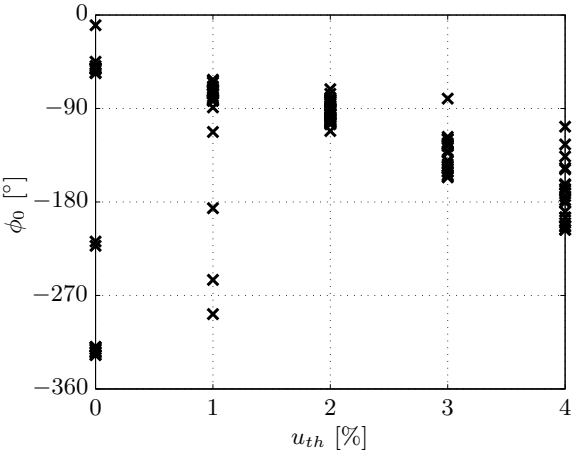

Figure 5.2.: Measured engine rest positions ϕ_0 for various throttle openings u_{th} during engine shutdown. At $\phi_0 = 0\,°$ the piston is located at the TDC after the compression stroke.

5.1.4. Throttle control during engine start

The throttle position setting found is only relevant during engine shutdown. In [9] it was shown that completely closing the throttle during the engine start phase is air- and time-optimal. A closed throttle implies that the intake manifold pressure decreases during the start. Hence, the compression work is reduced and the cylinder pressure is smaller when the CV opens which leads to a higher air mass flow and a higher torque. Therefore, for the subsequent design methodology the throttle is always assumed to be completely closed.

5.2. Design methodology

In this section the underlying optimization problem of the CV design is stated. The optimization problem is analyzed and discussed. A stepwise procedure for its solution is presented. The feasible set satisfying all the constraints is determined and specific design selections are introduced.

The objective of the proposed design methodology is to find values for the design variables which enable the engine to reach a prescribed speed $\omega_{e,s}$ within less than a prescribed start time $t_{s,max}$ and which at the same time minimize the amount of pressurized air used. The relevant design variables are:

$\phi_{CVO,s}$: CV opening angle,
$\phi_{CVC,s}$: CV closing angle,
d_{CV}: CV diameter.

Let $\Delta = \{\phi_{CVO,s}, \phi_{CVC,s}, d_{CV}\} \in \mathbb{R} \times \mathbb{R} \times \mathbb{R}^+$ be the parameter space considered of the relevant design variables. The variable δ denotes a single design in Δ.

The start time and the air consumption also depend on the initial tank pressure $p_{t,s}$. During the operation of the engine on a drive cycle the tank pressure varies. Fully variable CVs can adjust their valve timing to account for the changing tank pressure. However, the valve timing of CSD CVs is fixed. Hence, the design procedure has to consider the entire operating range of the tank pressure. To do so, the weighted sum of the air consumptions resulting for n different tank pressures $\boldsymbol{p}_{t,s} \in \mathbb{R}^{n,+}$ is minimized.

The optimization problem can be written as

$$\begin{aligned} & \min_{\delta \in \Delta} \sum_{i=1}^{n} w(\boldsymbol{p}_{t,s}(i)) \cdot m_{a,s}(\delta, \boldsymbol{p}_{t,s}(i)) \\ \text{s.t.} \quad & t_s(\delta, \boldsymbol{p}_{t,s}(i)) \leq t_{s,max}, \end{aligned} \tag{5.3}$$

where t_s is the time needed to reach the desired engine speed $\omega_{e,s}$ and $m_{a,s}$ denotes the amount of air used for the start. Both are calculated with the nonlinear process model f_{PM}

$$[m_{a,s}(\delta, p_{t,s}), t_s(\delta, p_{t,s})] = f_{PM}(\delta, p_{t,s}, \omega_{e,s}).$$

The air consumption $m_{a,s}$ is calculated by taking the integral over the mass flow through the CV $\dot{m}_{CV}$

$$m_{a,s} = \int_0^{\hat{t}_s} \dot{m}_{CV} dt, \tag{5.4}$$

where $\hat{t}_s$ implies an extension of the integration interval to $\hat{t}_s \geq t_s$. It is defined as the smallest $\hat{t}_s$ satisfying the following constraints

$$\omega_e(\hat{t}_s) \geq \omega_{e,s}, \tag{5.5}$$

$$\dot{m}_{CV}(\hat{t}_s) = 0. \tag{5.6}$$

This definition accounts for the fact that the CVs cannot be closed and deactivated immediately when $\omega_e = \omega_{e,s}$ is reached. In contrast to the fully variable valves used in [9], the CSD CVs can only be deactivated if $\phi \notin [\phi_{CVO,s}, \phi_{CVC,s}]$. Figure 5.3 visualizes the definitions of t_s and $\hat{t}_s$ for a pneumatic engine start.

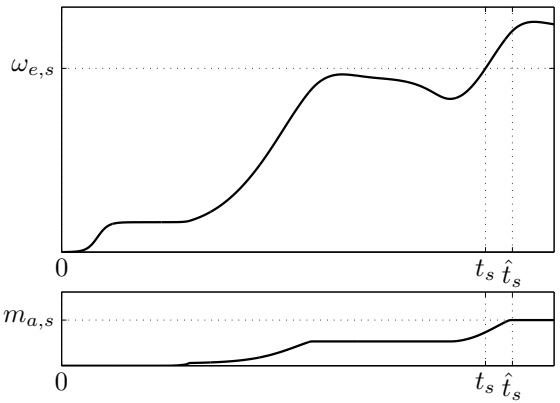

Figure 5.3.: Engine speed and cumulative air consumption for a pneumatic engine start. During the constant speed phase the engine is only driven by the ES. The variables t_s and $\hat{t}_s$ are labeled to clarify their definitions.

The scalar weighting function $w(p_{t,s}) \geq 0$ only depends on the initial tank pressure. It is used to select and penalize specific initial tank pressures in the optimization. Promoting high initial tank pressures results in an inferior design for low initial tank pressures and vice versa. A reasonable choice of $w(p_{t,s})$ is to make it large at small initial tank pressures. For low initial tank pressures, the air consumption can become a critical issue on a drive cycle. On the other hand, if the initial tank pressure is high, an increased air consumption can be accepted. Special attention should be paid to frequently occurring initial tank pressures during the drive cycle.

5.2.1. Properties of the optimization problem

Due to the reciprocating behavior of the engine and the highly nonlinear process model f_{PM} the optimization problem has special features. These are discussed below.

The feasible set is defined as

$$\Omega(p_{t,s}) := \{\Delta | t_s(\Delta, p_{t,s}) \leq t_{s,max}\}, \tag{5.7}$$

i.e., all designs which fulfill the performance constraint for the initial tank pressure $p_{t,s}$. The smallest initial tank pressure for which $\Omega(p_{t,s})$ is not empty is defined as the minimum tank pressure $\tilde{p}_{t,s,\Omega}$ of the feasible set. The tank pressures considered have to fulfill $\boldsymbol{p}_{t,s}(i) \geq \tilde{p}_{t,s,\Omega} \forall i$. However, since the minimum tank pressure is not known a priori, the choice of $\boldsymbol{p}_{t,s}$ is difficult. This fact makes it also difficult to formulate a reasonable weighting function $w(p_{t,s})$, such that the desired tank pressure range is promoted or penalized.

Furthermore, the reciprocating behavior of the engine implies a further difficulty for the solution of the optimization problem. The function $[m_{a,s}, t_s] = f_{PM}$ is piecewise continuous in both the air mass and the start time. This fact is shown by introducing the following consideration. Let δ_1 and δ_2 be two designs with $\|\delta_1 - \delta_2\|_\infty < \epsilon$ where $\|\cdot\|_\infty$ denotes the infinity norm and $\epsilon > 0$ is a very small number. Hence, the two designs only differ slightly. However, for specific choices of δ_1 and δ_2 the evaluation of $f_{PM}(\delta_i, p_{t,s})$ for the same initial tank pressure yields completely different results. It occurs when $\omega_{e,s}$ is reached in a different number of power strokes: $N_{ps}(\delta_1) \neq N_{ps}(\delta_2)$. Thus, there is a discontinuity in $m_{a,s}$ and t_s between δ_1 and δ_2. Discontinuities in the objective function can cause problems with numerical optimization algorithms.

5.2.2. Solution to the optimization problem

Depending on the objective and the prior knowledge two solving methods are proposed, namely numerical optimization and a brute-force approach. For the numerical optimization, the particle swarm optimization (PSO) is proposed since it copes well with the previously described properties of the problem. In Table 5.1 the properties of the proposed methods are listed. The numerical optimization is suited if the minimum tank pressure is known such that $\boldsymbol{p}_{t,s}$ can reasonably be selected. The derivation of the optimal solution is rather fast and a precise solution is found.

In the brute-force approach the process model is simulated for a multitude of CV design variables and tank pressures. Depending on the coarseness of the considered grid, this approach is computationally more demanding. The advantage of this method lays in the fact that the minimum tank pressure does not need to be known. It is derived in the approach. Furthermore, the simulation results can be used for sensitivity analyses. However, the precision of the solution is limited by the coarseness of the grid.

Table 5.1.: Comparison of the solving methods.

Method	numerical optimization	brute-force
Minimum tank pressure	needs to be known	is derived
Calculation time	fast	slow
Precision of solution	high	lower
Sensitivity analysis	not suited	suited

In the following the two solving methods are explained. Regardless of the solving method, the specifications have to be formulated first, i.e., $\omega_{e,s}$ and $t_{s,max}$.

1. Numerical optimization

If the minimum tank pressure $\tilde{p}_{t,s,\Omega}$ is known, a reasonable tank pressure range $\boldsymbol{p}_{t,s}$ and a reasonable weighting function can be defined. For the solution the PSO algorithm presented in [41] is proposed.

2. Brute-force

The brute-force approach visualized in Figure 5.4 starts with the definition of a grid $\Gamma = \{\Delta, p_{t,s}\}$ on which the process model is evaluated in the next step. The computational effort for the evaluation depends on the discretization chosen. Given $t_s(\Gamma) = f_{PM}(\Gamma, \omega_{e,s})$ the feasible set Ω and the minimum tank pressure $\tilde{p}_{t,s,\Omega}$ can be derived. Then, a reasonable tank pressure range $\boldsymbol{p}_{t,s}$ and a reasonable weighting function can be defined.

The optimal solution $\delta^* = \{\phi^*_{CVO,s}, \phi^*_{CVC,s}, d^*_{CV}\}$ is found by evaluating Equation (5.3) on the feasible set Ω. This minimum search is computationally not demanding if $\boldsymbol{p}_{t,s} \in \Gamma$, i.e., if $\boldsymbol{p}_{t,s}$ consists only of tank pressures that are also part of Γ. Then, no further model evaluations are necessary. Alternatively, a PSO can be conducted with the defined tank

pressure range and weighting function. It is computationally more demanding than the minimum search on an already existing grid. However, the solution found is more precise since it does not need to be on the grid.

Minimum tank pressure for optimal design The minimum tank pressure $\tilde{p}_{t,s}$ for the optimal design can be found by solving

$$\begin{aligned} &\tilde{p}_{t,s} = \min p_{t,s} \\ \text{s.t.} \quad &t_s(\delta^*, p_{t,s}) \leq t_{s,max}. \end{aligned} \tag{5.8}$$

Its value is important for the overall system design. More details on this topic can be found in Chapter 7.

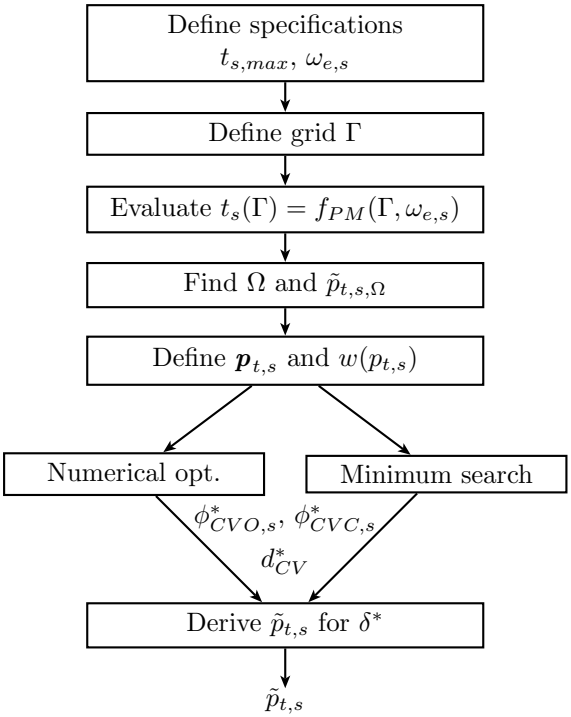

Figure 5.4.: CV design procedure for pneumatic engine start using the brute-force approach.

5.3. Design example

The following design example shows the application of the CV design methodology presented. The engine under consideration is the 0.75 l two-cylinder parallel twin engine described in Appendix A. Additional specifications of the engine are given in Table 5.2. The maximum CV lift is $y_{CV,max} = 4\,\text{mm}$ which corresponds to the value that can be realized on the test bench engine. The IV acceleration a_{IV} that guarantees safe operation up to the maximum engine speed $\omega_{e,max}$ is given in Appendix A. By applying Equation (5.2) the maximally allowable CV acceleration in the CA domain is found as $a_{CV,s} = 3.04 \cdot 10^{-5}\,\text{m}/^\circ\text{CA}^2$.

Table 5.2.: Design example parameterization.

Parameter	variable	value	unit
Max. start engine speed	$\omega_{e,s,max}$	1500	rpm
CV acceleration	$a_{CV,s}$	$3.04 \cdot 10^{-5}$	$\text{m}/^\circ\text{CA}^2$
Maximum valve lift	$y_{CV,max}$	4	mm
Initial engine position	ϕ_0	-95	°CA

Specifications

The desired start engine speed is set to $\omega_{e,s} = \omega_{e,idle} = 1200\,\text{rpm}$. The maximum start time is chosen as $t_{s,max} = 350\,\text{ms}$. These specifications are in accordance with [9, 38].

Grid definition

The grid Γ considered in the design example is given in Table 5.3.

Table 5.3.: Grid Γ used in design example.

Variable	lower bound	upper bound	step size
$\phi_{CVO,s}$	$-110\,^\circ$CA	$50\,^\circ$CA	$10\,^\circ$CA
$\phi_{CVC,s}$	$60\,^\circ$CA	$220\,^\circ$CA	$10\,^\circ$CA
d_{CV}	7 mm	21 mm	2 mm
$p_{t,s}$	7 bar	12 bar	1 bar

Evaluation of the process model

In this step the nonlinear process model is evaluated for Γ, i.e., $13,872$ model evaluations.

Determination of the feasible set and its minimum tank pressure

The analysis of the simulation results $t_s(\Gamma)$ yields a minimum tank pressure of $\tilde{p}_{t,s,\Omega} \approx 9.2\,\text{bar}$. Figure 5.5 visualizes this result. It shows the minimum start time achievable for fixed combinations of d_{CV} and $p_{t,s}$. The 350 ms line indicates the boundary of the feasible set in the $p_{t,s}$-d_{CV} subspace. All initial tank pressure and CV diameter combinations with $t_s \leq 350\,\text{ms}$ are part of the feasible set.

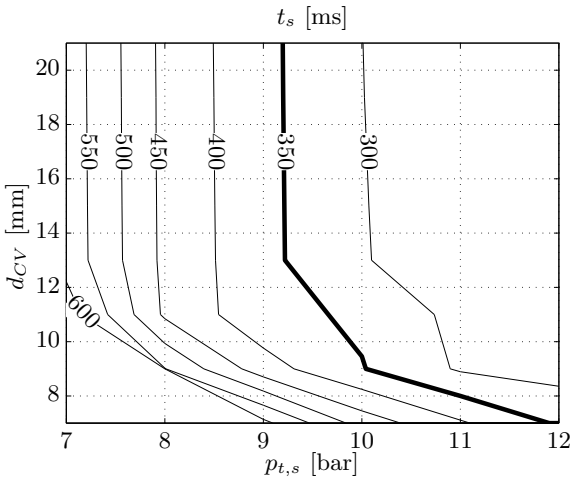

Figure 5.5.: Minimum start time for various CV diameters and initial tank pressures.

On the test bench, a CV with a diameter of $d_{CV} = 19\,\text{mm}$ is installed. Therefore this diameter is chosen for the design example and kept as fixed value throughout the rest of the optimization procedure.

Definition of the tank pressure range and the weighting function

Based on the data depicted in Figure 5.5 the tank pressure vector $\boldsymbol{p}_{t,s}$ can be defined. In this example only one tank pressure close to the boundary

of the feasible set is considered

$$\boldsymbol{p}_{t,s} = \{10\,\text{bar}\}. \tag{5.9}$$

Thus, no weighting is necessary

$$w(p_{t,s}) = 1. \tag{5.10}$$

Minimum search and numerical optimization

According to the procedure described in Section 5.2 the optimal CV design can be found by a minimum search on the feasible set. Since the tank pressure considered is on the grid, no further simulations are necessary. Table 5.4 lists the values for the design variables found by the minimum search and the numerical optimization using PSO, respectively, for $d_{CV} = 19\,\text{mm}$. The valve timings found with the two methods are very similar. The resulting start time is 350 ms. Thus, the maximum start time is fully exploited, and the solution is on the boundary of the feasible set.

Table 5.4.: Optimal values of the design variables for $d_{CV} = 19\,\text{mm}$.

	Minimum search	PSO
$\phi^*_{CVO,s}$	10 °CA	14.2 °CA
$\phi^*_{CVC,s}$	110 °CA	110.2 °CA
$m^*_{a,s}$	10.15 g	10.13 g
t^*_s	350 ms	350 ms

Figure 5.6 shows the air consumption for the relevant part of $\{\phi_{CVO,s}, \phi_{CVC,s}\} \in \Gamma$ and a tank pressure of 10 bar.

Minimum tank pressure $\tilde{p}_{t,s}$

Since only a tank pressure of 10 bar was considered in $\boldsymbol{p}_{t,s}$, this value also corresponds to the minimum tank pressure $\tilde{p}_{t,s}$ for which an engine start in $t_s = 350\,\text{ms}$ is achieved.

5.3.1. Discussion

The optimization procedure yields a CV opening angle after TDC. This result is advantageous because the first engine revolution would become

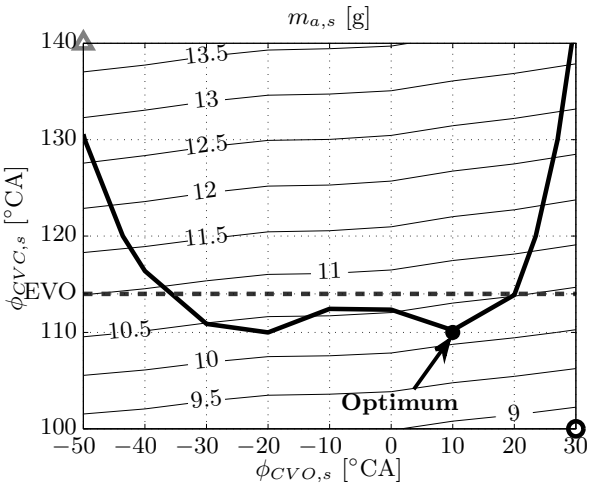

Figure 5.6.: Consumption of pressurized air for various CV opening and closing angles with $d_{CV} = 19\,\text{mm}$ and $p_{t,s} = 10\,\text{bar}$. The black line denotes the boundary of the feasible set, where all combinations above the line are feasible. The EV opening angle is denoted by EVO. Black circle: Minimum air consumption. Gray triangle: Maximum air consumption.

critical if the CV was to be opened before TDC and the initial tank pressure was large, i.e., significantly larger than the in-cylinder pressure at TDC. In that case, a negative torque would be produced by the injection of pressurized air before the piston passes TDC. If this torque were to exceed the torque produced by the ES, the engine could not be started pneumatically.

Figure 5.6 clearly shows that a later closing of the CV is unfavorable with respect to the air consumption. The reason for this fact is that the opening angle of the EV is at 114 °CA aTDC. A design where $\phi_{CVC,s} > 114\,°\text{CA}$ aTDC implies that pressurized air flows from the CV directly into the exhaust manifold. Such a design increases the air consumption without producing significantly larger torques and thus faster start times.

Sensitivity analysis

Based on the results depicted in the Figures 5.5, 5.6 and 5.7 a sensitivity analysis of the parameters in the set Γ can be performed.

Figure 5.5 shows that for small CV diameters the minimum tank pressure to satisfy $t_s \leq t_{s,max}$ increases significantly because less air can be transferred through the CVs due to the increased flow restriction. Thus, the torque is smaller. The increased flow restriction needs to be compensated by a higher density, i.e., a higher tank pressure. For $d_{CV} > 14\,\text{mm}$ the start time is almost constant for a fixed tank pressure. One would expect that higher values of d_{CV} result in more air being transferred and hence reduced start times. However, there is a counteracting effect. For large valve diameters the pressure difference between tank and cylinder decreases rapidly after the CV is opened. This effect results in a reduction of the mass flow rate.

Figure 5.7 shows the start time for various combinations of $\phi_{CVO,s}$ and $\phi_{CVC,s}$ for a fixed $p_{t,s} = 10\,\text{bar}$ and $d_{CV} = 19\,\text{mm}$. The maximum start time is 370 ms and is depicted by the gray triangle. The minimum start time is 341 ms and is indicated by the black circle. Thus, the maximum start time is 8% higher than the minimum start time, which indicates a rather small sensitivity. Around TDC, the start time t_s is almost constant for varying CV opening angles. On the other hand, the start time can be reduced by a later closing of the CV.

The air consumption shown in Figure 5.6 shows a rather high sensitivity to the CV timing. In the CV timing intervals depicted the minimum air consumption is 8.7 g (black circle). However, the maximum air consumption amounts to 13.8 g (gray triangle), which is 58% larger. analogously to the start time, around TDC there is a small variation of $m_{a,s}$ in terms of the CV opening angle. However, the gradient of the air consumption as a function of the CV closing angle points to the opposite direction of the gradient of the start time.

In general, it can be concluded that a later closing of the CV implies shorter start times but an increased air consumption. Comparing the time- and air-optimal designs indicated by the black circles in Figures 5.6 and 5.7 leads to the statement that accepting a 8% increase in the start time results in an air saving of 36%.

5.3.2. Experiments

In order to verify the quality of the model and the CV design found, the pneumatic start is implemented on a test bench engine with the optimal CV timings obtained from the design example. The CVs are actuated by a fully variable EHVS which can be used to emulate a wide variety of

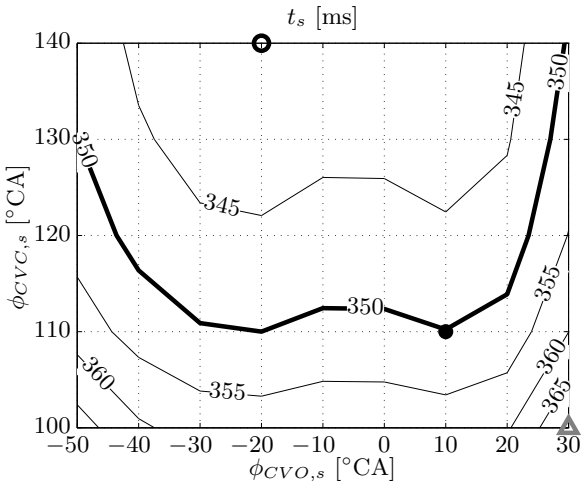

Figure 5.7.: Start times for various CV opening and closing angles for $p_{t,s} = 10\,\text{bar}$ and $d_{CV} = 19\,\text{mm}$. The black line denotes the boundary of the feasible set where all combinations above the line are feasible. Black circle: Minimum start time. Gray triangle: Maximum start time.

CV lift profiles. Figure 5.8 shows the desired and the emulated CV lift profiles of both cylinders for the engine start shown in Figure 5.9.

In Figure 5.9 the engine speed trajectories for a measured and a simulated pneumatic start are shown. The limit of $t_s = t_{s,max} = 350\,\text{ms}$ is fully exploited, which correponds to the result determined by simulation and presented in Table 5.4. The pressure drop in the air tank over the entire pneumatic engine start phase is approximately 300 mbar. The corresponding air consumption is 10.5 g which agrees with the value predicted by the process model. The discrepancy is 3%. Only four power strokes are required to reach the desired final engine speed $\omega_{e,s}$. During the first third of the start time the engine is only driven by the ES until $\phi_{CVO,s}$ is reached. This duration can only be reduced by a more powerful ES.

The good agreement between measurement and simulation data confirms the quality of the process model.

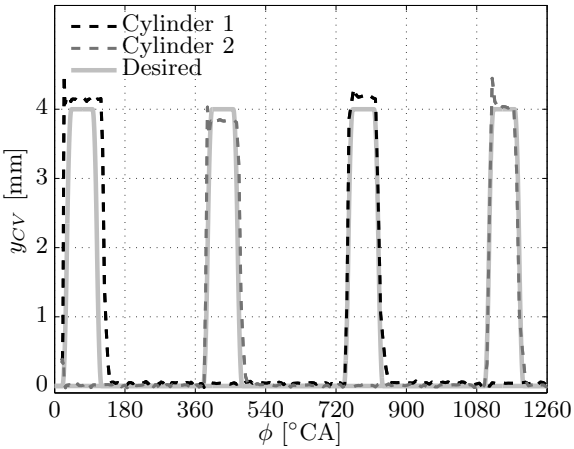

Figure 5.8.: Desired and emulated CV lift profiles.

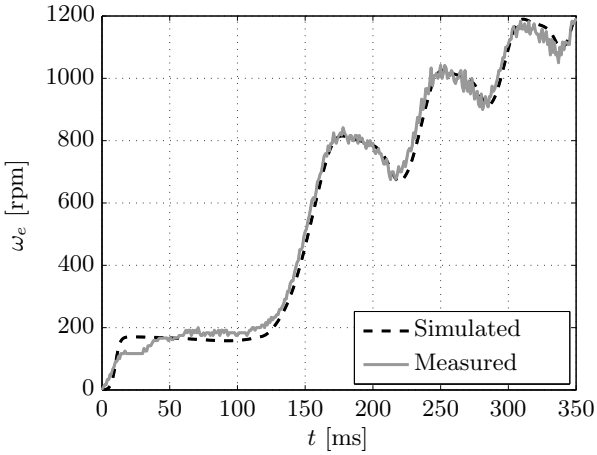

Figure 5.9.: Measured and simulated pneumatic engine start.

5.4. System analysis

The properly designed and validated system is used to study the behavior with respect to the varying parameters during the engine operation, namely the tank pressure and the initial engine position.

5.4.1. Variation of the initial tank pressure

During the operation of the engine, the tank pressure varies. In this section the start performance of a CSD CV with respect to the air used and the start duration is analyzed for various initial tank pressures. Figure 5.10 shows the results. The first subplot shows the total amount of air used $m_{a,s}$ and the amount of air used when the desired engine speed is reached. The second subplot shows the start time t_s and the time $\hat{t}_s$ when the valves are closed. The third subplot shows the number of power strokes N_{ps} required to reach the desired engine speed.

As stated in Equation (5.4), the amount of air used to start the engine is calculated as the integral of the air mass flow. Consequently, the same amount of air is used if a larger mass flow is present for a short time or if a small mass flow exists for a longer time duration. For instance, the air consumptions for $p_{t,s} = 9.3\,\text{bar}$ and $p_{t,s} = 12\,\text{bar}$ are equal. However, the start times are different.

A higher tank pressure leads to a higher air mass flow. The torque exerted is larger which leads to a shorter start time t_s. The total amount of air used for an engine start $m_{a,s}$ is a piecewise continuous function of the tank pressure. The steps occur when the number of power strokes changes. For an equal number of power strokes the amount of air used increases with an increasing tank pressure mainly because the valve cannot be closed when the desired engine speed is reached. If an immediately deactivatable CV is available the air consumption can be reduced to $m_a(t_s)$. However, the piecewise linearity remains.

5.4.2. Variation of the initial engine position

The throttle strategy during the engine shutdown presented in Section 5.1.3 showed fairly reliable results on the test bench. In this section the importance of the initial engine position is highlighted by simulating the engine start for various initial positions. Figure 5.11 shows the resulting air consumption and start time as a function of the initial engine position ϕ_0. If the start takes place closer to the CV opening position the start

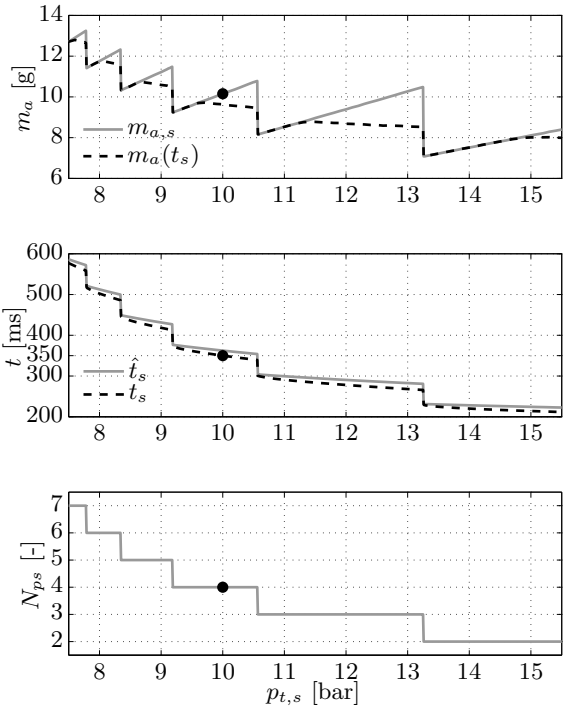

Figure 5.10.: Air consumption, start time and number of power strokes for various tank pressures for $\phi_{CVO,s} = 10\,°\text{CA}$, $\phi_{CVC,s} = 110\,°\text{CA}$ and $d_{CV} = 19\,\text{mm}$. The black dot indicates the optimal result of the design example.

time is shorter because it takes less time until pressurized air is injected and, thus, a high torque is applied. Furthermore, the first CV opening lasts longer since the engine speed is small. Hence, more air is injected, which yields a higher torque. The influence of the start position on the start time is significant. If the engine is started from the BDC, it takes 430 ms. The start from the TDC only takes 259 ms, which is 40% faster.

In contrast, the air consumption is not very sensitive to the initial engine position. For the start positions considered, an increase of just 5% can be observed. The air consumption is rather constant for start positions from BDC to 120 °CA bTDC. This can be explained by the open IVs, through

which air is blown out. The air consumption is highest if the initial position is just before the CV opening because then the engine speed and the cylinder pressure are rather low during the first air injection. Hence, the CV is open for a very long time and a lot of compressed air is injected.

It can be concluded that a good positioning of the engine during the shutdown substantially influences the start time while the air consumption is affected only slightly.

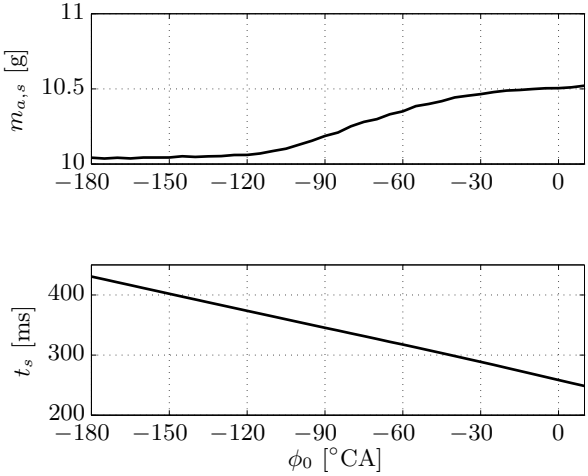

Figure 5.11.: Air consumption and start time for various initial engine positions ϕ_0 for $\phi_{CVO,s} = 10\,^\circ\text{CA}$, $\phi_{CVC,s} = 110\,^\circ\text{CA}$, $d_{CV} = 19\,\text{mm}$ and $p_{t,s} = 10\,\text{bar}$.

5.5. Conclusion

In this chapter, a general design methodology for CSD CVs used for pneumatic engine starts was presented. The design procedure was exemplified for a two-cylinder engine, and the results were experimentally verified. The discrepancy is 3%.

Pneumatic engine starts enable significantly reduced engine start times compared to conventionally started engines. In contrast to conventional combustion-based engine starts, a positive torque is produced already during the first expansion stroke, even without a preceding compression stroke. Another advantage of pneumatic engine starts is that they are

applicable on engines with port-fuel injection as well as those with direct injection.

Starting the engine without burning fuel also reduces the emission of hydrocarbons and carbon-monoxide caused by the incomplete combustion occurring at very low engine speeds.

To sum up, pneumatic engine starts offer the possibility to implement stop/start strategies that satisfy the comfort demands of the driver without significantly increasing the complexity and cost of the whole engine system.

6. Tank Filling

To enable in-cylinder boosting and pneumatic engine starts compressed air needs to be available. To avoid a negative impact on the fuel consumption the energy required for the air compression should not stem from the combustion. During the vehicle deceleration the braking energy can be used to compress air.

There are several ways to compress air. One option is to run the engine as a compressor during deceleration phases, as extensively discussed for HPEs [16, 42, 43]. When referring to this realization the terms internal tank filling or pump mode are used. Alternatively, an additional external compression device could be used. This approach is called external tank filling and is briefly discussed in Section 6.5.

The main focus of this chapter is on the characteristics and the design of a CSD CV used for the pump mode. In this mode the engine is operated as a compressor. During the compression stroke the CV is opened. For an ideal CV without any flow restriction it is optimal to open the valve when the cylinder pressure is equal to the tank pressure and to close it at the beginning of the expansion stroke when the cylinder pressure drops below the tank pressure [5]. However, since the tank pressure varies during the operation of the engine, the optimal CV timing cannot be achieved by a CSD CV with fixed timings.

In the realization with CSD CV, the engine torque cannot be controlled. It is a function of the tank pressure, the engine speed and the chosen CV design.

This chapter is structured as follows: In Section 6.1 the charateristics of the pump mode with a CSD CV are analyzed using a process model. Then, in Section 6.2 design methodologies are presented. One of them is applied in a design example in Section 6.3. In Section 6.4 the performances of a non-variable CSD CV and a variable CSD CV are compared. External tank filling is discussed in Section 6.5. The chapter ends with a conclusion.

6.1. Characteristics

To study the characteristics of the pump mode realized with a CSD CV, a process model of the engine specified in Appendix A is used. A detailed description of the process model can be found in Appendix C. The valve model and limitations from Section 5.1.2 are applied. Since the pump mode is operated in the entire engine operating range, the CV acceleration in the CA domain cannot be increased: $a_{CV,p} = a_{IV}$.

Figure 6.1 shows the air mass transferred per cycle $m_{a,p}$ and the average mass flow from the cylinder to the tank $\dot{m}_{a,p}$ for a fixed CV opening $\phi_{CVO,p}$ and fixed CV closing $\phi_{CVC,p}$.

The main effects which determine the air mass transferred per cycle for a constant tank pressure is the duration during which the CV is open and the cylinder filling at IVC. For low engine speeds, the duration is rather long. However, the cylinder filling is rather poor due to the late IVC of the engine considered ($\phi_{IVC} = 66\,°\text{CA}$ aBDC). As the engine speed increases the better filling performance first leads to an increased mass transfer to the tank. Eventually, the reduced opening duration becomes the dominant effect, and the air mass transferred is reduced. The value of $m_{a,p}$ decreases with an increasing tank pressure since it takes longer until the cylinder reaches the tank pressure which reduces the time duration with a high enough cylinder pressure. Consequently, as a result of the long duration with a large pressure difference, the air mass transferred per cycle is maximal at a low tank pressure and low engine speed.

However, the mean air mass flow to the tank is maximal at low tank pressure and high engine speed. The lower air mass per cycle is overcompensated by the higher number of air transfers per time.

These relations hold generally. The tank filling performance is best at low tank pressures and high engine speeds. Thus, it is always favorable to operate the pump mode at a high engine speed. The gear selection during the deceleration where the pump mode is operated could potentially be used to improve the tank filling performance. Thus, if a vehicle is equipped with an automatic or semi-automatic gear box, these characteristics should be included in the gear box control to promote operating points with a high filling performance, i.e., early downshift during deceleration.

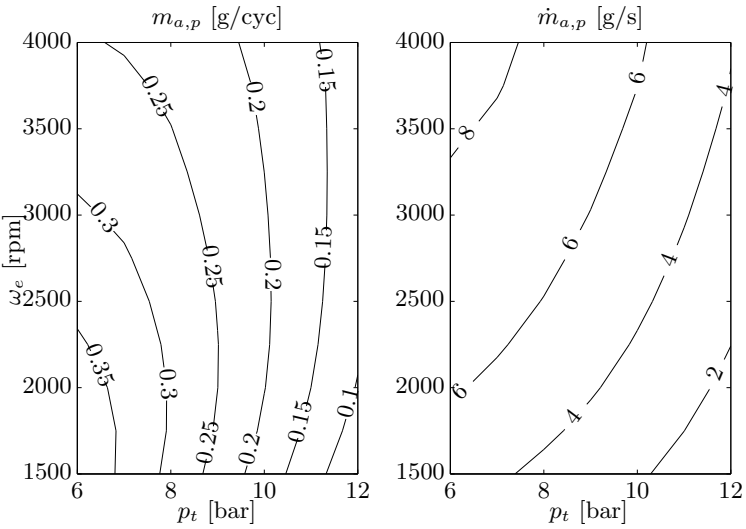

Figure 6.1.: Pump mode performance with fixed CV timing: $\phi_{CVO,p} = 125\,^{\circ}\text{CA}$, $\phi_{CVC,p} = 210\,^{\circ}\text{CA}$. Left: Air mass transferred per cycle from cylinder to tank. Right: Mean air mass flow from cylinder to tank.

6.2. CV design methodologies

The operating conditions, i.e., tank pressure and engine speed, vary substantially during the engine operation. As opposed to a variable CV, the timings of the considered CSD CV cannot be changed during the operation. The challenge is to find good values for the CV timing which perform well under various operating conditions. The objective of the CV design process is to find values for the relevant design variables, which are

$\phi_{CVO,p}$: CV opening angle,
$\phi_{CVC,p}$: CV closing angle.

In this section several approaches are proposed which can be used to determine the CV timings. They are either based on drive cycles or on operating points.

6.2.1. Drive cycle based method

The idea of the drive cycle based method is to optimize the CV timing such that the fuel consumption of the vehicle on a given drive cycle is minimized given that the tank pressure at the end of a drive cycle is not lower than at its beginning (charge sustaining) and the tank pressure is never lower than the minimum tank pressure $\tilde{p}_t = \max\{\tilde{p}_{t,s}, \tilde{p}_{t,b}\}$. By means of the process simulation, the air mass transfer map $\dot{m}_{a,p}(\omega_e, p_t)$ is generated for the CV timings provided by the optimizer. In a quasi-static simulation (QSS) [44] the fuel consumption of the vehicle on a given drive cycle is determined. It is provided to the optimizer, which calculates new CV timings until the optimal CV timings $\phi^*_{CVO,p}$ and $\phi^*_{CVC,p}$ are found. The particle swarm optimization [41] showed a good performance. Figure 6.2 illustrates the calculation procedure.

One prerequisite of this method is that the air transfer maps of the boost and the start mode need to be known.

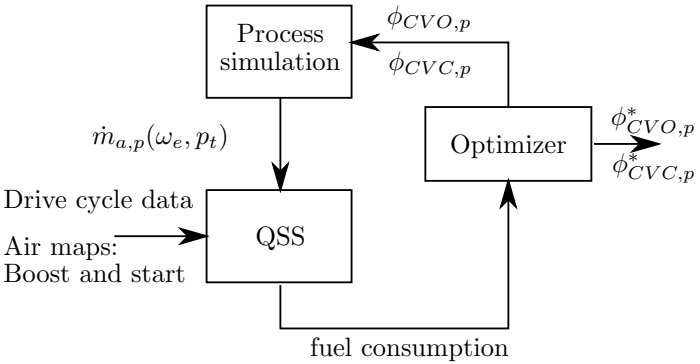

Figure 6.2.: Calculation procedure of drive cycle based method.

6.2.2. Operating point based method

In this method, the CV timing is determined by evaluating one or several operating points as opposed to an entire drive cycle. Each operating point is characterized by a tank pressure and an engine speed.

The goal is to find the optimal CV timings $\phi^*_{CVO,p}$ and $\phi^*_{CVC,p}$ which maximize the weighted sum of the air masses transferred in n operating

points $\Omega_i = \{\omega_{e,i}, p_{t,i}\} \in \Omega = \mathbb{R}^{n\times 2,+}$, that is

$$\{\phi^*_{CVO,p}, \phi^*_{CVC,p}\} = \text{argmax} \sum_{i=1}^{n} w_i \cdot \dot{m}_{a,p}(\Omega_i, \phi_{CVO,p}, \phi_{CVC,p}), \quad (6.1)$$

where $w_i \geq 0$ is the weighting factor of the operating point i. It can be used to penalize specific operating points or operating regions. The weighting factor can be chosen as a function of the tank pressure and/or the engine speed since they both vary during the operation. It is reasonable to penalize low tank pressures more strongly because then a good filling performance is desirable. The optimization problem can be solved with a numerical optimization method (e.g., particle swarm optimization [41]).

The n operating points in Ω should be selected reasonably, i.e., by considering the requirements of the other modes, e.g., minimum tank pressure for in-cylinder boosting or for the pneumatic start, or by considering the operating points which most frequently occur on a drive cycle.

Comparison to optimal values

Another possibility is to compare the performance of a CSD CV with fixed timing to the one with variable timing, e.g., by selecting the design

- for which the maximal absolute deviation from the value with variable CV timing is minimal, or
- for which the maximal relative deviation from the value with variable CV timing is minimal.

For this case the calculation procedure consists of the following steps:

1. Determine the maximal air mass $\dot{m}^*_{a,p}(\Omega)$ that can be transferred with a CSD CV that features variable timing in n operating points $\Omega_i = \{\omega_{e,i}, p_{t,i}\} \in \Omega = \mathbb{R}^{n\times 2,+}$.
2. Find the CV timings $\phi^*_{CVO,p}$ and $\phi^*_{CVC,p}$ which minimize the largest absolute deviation from the maximal air mass

   $$\{\phi^*_{CVO,p}, \phi^*_{CVC,p}\} = \text{argmin} \, \|\dot{m}^*_{a,p}(\Omega) - \dot{m}_{a,p}(\Omega, \phi_{CVO,p}, \phi_{CVC,p})\|_\infty, \quad (6.2)$$

   where $\dot{m}_{a,p}(\Omega, \phi_{CVO,p}, \phi_{CVC,p})$ is a vector which contains the air masses transferred in the operating points Ω for the CV timings $\phi_{CVO,p}$ and $\phi_{CVC,p}$. Alternatively, the largest relative deviation from the maximal air mass could be minimized.

As in the method described previously, the optimal design depends on the choice of Ω.

6.3. Design example

In this section a design example is presented. The criterion used is the following: Find the design which has the minimum absolute deviation in the mass flow from the maximal mass flow achievable with a variable valve-train, see Equation (6.2). The 25 operation points Ω considered are spanned by $p_t \in \{6, 7.5, 9, 10.5, 12\}$ bar and $\omega_e \in \{1500, 2100, 2750, 3400, 4000\}$ rpm.

With the design methodology the following optimal CV timings are found:

$$\phi^*_{CVO,p} = 106\,^\circ\text{CA} \tag{6.3}$$

$$\phi^*_{CVC,p} = 213.5\,^\circ\text{CA}. \tag{6.4}$$

These valve timings correspond to the optimal valve timing in the operating point $p_t = 6.85\,\text{bar}$ and $\omega_e = 2580\,\text{rpm}$. This operating point is located at the lower end of the tank pressure range considered and in the middle of the engine speed range considered. It reflects the best compromise. Figure 6.3 shows the mean air mass flow for the optimal fixed CV timing. Compared to data shown in Figure 6.1, the performance at a low tank pressure and a high engine speed is improved. However, it is worse for a high tank pressure and a low engine speed.

6.4. Comparison of CSD CV with fixed vs. variable timing

Any additional variability in the valve-train can be used to improve the tank filling performance. In this section the improvement of the tank filling performance is determined if fully variable CSD CV are used. Furthermore, the variabilities required in the CV opening and closing instants are quantified.

With a CSD CV with variable valve timing the valve opening and closing angles, $\phi_{CVO,p}$ and $\phi_{CVC,p}$, can be varied during the operation while the acceleration in the CA domain remains fixed and equal to the one with fixed CV timings.

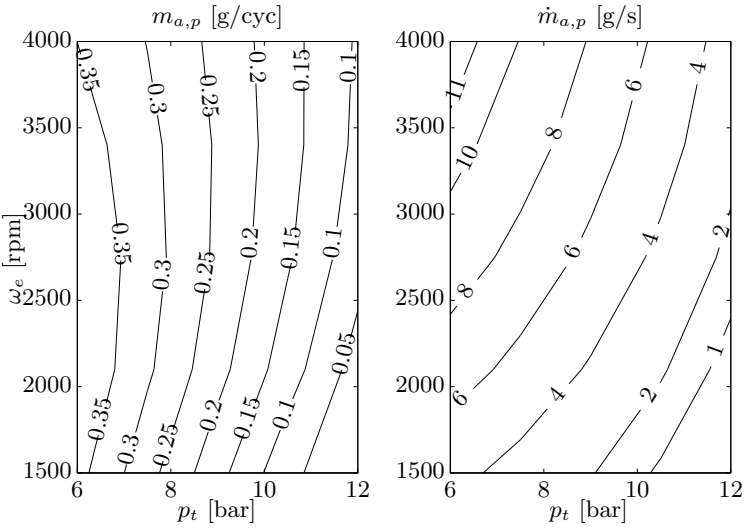

Figure 6.3.: Pump mode performance with fixed CV timing: $\phi^*_{CVO,p} = 106\,^\circ\text{CA}$, $\phi^*_{CVC,p} = 213.5\,^\circ\text{CA}$. Left: Air mass transferred per cycle from cylinder to tank. Right: Mean air mass flow from cylinder to tank.

Figure 6.4 shows the optimal performance with variable valve timing. The depicted values were found by optimizing the CV timings in each operating point. (The corresponding CV timings are depicted in Figure 6.6.) Clearly, the air mass per cycle predominately depends on the tank pressure. At a lower engine speed more time is available for the air exchange. At a high engine speed the cylinder filling and hence the pressure level is higher, which obviously compensates the shorter time duration. Furthermore, even at low speeds and high tank pressures air is transferred to the tank.

Figure 6.5 shows the absolute and the relative deviations in the air mass flows of the solution presented in Section 6.3 and the one achievable with variable valve timing. For the most part, the air mass transfer with fixed timing is smaller by less than 20%. In the region with a deviation of more than 20%, the air mass transfer is rather small (see Figure 6.3).

Particularly at low engine speeds and high tank pressures, the valve timing variability thus has clear advantages. Furthermore, the benefits

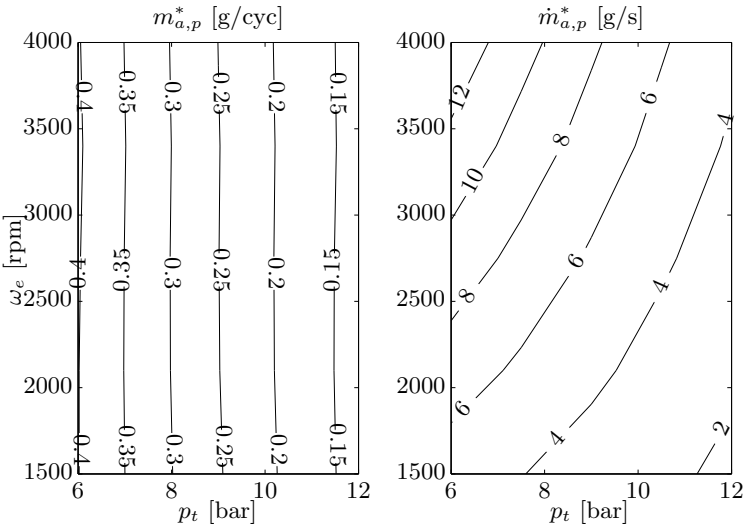

Figure 6.4.: Pump mode performance for a variable CSD CV. Left: Air mass transferred per cycle from cylinder to tank $m^*_{a,p}$. Right: Mean air mass flow from cylinder to tank $\dot{m}^*_{a,p}$.

of the variable valve timing increase with the size of the operating range considered, particularly the size of operating range of the tank pressure.

Analysis of optimal timing of variable CSD CV

The sensitivity of the CV timing remains to be analyzed. Figure 6.6 shows the optimal CV opening and CV closing angles for the variable CSD CV. The curves clearly show that:

- The higher the engine speed is the earlier the CV should open. At higher engine speeds the cylinder filling is better and hence the tank pressure is reached earlier in the compression;
- The higher the tank pressure is the later the CV should open because flow from the tank to the cylinder should be avoided. Hence, the CV should open once the cylinder pressure is higher than the tank pressure, which is closer to the TDC for higher tank pressures;
- The higher the engine speed is the later the CV should close;

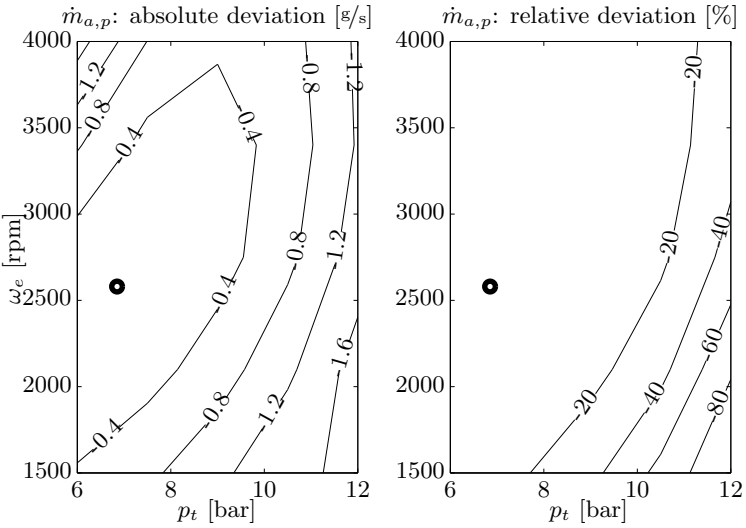

Figure 6.5.: Left: Absolute deviation in the air mass flow to the tank $m_{a,p} - m^*_{a,p}$. Right: Relative deviation in the air mass flow to the tank $m_{a,p}/m^*_{a,p} - 1$. For $\phi_{CVO,p} = 106\,^\circ$CA, $\phi_{CVC,p} = 213.5\,^\circ$CA.

- The higher the tank pressure is the later the CV should close.

The maximal difference in the optimal CV opening angle for the operating range considered amounts to 50°CA. The maximal difference in the optimal CV closing angle amounts to 20°CA. Thus, the sensitivity to the CV opening is larger.

6.5. External tank filling

In the case of external tank filling the compressed air is not directly added from the cylinder to the tank. There are several realizations possible.

Connection via intake or exhaust manifold

Several researchers have investigated so-called indirectly connected HPEs [45, 46, 47]. These realizations of HPEs are characterized by an indirect connection between the cylinder and the tank, e.g., via the intake or the exhaust manifold. Most of the solutions presented involve additional

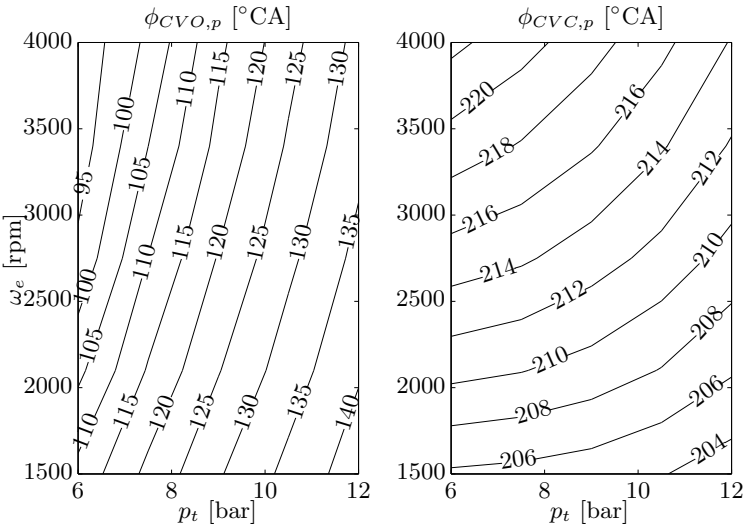

Figure 6.6.: Optimal valve timing in the pump mode for a variable CSD CV. Left: Optimal CV opening angle. Right: Optimal CV closing angle.

hardware or require variable valve timing on the intake and/or exhaust valves. Furthermore, higher losses of air are usually associated with such designs because the connecting pipes between engine valve and tank valve, e.g., intake manifold, have to be pressurized before air can be transferred to the tank. The filling of the connecting pipes takes time, and the air used thus cannot be transferred to the tank but is wasted.

Additional compression device

Another option is the use of an additional compressor which is driven either mechanically or electrically. The pneumatic engine start and in-cylinder boosting require a tank pressure which is substantially higher than the intake manifold pressure. Consequently, the compression ratio of the compression device needs to be rather high. In case of a single stage compression, piston compressors are best suited for the mass flows and tank pressures considered [48]. In the automotive industry, external piston compressors are commonly used for the braking system in heavy-duty road vehicles (e.g., trucks, busses) and trains. The compressors are

usually mechanically driven and can be engaged to the drive train with an additional clutch.

6.6. Conclusion

In this chapter internal and external tank filling were discussed. Design methodologies for the CV were presented with which suitable CV timings can be found. Simulations showed that it is best to determine the optimal CV timing for an operating point which is in the middle of the speed range considered and towards the lower end of the tank pressure range considered. In general, it is always favorable to operate the pump mode at high rotational speeds.

Furthermore, it was shown that the benefit of a CSD CV with variable timing in the operating range considered is rather small, particularly if the vehicle is equipped with an automatic gear box. The variability mainly pays off if the tank pressure range is very large.

7. Air Assist System Design

In the previous chapters, each mode has been analyzed and designed independently. However, in an air assisted TC SI engine the modes are linked to each other by the CV diameter and the tank pressure. Hence, a coordinated design of the modes is required. In particular, the minimum tank pressures of the boost mode and the pneumatic engine start should be chosen to match. Furthermore, the pump mode should be designed for the tank pressure region where the boost mode and the engine start are operated.

In this chapter a system design methodology is presented which merges the requirements of all modes. It is used to determine the minimum tank pressure and the valve lift profiles of each mode. Additionally, an appropriate tank size is derived.

The chapter is structured as follows: In Section 7.1 the system design methodology is presented. In Section 7.2 it is applied for a Nissan Micra, whose NA engine is replaced with an air assisted TC SI engine. The properly designed system is then used to study the system properties in Section 7.3. The chapter ends with a conclusion.

7.1. System design methodology

In this section a system design methodology is presented which merges the design methodologies presented in the Sections 3.3, 5.2 and 6.2. It aims at harmonizing the design processes, such that the system performance is optimized rather than the performance of each mode individually.

For the following derivations it is assumed that the CV diameter d_{CV} is given, e.g., as large as possible. Furthermore, each mode is realized with a separate cam, i.e., at least three different cams are necessary.

The proposed system design consists of four steps:

1. Design of air usage modes;
2. Design of tank filling mode;
3. Generation of air transfer maps;

4. Tank sizing.

The design process is iterative. In the following sections each step is discussed. Figure 7.1 illustrates the entire design procedure.

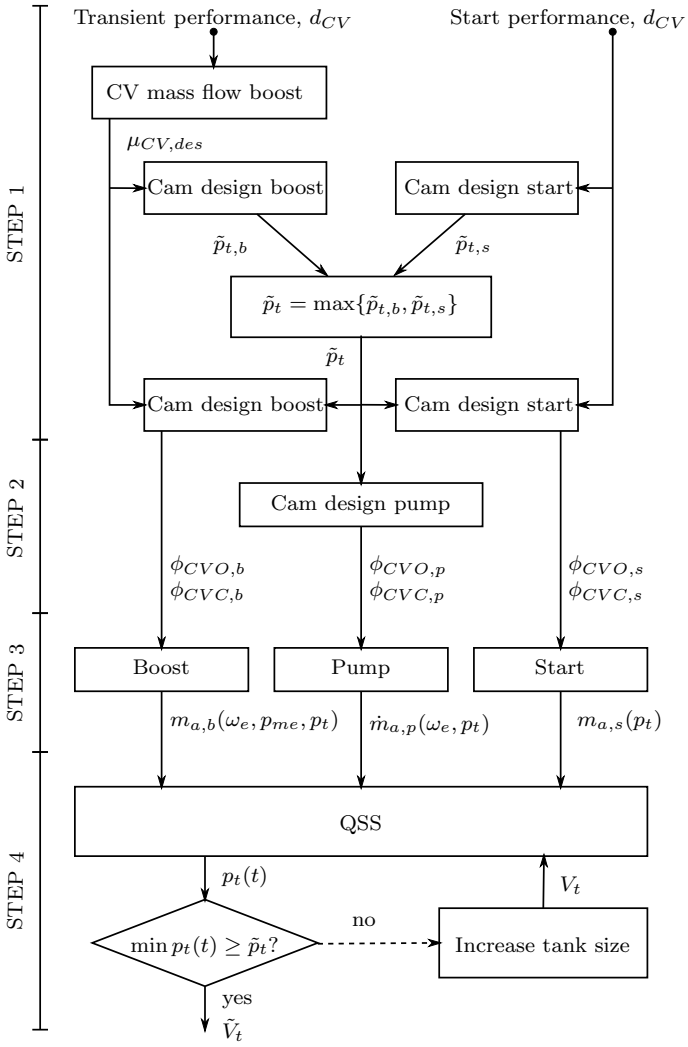

Figure 7.1.: Design procedure for an air assisted TC SI engine.

Step 1: Design of air usage modes

The pneumatic start and the boost mode both have a minimum tank pressure. The goals of the first step are to bring the minimum tank pressures $\tilde{p}_{t,s}$ and $\tilde{p}_{t,b}$ into agreement and to determine the CV timings as well as the CV acceleration of the two modes.

The design process starts with the determination of the CV timings, the CV acceleration and the minimum tank pressure $\tilde{p}_{t,s}$ of the pneumatic engine start. The process model is used for this.

Simultaneously, the CV mass flow $\mu_{CV,des}$ is determined using the mean value model of the engine. It is followed by the determination of the CV timings, the CV acceleration and the minimum tank pressure $\tilde{p}_{t,b}$ for the boost mode.

Then, the minimum tank pressure of the system is determined as $\tilde{p}_t = \max\{\tilde{p}_{t,b}, \tilde{p}_{t,s}\}$. Most likely, the cam design of the boost or the start mode is conducted again with the minimum tank pressure $\tilde{p}_t$ to find new valve lift parameters. The results of this step are the minimum tank pressure $\tilde{p}_t$ and the CV lift profile parameters for the boost $\{\phi_{CVO,b}, \phi_{CVC,b}, a_{CV,b}\}$ and the start mode $\{\phi_{CVO,s}, \phi_{CVC,s}, a_{CV,s}\}$.

Step 2: Design of tank filling mode

The second step aims at finding the CV timings of the pump mode. For that purpose, the pump mode design methodology described in Section 6.2 is applied using the process model. In order to define reasonable operating points Ω in the operating point based method, it is necessary to know the minimum tank pressure $\tilde{p}_t$. The results of this step are the CV timings of the pump mode $\{\phi_{CVO,p}, \phi_{CVC,p}\}$.

Step 3: Generation of air transfer maps

Now that the CV profiles of all modes are known, the air transfer map of each mode is generated.

Step 4: Tank sizing

With all air transfer maps at hand, a quasi-static simulation (QSS) can be run to determine the tank pressure trajectory on a drive cycle. The mode selection is crucial for the determination of the tank pressure trajectory. In the HPE [6] the mode selection was done based on the solution of an optimal control problem. The optimization was necessary because for

certain driving conditions the torque could have been provided by either the combustion mode or the pneumatic motor mode. Since the pneumatic motor mode is omitted in the air assisted TC SI engines this degree of freedom is not available anymore. Thus, an optimization is not necessary. The activation criteria for the pump and the start mode are trivial, i.e., pump when the kinetic energy loss is larger than the work necessary to compress air and start the engine after it was stopped, respectively. The boost mode activation criterion is more challenging. It is discussed in the following section.

Given that all criteria are known, the tank pressure trajectory can be calculated for a given tank volume V_t. The minimum tank pressure of the resulting tank pressure trajectory should be larger than or equal to the minimum tank pressure $\tilde{p}_t$. Furthermore, a charge sustaining solution is desirable, i.e., the tank pressure at the end of the drive cycle is larger than or equal to the initial tank pressure.

The continuation of the design process depends on its goal, which could be

- to check the feasibility of a given tank size: The result is yes or no.
- to find the minimum tank volume $\tilde{V}_t$: For that purpose the tank volume is adjusted until the minimum tank pressure on the drive cycle is equal to the minimum tank pressure $\tilde{p}_t$, i.e.,

$$\min_t p_t(t) = \tilde{p}_t, \tag{7.1}$$

  and the solution is charge sustaining.

7.1.1. Boost mode activation criterion

The conditions which have to be fulfilled for a boost mode activation substantially influence the air consumption and thus the tank size. They can be used to map various driving styles. Its formulation is up to the OEM. In this section ideas and aspects are discussed which need to be considered. Here only activation criteria are discussed that can be used for the derivation of the tank size. The implementation of the boost mode activation on the vehicle's engine control unit is not considered.

In the following, three boost mode activation critieria for the derivation of the tank size are presented. This list does not claim to be complete but rather presents ideas for how to tackle the problem. For the evaluation of the criteria in the QSS framework the current (k) and zhe previous ($k-n$) operating points are used.

Model-based activation criterion

As opposed to an NA engine, due to the turbo lag, a TC SI engine cannot perform every change in operating points within 1 s (= typical sample time T_s in QSS). By means of a dynamic engine model, a formulation of the turbo lag suitable for QSS can be derived. The boost mode is thus activated if the requested operating point change from time step $k-1$ to k cannot be performed without boosting:

$$p_{me}(k) \geq p_{me,max}(\omega_e(k), p_{me}(k-1), \omega_e(k-1)), \tag{7.2}$$

where $p_{me,max}$ denotes the highest torque that can be reached in the sample time T_s without boosting.

Rule-based activation criterion

Another option is to formulate the activation criterion as a list of conditions which have to be fulfilled, e.g.

$$\begin{aligned} p_{me}(k) - p_{me}(k-n) > \Delta p_{me,thr}(.) \quad &\wedge \\ p_{me}(k) > p_{me,thr}(.), & \end{aligned}$$

where $k \geq n \geq 1$. In this formulation the boost mode is activated if the torque change is larger than a threshold value $\Delta p_{me,thr}(.)$ and the desired torque is larger than a threshold value $p_{me,thr}(.)$ (which is typically in the turbocharged region). The list of conditions can arbitrarily be extended with conditions on the engine speed, the turbocharger speed, etc. Furthermore, the threshold values can either be constants or functions, e.g., of the engine speed.

Interpretation of accelerator signal

If measurement data of a drive cycle is available, the accelerator signal u_{th} can be used to determine the boost activation instead of the torque signal. The accelerator signal is better suited because it contains information about the driver's wish. As before, the activation criterion can be formulated as a list of conditions

$$\begin{aligned} u_{th}(k) - u_{th}(k-n) > \Delta u_{th,thr}(.) \quad &\wedge \\ u_{th}(k) > u_{th,thr}(.). & \end{aligned}$$

This formulation can be extended with additional conditions as described above.

7.1.2. Drive cycle dependency

Apart from the activation criterion, the drive cycle considered influences the tank sizing, e.g., the number of starts or the number of boosts. Drive cycles developed for the determination of the fuel consumption generally are not suitable for the tank sizing. The velocity trajectories of most of them, e.g., NEDC, WLTP, FTP, are too gradual to require boosting. For the tank size evaluation a designated drive cycle needs be used, e.g., a drive cycle which captures the most aggressive driving that is desired with the vehicle considered.

For a worst case analysis, the drive cycle should contain many boosts at low speeds and many engine starts.

7.2. Design example

In this section the design methodology presented previously is applied in a design example. The goal is to determine the cam profile of all modes and the minimum tank size of the air assisted 0.75 l TC SI engine described in Appendix A. This engine replaces the 1.24 l NA engine of a Nissan Micra. Both engines have approximately the same rated power. In [6] a fuel saving potential of 28% was validated by experiments on the FTP for this replacement.

The relevant data for the design of pneumatic modes are $d_{CV} = 19\,\text{mm}$ and $\phi_{IVC} = 66\,^{\circ}\text{CA}$. The vehicle parameters are given in Table 7.1. The friction coefficients are identified from rolling tests conducted by the Swiss Federal Laboratories for Material Science and Technology (EMPA).

The drive cycle chosen for the tank sizing is an aggressive version of the NEDC drive cycle, called the aNEDC. The vehicle acceleration on the aNEDC is three times higher than in the regular NEDC. The gears are selected in accordance with the regular version, i.e., shifting occurs at the same vehicle speed. Figure 7.2 shows the speed and gear profiles of both drive cycles.

In the following sections the steps described above are performed to find the minimum tank size.

Step 1: Design of air usage modes

For the engine start the performance requirements of Section 5.3 hold, i.e., a pneumatic engine start from 0 to 1200 rpm should be achieved in

Table 7.1.: Vehicle parameters: Nissan Micra.

vehicle base mass	1150	kg
wheel radius	0.2851	m
$c_{r,0}$	0.0076	
$c_{r,1}$	$5.1 \cdot 10^{-6}$	$^{s}/_{m}$
$A_f c_d$	0.8575	m^2
final gear ratio	4.07	
1st gear ratio	3.73	
2nd gear ratio	2.15	
3rd gear ratio	1.39	
4th gear ratio	1.03	
5th gear ratio	0.82	

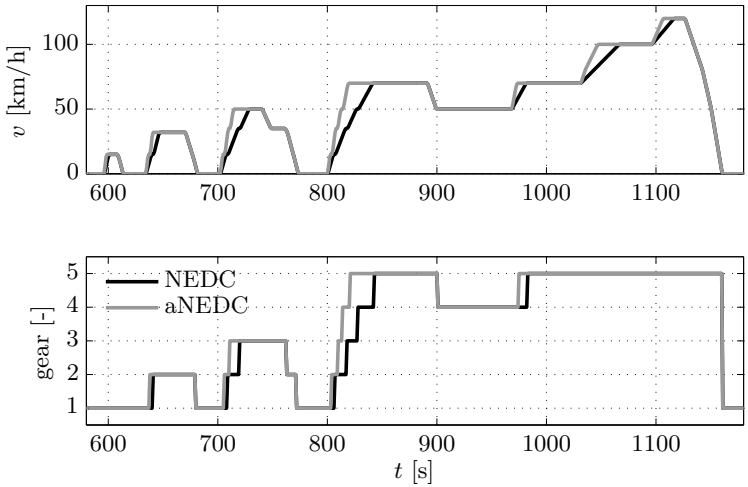

Figure 7.2.: Comparison of velocity and gear trajectories of the NEDC and the aNEDC on the last part of the ECE and on the EUDC.

0.35 s. According to the results presented in Section 5.3 the minimum tank pressure required is $\tilde{p}_{t,s} = 10$ bar.

The performance requirements of the boost mode stated in Section 3.4 also hold in this example, i.e., a torque step from 1.7 bar to the full load

at 2000 rpm should take 1 s. Consequently, the desired CV mass flow is $\mu_{CV,des} = 34.9\,\mathrm{g/s}$. According to Table 3.2, the minimum tank pressure for the boost mode is $\tilde{p}_{t,b} = 8.3\,\mathrm{bar}$.

Consequently, the minimum tank pressure is $\tilde{p}_t = \tilde{p}_{t,s} = 10\,\mathrm{bar}$. Since the minimum tank pressure is larger than $\tilde{p}_{t,b}$, the boost cam design is adjusted. Specifically, the CV closes earlier which increases the robustness of mixture flow to the tank. The resulting values for the CV profiles are listed in Table 7.2. The accelerations were derived from the corresponding specifications on the engine speed $\omega_{e,b}$ and $\omega_{e,s,max}$, respectively.

Table 7.2.: CV timings of boost and start cams. Note: $\phi = 0\,^\circ\mathrm{CA}$ is at BDC before the compression stroke.

Boost	start
$\phi_{CVO,b} = 66.0\,^\circ\mathrm{CA}$	$\phi_{CVO,s} = 190.0\,^\circ\mathrm{CA}$
$\phi_{CVC,b} = 120.4\,^\circ\mathrm{CA}$	$\phi_{CVC,s} = 290.0\,^\circ\mathrm{CA}$
$a_{CV,b} = 4 \cdot 10^{-6}\,\mathrm{m/^\circ CA^2}$	$a_{CV,s} = 30.4 \cdot 10^{-6}\,\mathrm{m/^\circ CA^2}$

Step 2: Design of tank filling mode

To find the CV profile for the pump mode cam, the single operating point optimization is chosen. According to the results presented in Section 6.3, it is reasonable to determine the CV timings for a tank pressure close to the lower end of the operating range considered and for a medium engine speed. Figure 7.3 shows the histogram of the engine speeds occurring during the deceleration phases on the aNEDC. Based on this result, the optimization for the CV timings is performed for $\omega_e = 2000\,\mathrm{rpm}$ and $p_t = 10.5\,\mathrm{bar}$.

The resulting values for the valve timings are $\phi_{CVO,p} = 133\,^\circ\mathrm{CA}$ and $\phi_{CVC,p} = 207\,^\circ\mathrm{CA}$.

Step 3: Generation of air transfer maps

This step is straightforward. The values of $m_{a,b}(\omega_e, p_{me,b}, p_t)$ are taken from Section 4.6. The values of $m_{a,s}(p_t)$ are those presented in Figure 5.10.

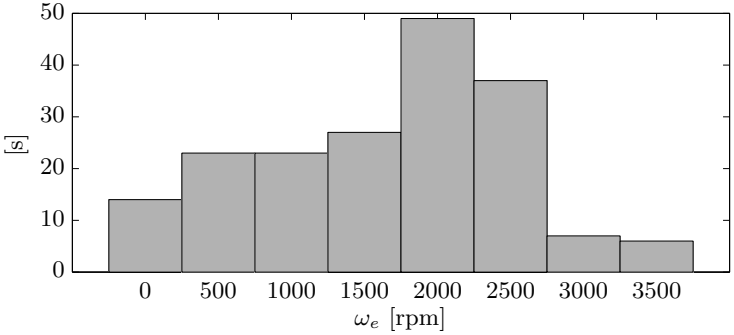

Figure 7.3.: Histogram of engine speed during deceleration phases on NEDC.

Step 4: Tank sizing

With all air transfer maps at hand, the tank volume can be determined. The sample time of the drive cycle data is $T_s = 1\,\mathrm{s}$. The activation criterion used is

$$p_{me}(k) > 12\,\mathrm{bar} \quad \wedge$$
$$p_{me}(k) - p_{me}(k-1) > 5\,\mathrm{bar}.$$

For the evaluation of the boost air map the maximum torque value of the following 3 s is used

$$p_{me,b}(k) = \max_{i \in [k, k+3\,\mathrm{s}/T_s]} p_{me}(i). \tag{7.3}$$

The tank is assumed to be iso-thermal with a temperature of $\vartheta_t = 308\,\mathrm{K}$. The value of the initial tank pressure is $p_t(0) = 12\,\mathrm{bar}$.

7.2.1. Results

The evaluation of Step 4 results in a minimum tank volume of $\tilde{V}_t = 9.25\,\mathrm{l}$. Figure 7.4 shows the resulting trajectories of the torque, the engine speed and the tank pressure. In general, boosting is necessary when shifting up or during accelerations in high gears. The tank volume is limited by the minimum tank pressure since at $t = 127\,\mathrm{s}$ the tank pressure is equal to the minimum tank pressure. The resulting solution is charge sustaining since the pressure at the end is 2.4 bar higher than the pressure at the beginning. Thus, the net increase in air stored $\Delta M_{a,t}$ amounts to 25 g.

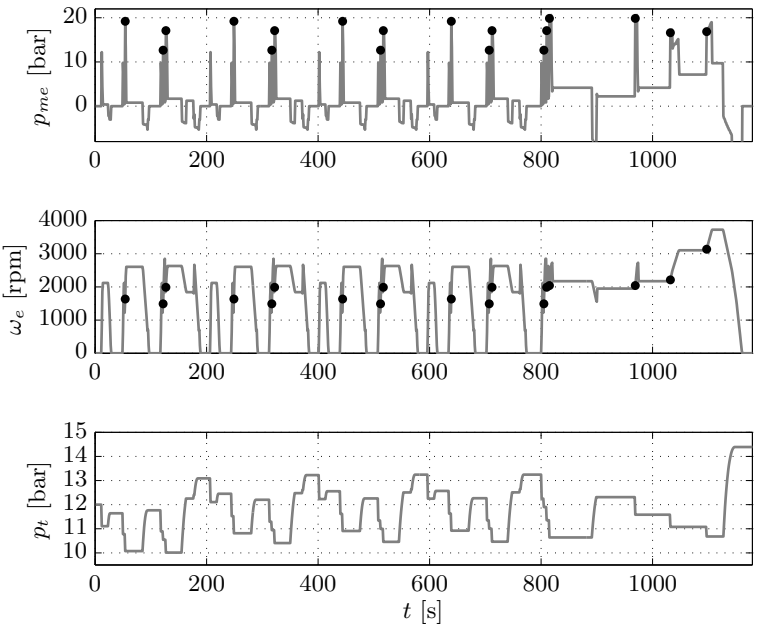

Figure 7.4.: Mean effective pressure p_{me}, engine speed ω_e and tank pressure p_t trajectories on the aNEDC drive cycle. The black dots indicate boosting.

In Table 7.3 the values of the cumulative air masses transferred in each mode $M_{a,i}$ are listed. The drive cycle chosen requires 18 boosts and has 13 engine starts. More air is used for starting than for boosting. In the pump mode 253 g air are charged during 135 s.

Table 7.3.: Cumulative air masses transferred in each mode on the aNEDC for the minimum tank size.

Mode	boost	start	pump
$M_{a,i}$	101 g	127 g	253 g
number	18	13	135 s

Dependence on initial tank pressure

If the initial tank pressure is small, i.e., close to the minimum tank pressure, a large tank volume is necessary to avoid a pressure drop below the minimum value during the first engine start. At a large initial tank pressure the tank volume can be much smaller. Figure 7.5 shows the relation between the initial tank pressure and the minimum tank size. Thus, it is recommended to select an initial tank pressure which is in the middle between the minimum (=10 bar) and the maximum (=15.5 bar) tank pressures.

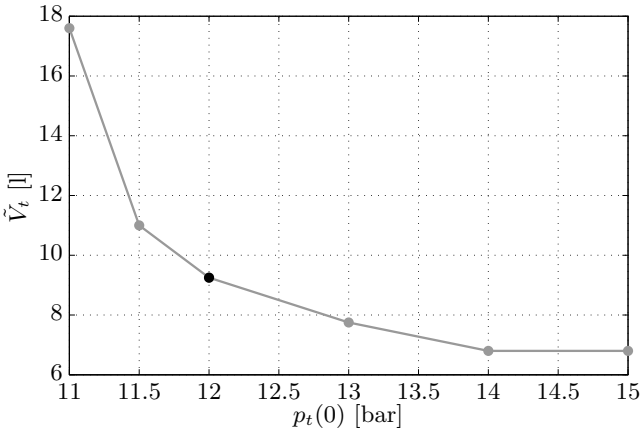

Figure 7.5.: Minimum tank volume $\tilde{V}_t$ as a function of the initial tank pressure $p_t(0)$.

7.3. System properties

The well-designed system is used to study the system properties. The tank pressure change depends on the tank size and the air mass transferred:

$$p_t(k+1) = p_t(k) + \frac{R_a \cdot \vartheta_t}{V_t} \cdot m_{a,l}(p_t(k), \omega_e(k), p_{me}(k)), \tag{7.4}$$

where $l = \{b, p, s\}$ indicates the mode and $m_{a,p} = \dot{m}_{a,p} \cdot T_s$.

In the pump mode the air mass transferred $m_{a,p}$ is sensitive to the tank pressure and the engine speed. The air consumption for the engine start

shows a medium sensitivity to the tank pressure, mainly because of its piece-wise continuous characteristics. On the other hand, boosting is not very sensitive to the tank pressure. The consequences of these differing dependencies are highlighted in this section by studying the system behavior for various tank sizes and various gear profiles during the vehicle deceleration.

7.3.1. Tank volume

As stated in Equation (7.4) the tank size influences the tank pressure trajectory. It acts as a low-pass filter. In this section the differences between a small and a large tank volume are discussed. For that purpose, a QSS is performed for $V_t = 9.25\,\mathrm{l}$ and $V_t = 18.5\,\mathrm{l}$. Figure 7.6 shows the resulting tank pressure trajectories. The filter properties of the large tank are well noticeable by the lower amplitude of the pressure oscillations.

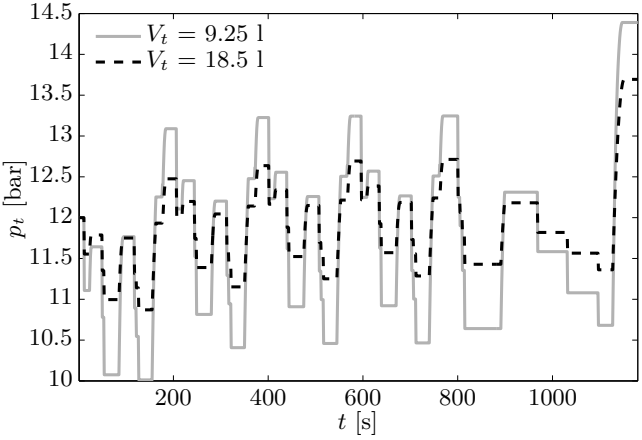

Figure 7.6.: Tank pressure trajectories for two different tank volumes.

Table 7.4 lists the total amount of air transferred in each mode. Boosting requires the same amount of air with both tank sizes due to its low sensitivity to the tank pressure. With the larger tank, starting requires slightly less air since the tank pressure at the engine start is lower. However, in the pump mode 3% more air is transferred to the larger tank. On the one hand this increase is due to the longer duration with pumping (+8 s). On the other hand it is a result of the better filling performance

which generally increases with a decreasing tank pressure. For a small tank, the filling performance at the beginning of a deceleration phase is usually better than the one with a large tank due to the lower tank pressure. However, as a result of the small tank the tank pressure increases faster, which leads to a decrease of the filling efficiency below the one achieved with a large tank. Furthermore, the instant at which no more air can be transferred is reached earlier with a smaller tank. Thus, the filling duration with a small tank tends to be shorter.

Finally, the increase of the air mass $\Delta M_{a,t}$ in the large tank is 44% higher than the one in the small tank.

Aside from the increased air mass at the end of the drive cycle, the safety margin, i.e., the margin to the minimum tank pressure, is considerably larger with a larger tank. Hence, the system design is more robust to errors in the assumptions and to disturbances.

Table 7.4.: Cumulative air mass transferred in each mode on the aNEDC for two different tank sizes.

	$V_t = 9.25\,\mathrm{l}$	$V_t = 18.5\,\mathrm{l}$	
$M_{a,b}$	101 g	101 g	+0.0%
$M_{a,s}$	127 g	124 g	−2.4%
$M_{a,p}$	253 g	261 g	+3.2%
$\Delta M_{a,t}$	25 g	36 g	+44.0%
t_p	135 s	143 s	+5.9%

7.3.2. Gear selection during deceleration

Besides the dependence on the tank pressure, the filling performance is also influenced by the engine speed. In general, the performance is better at high engine speeds. Therefore, the system behavior is analyzed for two additional gear profiles which have higher engine speeds during the deceleration phases. In profile 1, the standard gear is decreased by 1 during the deceleration phases given that the pump mode can be enabled in the lower gear, i.e., torque is high enough. In profile 2, the standard gear is always decreased by at least one gear during the deceleration phases. Additionally, the standard gear is decreased by two on the EUDC provided that the maximum engine speed is not exceeded. Table 7.5 lists the results and Figure 7.7 shows the resulting engine speed and tank pressure trajectories.

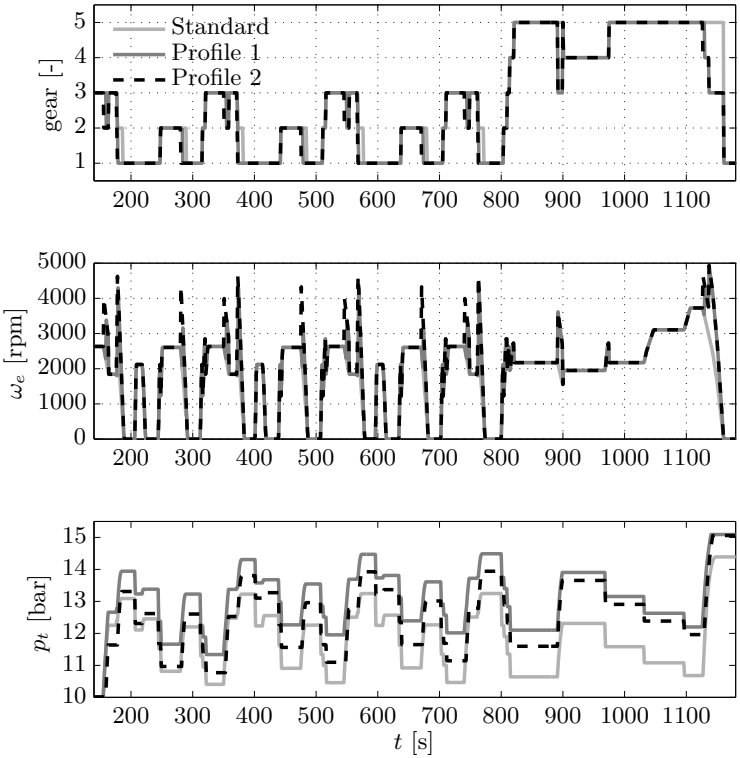

Figure 7.7.: Gear number, engine speed and tank pressure trajectories for 3 different gear profiles for $t \geq 140\,\mathrm{s}$.

With profile 1, the average tank pressure $\bar{p}_t$ is larger than the one with the standard profile. Thus, the tank filling performance is lower. However, the tank pressure at the start is often high enough to achieve the pneumatic start with fewer power strokes, which substantially lowers the air consumption. All in all, more air is in the tank at the end of the drive cycle than with the standard gear profile, which is mainly due to the lower air demand of the engine starts.

In profile 2, the average tank pressure is between the standard and the profile 1. This pressure level also allows for some engine starts with a decreased air consumption. The resulting charging time t_p is rather short because an early downshift leads to phases with too low a torque for the compression of air. Nevertheless, more air is charged than with the standard gear profile. The improved filling efficiency results from the

high mean engine speed during the deceleration $\bar{\omega}_{e,dec}$. All in all, the tank pressure at the end of the drive cycle is equal to the one with profile 1 and thus higher than the one of the standard profile.

The influence of the gear profile on the amount of air used for boosting is negligible, which is due to the rather low sensitivity to the tank pressure.

It can be concluded that a higher tank pressure level leads to a lower pump performance and a decreased air demand for the starts. The same overall performance can be achieved with a slightly lower tank pressure level but with higher engine speeds.

Table 7.5.: Cumulative air mass transferred in each mode on the aNEDC for various gear profiles.

Gear profile	standard	profile 1		profile 2	
$M_{a,b}$	101 g	102 g	+1.0%	102 g	+1.0%
$M_{a,s}$	127 g	108 g	−15.0%	121 g	−4.7%
$M_{a,p}$	253 g	242 g	−4.3%	255 g	+0.8%
$\Delta M_{a,t}$	25 g	32 g	+28.0%	32 g	+28.0%
t_p	135 s	128 s	−5.2%	113 s	−16.3%
$\bar{p}_t$	11.7 bar	12.8 bar		12.3 bar	
$\bar{\omega}_{e,dec}$	1700 rpm	2300 rpm		2600 rpm	

7.4. Conclusion

In this section the design methodologies of all modes are merged to a system design procedure. It consists of four steps: Equalize the minimum tank pressures and design the boost and start mode, design the pump mode for the corresponding tank pressure level, generate the air transfer maps, and find the tank size.

The properly designed system was then analyzed. The air exchange in the pump and the start mode show a strong dependency on the tank pressure. However, the air consumption of the boost mode is rather robust to the tank pressure. From a design perspective the tank pressure trajectory can be influenced mainly by the tank size and the gear shifting strategy.

8. Conclusions and Outlook

It is not the objective of this chapter to provide conclusions about all aspects of this work, as this has been done in each of the previous chapters. The aim is to provide general conclusions for the field of air assisted TC SI engines. Furthermore, arising challenges are discussed, and an outlook on future research in this field is given.

Conclusions

In spite of all its well-known weaknesses, the internal combustion engine will continue to be the most important means of automobile propulsion and is expected to remain so for at least another one or two decades. Directly air assisted TC SI engines offer a great potential to reduce the fuel consumption of compact class vehicles. For reasons of driveability and cost strong downsizing and turbocharging has not yet been applied in this largest market segment. By using a CSD CV the additional system costs and complexity are reduced in comparison to a HPE with fully variable valves. In-cylinder boosting as well as the engine start can still be realized while the pneumatic motor mode is omitted. The performance of the pump mode with CSD CV is somewhat worse than with fully variable valves. However, the overall air demand is substantially lower since the pneumatic motor mode is omitted. As a consequence, the tank size can be reduced.

All in all, the fuel consumption can still be improved by approximately 28% compared to a larger NA SI engine with the same rated power.

The focus of this thesis was on the design of the valve profile in each mode and on the control strategies which can cope with the limited valvetrain variability. For each mode a design methodology was derived which generally holds. The individual design methodologies were then combined to a system design procedure which ensures that the best overall performance of the system rather than of each individual mode is obtained.

Challenges

Methodologies for the design of the lift profile are now available. For the following reasons, the major challenges remaining are the valve-train actuator system and its integration in the cylinder head:

- The CV requires space. One possibility to gain space is to replace one of the regular air exchange valves, which results in a trade-off. Removing an EV results in an increased back pressure, while removing an IV limits the air intake and thus the rated power. Alternatively and preferably, a valve is added.
- Due to the large pressure difference across the CV, the spring and rocker system have to be modified.
- Valve-train systems with three shiftable cams are available today. Since the pin actuator used in those systems is operated in the time domain, the engine speed up to which the cam profile can be changed is limited. The question of whether the requirements can be fulfilled has to be evaluated.
- Aside from the valve, the valve actuator requires space, too. Its integration on the cylinder head will be challenging.
- For the pneumatic engine start the valve is initially actuated with the starter. Since it is used as a stop/start functionality, the starter is used more often than in a conventional engine. Hence, its durability has to be improved. Alternatively, a valve actuator could be developed that can actively open the valve at least once in order to get the engine rotating. A third option is to combine the pneumatic start with the direct start studied for direct injection engines [39, 40].

The focus of this work was on the realization of the pneumatic modes with CSD CV. In future investigations the impact of various turbine sizes on the fuel consumption and the associated air demand for the turbo lag compensation should be addressed.

Outlook

This thesis is a contribution to the field of air assisted TC SI engines, answering the question of how the system can be realized with camshaft

driven valves for the air exchange between the air tank and the combustion chamber. As a next step an appropriate valve actuator has to be developed and installed on a new prototype engine. Subsequent tests could serve to verify the results obtained with the old one. If a good solution is found for the valve actuator, the engine concept presented will have a perspective for automobile markets which ask for an excellent driveability and are cost sensitive.

Appendix A.

Test Bench Engine

Table A.1.: Data of modified MPE750 engine: Geometry.

engine type		gasoline SI	
injection		PFI	
rated power	P_{max}	61	kW at 6000 rpm
rated torque	T_{max}	131	Nm at 3000 rpm
idling speed	$\omega_{e,idle}$	1200	rpm
max. engine speed	$\omega_{e,max}$	6000	rpm
displacement	V_d	0.75	l
stroke	S	66	mm
bore	B	85	mm
connecting rod	l	115	mm
compression ratio	ε	9.0	
no. of cylinders	N_{cyl}	2	360° parallel twin

Table A.2.: Data of modified MPE750 engine: Valves.

intake valve			
no. of IVs per cyl.	N_{IV}	2	
diameter	d_{IV}	32.5	mm
IV opening	ϕ_{IVO}	24	° CA bTDC
IV closing	ϕ_{IVC}	66	° CA aBDC
IV acceleration	a_{IV}	$0.19 \cdot 10^{-5}$	$\mathrm{m}/{}^{\circ}\mathrm{CA}^2$
exhaust valve			
no. of EVs per cyl.	N_{EV}	1	
diameter	d_{EV}	29.5	mm
EV opening	ϕ_{EVO}	66	° CA bBDC
EV closing	ϕ_{EVC}	24	° CA aTDC
EV acceleration	a_{EV}	$0.19 \cdot 10^{-5}$	$\mathrm{m}/{}^{\circ}\mathrm{CA}^2$
charge valve			
no. of CVs per cyl.	N_{CV}	1	
diameter	d_{CV}	19	mm
tank volume	V_t	30	l

Appendix B.

In-Cylinder Boosting

B.1. Engine mass flow

The engine's volumetric efficiency is mainly affected by the amount of residual gas, the amount of fuel and by the engine speed: $\eta_{vol}(\lambda_{ip}) = \eta_{vol,rg} \cdot \eta_{vol,f}(\lambda_{ip}) \cdot \eta_{vol,\omega}$. The fuel dependent part, which accounts for the rich intake conditions, becomes

$$\eta_{vol,f}(\lambda_{ip}) = \frac{1}{1 + \frac{1}{\lambda_{ip} \cdot \sigma_0}}. \tag{B.1}$$

Compared to the measured intake manifold temperature ϑ_{im}, the temperature of the charge entering the cylinder $\vartheta_{im,cc}$ is lower due to the cooling effect of the fuel evaporation. It is modeled as

$$\vartheta_{im,cc}(t) = \vartheta_{im}(t) - C_{cc} \cdot \frac{1 - \lambda_{ip}(t)^2}{\lambda_{ip}(t)^2}. \tag{B.2}$$

The term C_{cc} denotes a constant which has to be identified by measurements. A similar approach is presented in [37].

B.2. Air mass flow through the charge valve

The CV mass is determined by integration of the CV mass flow over the CV opening period. The CV is modeled as an isothermal orifice [29]. The following assumptions are made for the derivations:

- Air is an ideal gas with $\kappa_a = 1.4$.
- The engine speed, the tank temperature and the tank pressure are constant during the CV opening period. Since this interval is in the order of milliseconds, this assumption is reasonable.

- During the opening period the flow is at sonic conditions. Consequently, the flow function is constant and equal to Ψ_{crit}.
  Since any flow-to-tank has to be avoided, the largest error resulting from the sonic flow assumption occurs if the cylinder pressure at CV closing is equal to the tank pressure. By means of a process simulation it was found that the error in the CV mass transferred is below 1%.

B.3. Maximum in-cylinder mass

For the evaluation of the flow-to-tank condition the maximum in-cylinder mass $m_{cyl,max}$ is used. It consists of the air masses from the intake and the tank, the fuel mass and the residual gas mass:

$$\begin{aligned} m_{cyl,max} &= \frac{1}{x_a} \cdot \max_{\omega_e} \left\{ m_{\beta,max}(\omega_e) + \frac{\mu_{CV,des}}{\omega_e} \right\} \\ &= \frac{1}{x_a} \cdot \left(m_{\beta,max}(\omega_e^*) + \frac{\mu_{CV,des}}{\omega_e^*} \right), \end{aligned} \tag{B.3}$$

where $m_{\beta,max}$ is the maximum intake air mass, i.e., at full load. The air mass fraction x_a is defined as

$$x_a = \frac{1}{\left(1 + \frac{1}{\lambda_c \cdot \sigma_0}\right)} \cdot (1 - x_{rg}), \tag{B.4}$$

where x_{rg} denotes the residual gas mass fraction and λ_c is the normalized air/fuel ratio.

The value of $m_{\beta,max}(\omega_e)$ can either be determined by inversion of the torque model or approximated by the following relation

$$m_{\beta,max}(\omega_e) = \frac{p_{me,max}(\omega_e) \cdot \sigma_0 \cdot \lambda_c \cdot V_d}{H_l \cdot \eta_e \cdot N_{cyl}}, \tag{B.5}$$

where η_e is the engine efficiency at full load. The normalized air/fuel ratio λ_c is also considered since at full load TC SI engines are often run under rich conditions. Typical values for the conditions at full load are: $x_{rg} = 0.1$, $\lambda_c = 0.95$, $\eta_e = 0.31$.

Note that if overboosting is applied, the maximum dynamic torque line has to be considered instead of the stationary full load curve.

B.4. Flow-to-tank condition for higher tank pressure

If the tank pressure is larger than $\tilde{p}_{t,b}$, the air mass transferred through the CV increases. However, the tank pressure and, thus, the cylinder mass at which flow-to-tank occurs are also higher due to the higher tank pressure.

As long as the upper limit of the intake air mass for which no flow-to-tank occurs $m_{\beta,ul}$ is higher than $m_{\beta,max}$, no flow-to-tank will occur

$$m_{\beta,max}(\omega_e) \leq m_{\beta,ul}(\omega_e, p_t) \quad \forall \omega_e \in [\omega_{e,min}, \omega_{e,b}], \tag{B.6}$$

where $m_{\beta,ul}$ is calculated as the difference of the maximum cylinder air mass minus the CV air mass

$$m_{\beta,ul}(\omega_e, p_t) = \frac{x_a \cdot p_t \cdot V_{cyl}(\phi_{CVC,b})}{f_s \cdot R_{cyl} \cdot \vartheta_{cyl}(\phi_{CVC,b})} - \frac{\mu_{CV,p} \cdot p_t}{\omega_e}. \tag{B.7}$$

From Section 3.3.2 it is known that for $p_t = \tilde{p}_{t,b}$, the following inequality holds

$$m_{\beta,max}(\omega_e) \leq \left(\frac{x_a}{f_s} \cdot \frac{V_{cyl}(\phi_{CVC,b})}{R_{cyl} \cdot \vartheta_{cyl}(\phi_{CVC,b})} - \frac{\mu_{CV,p}}{\omega_e} \right) \cdot \tilde{p}_{t,b}. \tag{B.8}$$

Thus, Equation (B.6) also holds for $p_t > \tilde{p}_{t,b}$ since $m_{\beta,max}(\omega_e)$ is independent of p_t.

B.5. Spring stiffness design

For a typical realization of the CV with a return spring it has to be considered that the tank pressure is significantly higher than the one in the cylinder during the intake stroke. The pre-load of the valve spring $F_{s,0}$ has to be larger than the gas force on the CV in order to keep the CV closed:

$$F_{s,0} \geq \frac{d_{CV}^2 \cdot \pi}{4} \cdot p_{t,max} \geq F_{gas}(\Delta p(t), d_{CV}), \tag{B.9}$$

where F_{gas} is the force which results from the pressure distribution $\Delta p(t)$ across the CV and $p_{t,max}$ is the maximum tank pressure, which should not be exceeded.

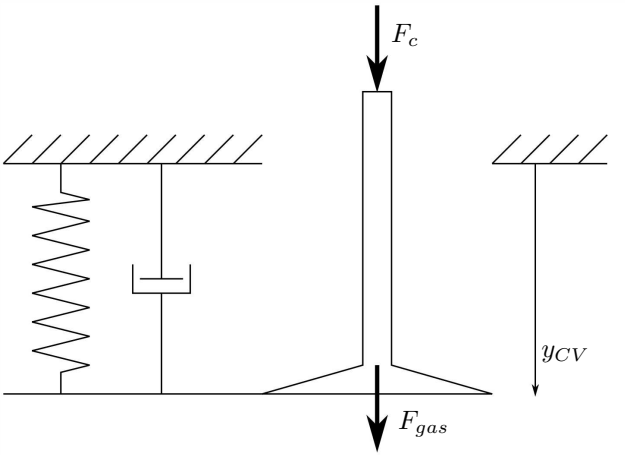

Figure B.1.: Forces exerted on the CV.

The dynamics of the CV realized with a spring and a damper as illustrated in Figure B.1 can be described by

$$\begin{aligned} m_v \cdot \ddot{y}_{CV}(t) = \quad & F_c(t) + F_{gas}(\Delta p(t), d_{CV}) \\ & -k_s \cdot y_{CV}(t) - F_{s,0} - b_s \cdot \dot{y}_{CV}(t), \end{aligned} \tag{B.10}$$

where k_s is the spring stiffness, m_v denotes the valve mass, b_s indicates the friction coefficient and $F_c(t)$ is the reaction force between the lobe and the CV. Note that the gravity is neglected here since its effect is very small as will be shown later.

Besides the static constraint there are also dynamic ones. Cam lobes are not rigidly linked to poppet valves. Hence, the valve spring has to be designed such that no detachment occurs, i.e., the reaction force $F_c(t)$ between the cam and the valve has to be positive at all times, but as small as possible in order to reduce friction losses. This leads to the following constraint

$$F_c(t) = m_v \cdot \ddot{y}_{CV}(t) - F_{gas} + F_{s,0} + k_s \cdot y_{CV}(t) + b_s \cdot \dot{y}_{CV}(t) \geq 0. \tag{B.11}$$

For the simplified acceleration profile, a value for the valve spring stiffness can be found. The worst case which has to be considered is when all of the following conditions are fulfilled:

- The engine speed is equal to the maximum engine speed for which boosting is allowed, $\omega_e = \omega_{e,b}$, since the accelerations in the time domain are highest.

- The tank pressure is maximal: $p_t = p_{t,max}$. In that case, $F_{s,0} - F_{gas}(t) \geq 0$ due to the condition of Equation (B.9). As a conservative guess for the design it is assumed that $F_{s,0} - F_{gas}(t) = 0$ at all times. Once the valve is open, $F_{gas}(t)$ decreases as a result of the flowing fluid (pressure drop).

- The most critical instant at which a lift-off can occur is half way during the valve closing (transition from deceleration to acceleration) since the valve speed and thus the friction are largest:

$$\phi_{crit} = \phi_{CVO,b} + \frac{3\Delta\phi_{CV,b}}{4}, \tag{B.12}$$

  where $\Delta\phi_{CV,b} = \phi_{CVC,b} - \phi_{CVO,b}$ is the total opening duration.

Given the stated conditions and assuming that the engine speed is constant ($\dot{\omega}_e = 0$), Equation (B.11) can be transformed to

$$\begin{aligned} F_{c,crit} &= -a_{CV,b} \cdot m_v \cdot \omega_{e,b}^2 + k_s \cdot \frac{a_{CV,b}}{2} \left(\frac{\Delta\phi_{CV,b}}{4} \right)^2 \\ &\quad -b_s \cdot a_{CV,b} \cdot \omega_{e,b} \cdot \frac{\Delta\phi_{CV,b}}{4} \geq 0. \end{aligned} \tag{B.13}$$

Solving for the spring stiffness k_s results in

$$k_s \geq k_{s,crit} = 8 \cdot \frac{\omega_{e,b}}{\Delta\phi_{CV,b}} \cdot \left(b_s + m_v \cdot \frac{4 \cdot \omega_{e,b}}{\Delta\phi_{CV,b}} \right). \tag{B.14}$$

In Figure B.2 the force between the valve and the cam is depicted for two different values of the spring stiffness and a friction value of $b_s = 10\,\mathrm{Ns/m}$. During the closing of the valve at ϕ_{crit}, the spring force has to be larger than the inertia force and the friction, which act against the moving direction. The contribution of the gravity is 0.49 N and thus substantially smaller than F_c. If no friction is considered, the conditions at half-way open (just after transition from acceleration to deceleration) are equal to those at half-way closed (just before the transition from deceleration to acceleration).

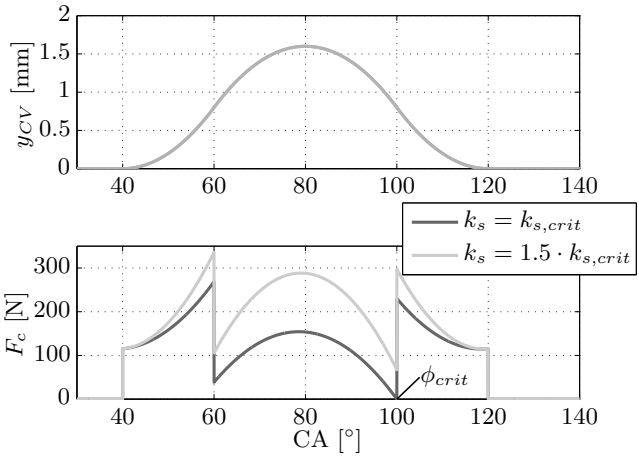

Figure B.2.: Force between valve and cam in the worst case: $m_v = 50\,\mathrm{g}$, $b_s = 10\,{}^{\mathrm{Ns}}/_{\mathrm{m}}$.

The most important variables for the determination of the valve spring stiffness are the maximum boost speed and the valve opening period. A realization with this spring stiffness will guarantee that no lift-off occurs, also for a smoother acceleration profile.

B.6. Constant tank pressure assumption

In the results presented in Chapter 4, it was assumed that the tank pressure remains constant during the turbo lag compensation. In this section this assumption is discussed.

During the turbo lag compensation the tank pressure drops due to the outflow of mass. The pressure drop associated with a certain air mass depends on the tank volume. Figure B.3 shows the simulation results for two engine speeds and a varying tank volume. The upper plot shows the ratio of the air used with a reduced tank volume and the one used with an infinitely large tank. As a result of the decreasing tank pressure, m_{CV} decreases. The boost time slightly increases, however, the effect of the decreasing boost mass is stronger. Consequently, the total amount of air mass used is smaller for a smaller tank. The largest error is 4% for $\omega_e = 4000\,\mathrm{rpm}$ and a tank volume of $V_t = 5\,\mathrm{l}$.

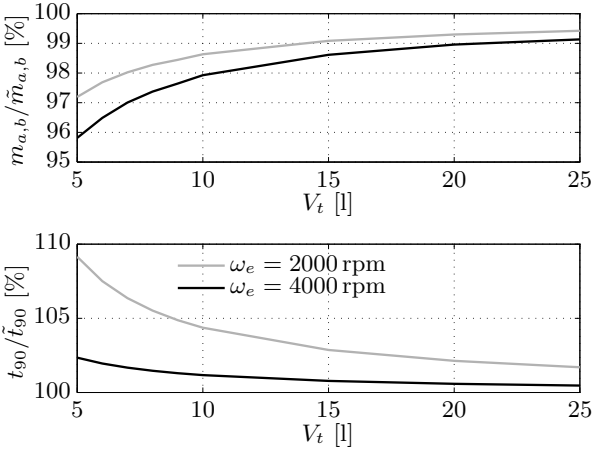

Figure B.3.: Influence of tank size on air mass used and torque rise time for a torque step from 1.7 bar to 17 bar for two different engine speeds.

The air economy comes at the cost of a slower torque rise. The lower plot shows the ratio of the torque rise time t_{90} with a reduced tank volume and the one obtained with an infinitely large tank. The largest penalty is 9% for $\omega_e = 2000\,\mathrm{rpm}$ and $V_t = 5\,\mathrm{l}$.

Since the relative error in the air mass used is small, this effect can be neglected. Furthermore, the air mass used with the infinitely large tank assumption overestimates the real demand. Hence, it is uncritical for the system design process.

Appendix C.

Process Model

In this Appendix the most important relations used in the process model are given. The engine cylinders are modeled as receivers with variable volume. Each cylinder $i \in \{1, ..., N_{cyl}\}$ has its crank angle position ϕ_i. For $\phi_i = 0\,^\circ$, the piston is located at the BDC before the compression stroke.

Mass balance

The air mass of every cylinder $m_{cyl,i}$ is determined by the mass flows $\dot{m}_{k,i}$ through each valve type $k = \{IV, EV, CV\}$

$$\frac{dm_{cyl,i}(t)}{dt} = \dot{m}_{IV,i} + \dot{m}_{CV,i} - \dot{m}_{EV,i}. \tag{C.1}$$

Blow-by is neglected. The mass flow through the valves is modeled as a compressible flow restriction, see [29]. The relation for the discharge coefficient of [30] is used for all valves.

Energy balance

The internal energy balance of every cylinder is given by the enthalpy flows $\dot{H}_{k,i}$, the heat transfer and the instantaneous work done

$$\frac{dU_i}{dt} = \dot{H}_{IV,i} + \dot{H}_{CV,i} - \dot{H}_{EV,i} - \dot{Q}_i - p_{cyl,i} \cdot \dot{V}_{cyl,i}, \tag{C.2}$$

where $\dot{Q}_i$ is the heat transfer to and from the walls. The cylinder volume $V_{cyl,i}$ depends on the cylinder's crank angle position

$$\begin{aligned} V_{cyl,i}(\phi_i) &= V_{cyl,TDC} + A_{cyl} \\ &\quad \cdot \left(l + r \cdot (1 + \cos\phi_i) - \sqrt{l^2 - r^2 \cdot \sin^2\phi_i} \right), \end{aligned} \tag{C.3}$$

where $r = S/2$ is the crank radius. The cylinder temperatures and pressures are calculated using the definition of the internal energy as well as the ideal gas equation:

$$\vartheta_{cyl,i} = \frac{U_i}{m_{cyl,i} \cdot c_{v,a}}, \tag{C.4}$$

$$p_{cyl,i} = \frac{m_{cyl,i} \cdot R_a \cdot \vartheta_{cyl,i}}{V_{cyl,i}}, \tag{C.5}$$

where $c_{v,a}$ is the specific heat at a constant volume of air. The instantaneous torque T_i of each cylinder is defined as

$$T_i = p_{cyl,i} \cdot A_{cyl} \cdot \left[-r \cdot \sin\phi_i + \frac{r^2 \cdot \sin\phi_i \cdot \cos\phi_i}{\sqrt{l^2 - r^2 \cdot \sin^2\phi_i}} \right]. \tag{C.6}$$

Conservation of angular momentum

The law of the conservation of angular momentum determines the engine's acceleration

$$J_e \cdot \frac{d\omega_e}{dt} = \sum T_i - T_{fric}(\omega_e) + T_{ES}(\omega_e), \tag{C.7}$$

where J_e is the engine's inertia, T_{fric} is the friction torque and T_{ES} is the torque supplied by the electric starter. The engine speed ω_e is the time derivative of any crank angle

$$\frac{d\phi_i}{dt} = \omega_e. \tag{C.8}$$

Nomenclature

Acronyms

AA	air assisted
aBDC	after bottom dead center
aNEDC	aggressive New European Drive Cycle
aTDC	after top dead center
BDC	bottom dead center
bBDC	before bottom dead center
bTDC	before top dead center
CA	crank angle
CSD	camshaft driven
CV	charge valve
CVC	charge valve closing
CVO	charge valve opening
ECE	urban part of NEDC
EHVS	electro-hydraulic valve system
EMPA	Swiss Federal Laboratories for Material Science and Technology
ES	electric starter
EUDC	extra-urban part of NEDC
EV	exhaust valve
EVO	exhaust valve opening
FTP	Federal Test Procedure
HEV	hybrid electric vehicle
HPE	hybrid pneumatic engine
ICE	internal combustion engine
IV	intake valve
IVC	intake valve closing
MBT	maximum brake torque
MVM	mean value model
NA	naturally aspirated
NEDC	New European Drive Cycle
OEM	original equipment manufacturer
PFI	port-fuel injected

PM	process model
PSO	particle swarm optimization
QSS	quasi-static simulation
SI	spark-ignited
TC	turbocharger, turbocharged
TDC	top dead center
TWC	three-way catalyst
VT	valve-train
WLTP	Worldwide Harmonized Light-duty Test Procedure
WOT	wide-open throttle

Latin symbols

a	acceleration
b	damping coefficient
c	constant
c_d	aerodynamic coefficient
c_v	specific heat under constant volume
d	diameter
e	engine efficiency
f	factor, function
k	constant
l	connecting rod length
m	mass
$\dot{m}$	mass flow
$\tilde{m}$	nominal mass
p	pressure
$\tilde{p}$	minimum pressure
r	crank radius
t	time, time instant
u	control input
w	weighting factor/function
x	mass fraction
y	valve lift

A	area
B	bore
C	constant

F	force
H	enthalpy
J	inertia
M	total mass on a drive cycle
N	number
P	power
$\dot{Q}$	heat transfer
R	ideal gas constant
S	stroke
S	sensitivity
T	torque
T_s	sample time
U	internal energy
V	volume
$\tilde{V}$	minimum volume

Greek symbols

α	position
δ	design variables
Δ	difference
ϵ	compression ratio
η	efficiency
ϑ	temperature
κ	ratio of specific heats
λ	normalized air/fuel ratio
μ_{CV}	CV air mass flow
$\mu_{CV,p}$	CV size
$\mu\sigma$	flow function
σ_0	stoichiometric air/fuel mass ratio
ϕ	crank angle
Ψ	flow function
ω	rotational speed

Subscripts

a	air
aC	after compressor

b	boost mode
c	cam
c	at point of ignition
cc	charge cooling
$crit$	critical
cyl	cylinder
d	displacement
dec	deceleration
des	desired
e	engine
eff	effective
f	fuel
f	frontal
$fric$	friction
ign	ignition dependent
im	intake manifold
ip	intake port
lin	linearized
max	maximal
me	brake mean effective
mf	fuel mean effective
opt	optimal
p	pump mode
ps	power stroke
r	road friction
rg	residual gas
s	start mode
s	valve spring
ss	safety
sim	simulated
spd	spark delay
t	tank
th	throttle
thr	threshold
ul	upper limit
v	valve
vol	volumetric
β	intake manifold to cylinder
ω	engine speed dependent

List of Figures

List of Tables

Bibliography

[1] L. Guzzella, U. Wenger, and R. Martin, "IC-engine downsizing and pressure-wave supercharging for fuel economy," *SAE Paper 2000-01-1019*, 2000.

[2] S. Berns, J. Hammer, K. Benninger, M. Klenk, and R. Frei, "Reduction of CO_2-emissions while maintaining good driveability: Suggestions for overall powertrain optimization," in *31st International Vienna Motor Symposium*, 2010.

[3] P. Higelin and A. Charlet, "Thermodynamic cycles for a new hybrid pneumatic-combustion engine concept," *SAE Paper 2001-24-0033*, 2001.

[4] I. Vasile, P. Higelin, A. Charlet, and Y. Chamaillard, "Downsized engine torque lag compensation by pneumatic hybridization," in *13th International Conference on Fluid Flow Technologies*, 2006.

[5] C. Dönitz, I. Vasile, C. H. Onder, and L. Guzzella, "Realizing a concept for high efficiency and excellent driveability: The downsized and supercharged hybrid pneumatic engine," *SAE Paper 2009-01-1326*, 2009.

[6] C. Dönitz, C. Voser, I. Vasile, C. H. Onder, and L. Guzzella, "Validation of the fuel saving potential of downsized and supercharged hybrid pneumatic engines using vehicle emulation experiments," *J. Eng. Gas Turbines Power*, vol. 133, no. 9, p. 092801, 2011.

[7] C. Dönitz, "Hybrid pneumatic engines," Ph.D. thesis, No. 18761, ETH Zürich, 2009.

[8] P. Higelin, A. Charlet, and Y. Chamaillard, "Thermodynamic simulation of a hybrid pneumatic combustion engine concept," *Int. J. of Applied Thermodynamics*, vol. 5, no. 1, pp. 1–11, 2002.

[9] I. Vasile, C. Dönitz, C. Voser, J. Vetterli, C. Onder, and L. Guzzella, "Rapid start of hybrid pneumatic engines," in *IFAC Workshop*

on Engine and Powertrain Control, Simulation and Modeling (E-COSM09), 2009, pp. 123–130.

[10] C. Voser, C. Dönitz, G. Ochsner, C. H. Onder, and L. Guzzella, "In-cylinder boosting of turbocharged spark-ignited engines. Part 1: Model-based design of the charge valve," *Proc. IMechE, Part D: J. Automobile Engineering*, vol. 226, no. 10, pp. 1408–1418, 2012, DOI: 10.1177/0954407012443765.

[11] C. Voser, C. Dönitz, C. H. Onder, and L. Guzzella, "Turbocharged reciprocating piston engine having a conducted pressure tank for bridging the turbo lag, and method for operating said engine / Turboaufgeladene Hubkolbenkraftmaschine mit angeschlossenem Drucktank zur Turbolochüberbrückung und Verfahren zum Betrieb derselben," Patent WO2011015 336 A1, 2011.

[12] C. Voser, T. Ott, C. Dönitz, C. H. Onder, and L. Guzzella, "In-cylinder boosting of turbocharged spark-ignited engines. Part 2: Control and experimental verification," *Proc. IMechE, Part D: J. Automobile Engineering*, vol. 226, no. 11, pp. 1564–1574, 2012, DOI: 10.1177/0954407012443766.

[13] M. Moser, C. Voser, C. Onder, and L. Guzzella, "Design methodology of camshaft driven charge valves for pneumatic engine starts," in *IFAC Workshop on Engine and Powertrain Control, Simulation and Modeling (E-COSM12)*, 2012, pp. 53–60.

[14] L. Guzzella, C. H. Onder, C. Dönitz, C. Voser, and I. Vasile, "Das Downsizing-Boost Konzept auf Basis der pneumatischen Hybridisierung von Ottomotoren / The pneumatic hybridization concept for downsizing and supercharging gasoline engines," *Motortechnische Zeitschrift MTZ*, vol. 71, no. 1, pp. 52–58, 2010.

[15] C. Dönitz, I. Vasile, C. H. Onder, and L. Guzzella, "Dynamic programming for hybrid pneumatic vehicles," in *Proceedings 28th American Control Conference*, 2009, pp. 3956–3963.

[16] C. Dönitz, I. Vasile, C. H. Onder, and L. Guzzella, "Modelling and optimizing two- and four-stroke hybrid pneumatic engines," *Proc. IMechE, Part D: J. Automobile Engineering*, vol. 223, no. 2, pp. 255–280, 2009.

[17] V. Korte, H. Blaxill, F. Schneider, and H. Hoffmann, "Variable valve timing: General options and technologies," in *SIA Conference on Variable Valve Actuation*, 2006.

[18] R. Flierl and M. Klüting, "The third generation of valvetrains − New fully variable valvetrains for throttle-free load control," *SAE Paper 2000-01-1227*, 2000.

[19] L. Bernhard, A. Ferrari, D. Micelli, A. Perotto, R. Rinolfi, and F. Vattaneo, "Elektrohydraulische Ventilsteuerung mit dem "MultiAir"-Verfahren," *Motortechnische Zeitschrift MTZ*, vol. 70, no. 12, pp. 892–899, 2009.

[20] M. Haas, "UniAir − The first fully-variable, electro-hydraulic valve control system," in *Schaeffler Symposium, Detroit*, 2010, pp. 250–263.

[21] H. Unger, *Valvetronic: Der Beitrag des Ventiltriebs zur Reduzierung der CO2-Emissionen des Ottomotors*. Moderne Industrie, 2004.

[22] F. Himsel, C. Faria, P. Solfrank, U. Grau, and U. Geiger, "INA EcoValve − A continuously variable valve lift (CVVL) system," *SAE Paper 2004-01-1391*, 2004.

[23] C. Brüstle and D. Schwarzenthal, "VarioCam plus − a highlight of the Porsche 911 turbo engine," *SAE Paper 2001-01-0245*, 2001.

[24] R. Huber, P. Klumpp, and H. Ulbrich, "Dynamic analysis of the Audi valvelift system," *SAE Paper 2010-01-1195*, 2010.

[25] N. Nitz, H. Elendt, A. Ihlemann, and A. Nendel, "Cam shifting system," in *Schaeffler Symposium, Detroit*, 2010, pp. 226–237.

[26] J. Schäfer, S. Zwahr, and M. Wensing, "The continuously variable cam shifting valve train," in *Schaeffler Symposium, Detroit*, 2010, pp. 238–249.

[27] M. Rebbert, G. Kreusen, and S. Lauer, "A new cylinder deactivation by FEV and Mahle," *SAE Paper 2008-01-1354*, 2008.

[28] H. Hoffmann, A. Loch, R. Widmann, G. Kreusen, D. Meehsen, and M. Rebbert, "Zylinderabschaltung für Ventiltriebe mit Rollenschlepp- hebeln," *Motortechnische Zeitschrift (MTZ)*, vol. 70, pp. 302–307, 2009.

[29] L. Guzzella and C. H. Onder, *Introduction to modeling and control of internal combustion engine systems*. Springer, Berlin, 2010.

[30] R. Pischinger, G. Krassnig, G. Taucar, and T. Sams, *Thermodynamik der Verbrennungskraftmaschine*, H. List and A. Pischinger, Eds. Springer, Wien New York, 1989.

[31] H. Hirooka, S. Mori, and R. Shimizu, "Effects of high turbulence flow on knock characteristics," *SAE Paper 2004-01-0977*, 2004.

[32] Y. Wang, *Introduction to Engine Valvetrains*. SAE International, 2007.

[33] J. Gerhardt, H. Hönninger, and H. Bischof, "A new approach to functional and software structure for engine management systems − BOSCH ME7," *SAE Paper 980801*, 1998.

[34] M. Livshiz, M. Kao, and A. Will, "Engine torque control variation analysis," *SAE Paper 2008-01-1016*, 2008.

[35] S. Frei, "Performance and driveability optimization of turbocharged engine systems," Ph.D. thesis, No. 11520, ETH Zürich, 2004.

[36] J. H. Buckland, J. Freudenberg, J. W. Grizzle, and M. Jankovic, "Practical observers for unmeasured states in turbocharged gasoline engines," in *Proceedings 28th American Control Conference*, 2009.

[37] P. Andersson and L. Eriksson, "Cylinder air charge estimator in turbocharged SI-engines," *SAE Paper 2004-01-1366*, 2004.

[38] T. Fesefeldt and S. Müller, "Optimization and comparison of quick and hybrid start," *SAE Paper 2009-01-1340*, 2009.

[39] U. Kramer, "Potentialanalyse des Direktstarts für den Einsatz in einem Stopp-Start-System an einem Ottomotor mit strahlgeführter Benzin-Direkteinspritzung unter besonderer Berücksichtigung des Motorauslaufvorgangs," Ph.D. thesis, University of Duisburg-Essen, 2005.

[40] A. Kulzer, J. Laubender, U. Lauff, D. Mössner, and U. Sieber, "Der Direktstart," *Motortechnische Zeitschrift (MTZ)*, vol. 67, no. 9, pp. 636–644, 2006.

[41] S. Ebbesen, P. Kiwitz, and L. Guzzella, "A generic particle swarm optimization Matlab function," in *Proceedings of American Control Conference*, 2012, pp. 1514–1524.

[42] M. Schechter, "Regenerative compression braking − a low cost alternative to electric hybrids," *SAE Paper 2000-01-1025*, 2000.

[43] S. Trajkovic, P. Tunestal, B. Johansson, U. Carlson, and A. Höglund, "Introductory study of variable valve actuation for pneumatic hybridization," *SAE Paper 2007-01-0288*, 2007.

[44] L. Guzzella and A. Sciarretta, *Vehicle Propulsion Systems*, 2nd ed. Springer, Berlin, 2007.

[45] A. Fazeli, A. Khajepour, C. Devaud, and N. L. Azad, "A new air hybrid engine using throttle control," *SAE Paper 2009-01-1319*, 2009.

[46] C.-Y. Lee, H. Zhao, and T. Ma, "A low cost air hybrid concept," in *Les Rencontres Scientifiques de l'IFP − Advances in Hybrid Powertrains*, 2008.

[47] H. Kang, C. Tai, X. Wang, T.-C. Tsao, P. N. Blumberg, and J. Stewart, "Demonstration of air-power-assist (APA) engine technology for clean combustion and direct energy recovery in heavy-duty application," *SAE Paper 2008-01-1197*, 2008.

[48] H. Sigloch, *Strömungsmaschinen: Grundlagen und Anwendungen*. Hanser, München, 2009.